N64-18440

OTS PRICE

XEROX $ 10.50 ph

MICROFILM $ 4.31 mf

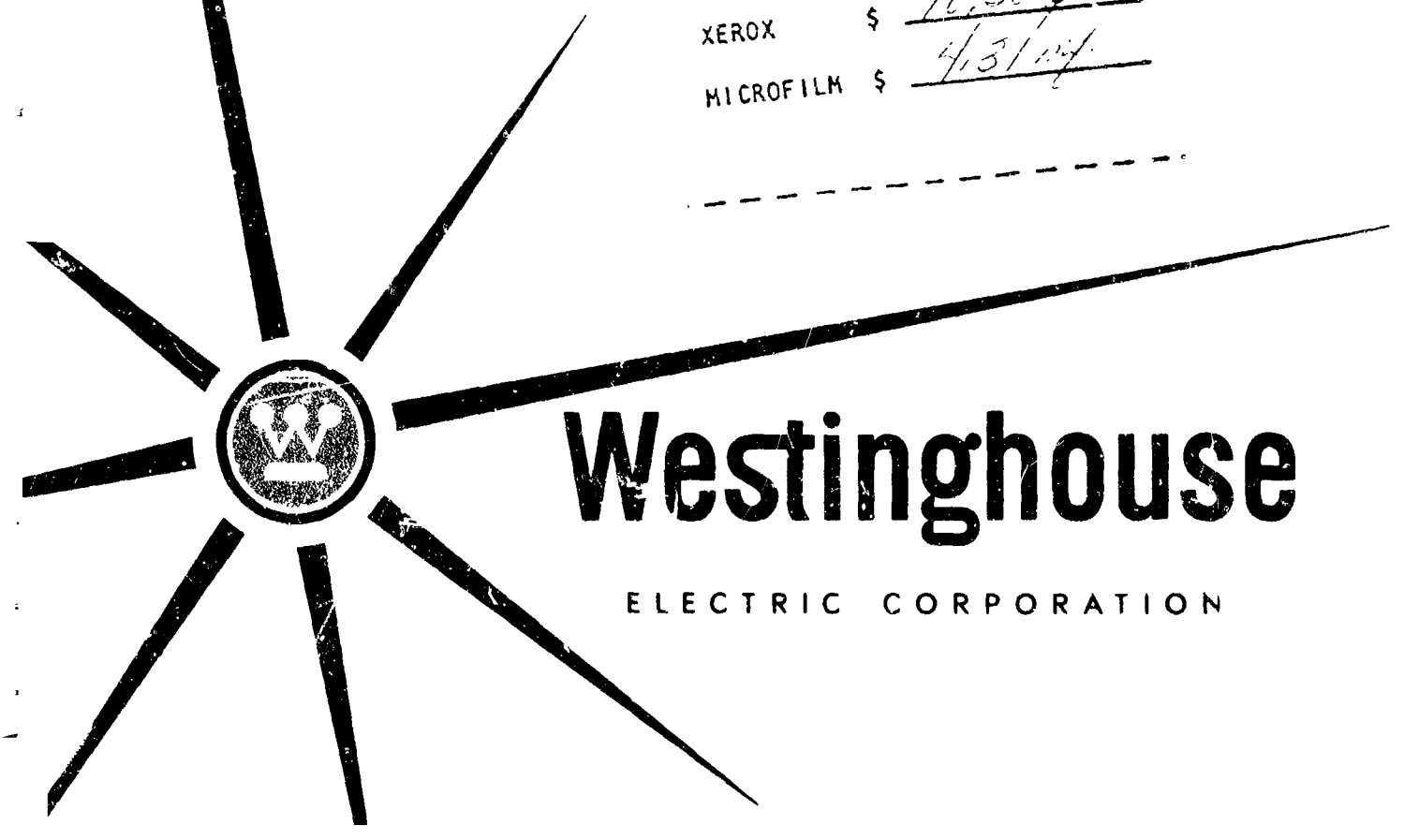

Westinghouse

ELECTRIC CORPORATION

ORBIT POSITION CONTROL

SYSTEMS COMPARISON

AND SELECTION STUDY REPORT

November 8, 1963

An Interim Report Prepared Under Contract NAS1-3131 for The

NATIONAL AERONAUTICS AND
SPACE ADMINISTRATION
Langley Research Center, Virginia

by the

Westinghouse Electric Corporation
Aerospace Division
Baltimore, Maryland

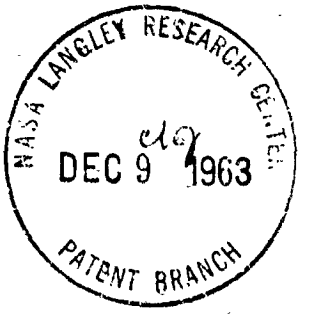

TABLE OF CONTENTS

TABLE OF CONTENTS (Continued)

TABLE OF CONTENTS (Continued)

TABLE OF CONTENTS (Continued)

1.0 INTRODUCTION

This study concerns a system in which solar flux is exploited as a force to change orbital parameters of a passive communication satellite in a manner which when controlled will permit sufficient change of these parameters to provide means for station keeping of a satellite with respect to others in the same orbital plane. The purpose is to be able to maintain spacing of a minimum number of these satellites to provide maximum communications coverage around the earth's surface as opposed to random placement of similar satellites. The method of controlling the force upon the satellite due to solar flux is to position surfaces of varying solar force characteristics toward the sun as a function of orbital position by torquing against the earth's magnetic field with currents in three mutually orthogonal coils rigidly fixed to the satellite.

The first four months effort has been divided into three major headings; control, structure and orbital computations. Considered under these headings are feasibility with regard to control accuracy and stability; structural weight; thermal balance; reliability and component life; optimum coil weight vs power supply weight; and mobility in terms of orbital parameters.

The study was made by comparing two approaches. One, called the "dual flip ", in which the satellite was flipped twice per orbit in the near ecliptic plane to place alternate sides towards the sun when the sun line was most nearly tangental to the satellite's velocity vector. The other, a vertically oriented system, where one axis of the satellite is pointed toward the earth's center at all times, thus pointing alternate surfaces towards the sun when the sun line is tangential to the velocity vectors.

Two objectives were to be accomplished during the first four months of this study program. First, to select the most promising system and second, to demonstrate feasibility. This report will present first those parameters which will be significantly different for the aforementioned two systems studied in order

to establish a basis for the recommended choice. Following this will be presented those additional areas studied to complete the feasibility picture.

2.0 RECOMMENDATION

The results of the first four months study have shown that the vertical oriented system is a more readily attainable system. At first it was believed that the dual flip system would better utilize the effects of solar forces because the satellite could be controlled in attitude to directly point the desired face toward the sun during large portions of each orbit by solar vectoring. The vertically oriented satellite must by contrast accept an offset equal to the angle of the orbital plane to the ecliptic plane. However, upon evaluating secondary solar forces, specifically the earth's albedo and radiation, it was found that slightly greater total differential forces were obtained in the vertically oriented system. Further basis for this recommendation is presented in section 3.0

This page left intentionally blank

3.1 CONTROL SYSTEM

3.1.1 Control System Goals

The function of the control system is to align the symmetrical axis of the vehicle along a predetermined direction vector. For the dual flip system configuration the sunline forms the reference vector and for the vertical configuration the orbit velocity vector forms the external reference. At appropriate times the desired pointing direction is reversed (flip operation) to establish a new direction and/or magnitude of orbit correction forces. The control system should point the symmetrical axis along the external reference vector with minimum error consistent with meeting the other requirements of the system.

Due to the high reliability requirement imposed by the expected life of the vehicle, the following conditions were assumed in designing the fundamental control system:

(a) Directional information is to be obtained from sun sensors and magnetometers. These information sources contain no moving parts, a basic requirement for long life. Alternate sensing elements such as horizon scanners, directional gyros, stable tables and star trackers all contain moving parts, while the use of radar error detection depends on the continuous availability of ground stations for reference signal generation.

(b) Damping information is to be obtained from operation on the basic error signals. The long expected life precludes the use of gyros.

(c) The torque source for error correction and maneuver is limited to the interaction between electromagnets and the earth's magnetic field. Mass expulsion systems and reaction wheels both contain undesirable moving parts. The system is to be evaluated for three phases of operation: settling time for a large initial error (>30°), normal pointing error under nonmaneuvering conditions and performance during a maneuver (flip).

3.1.2 General System Descriptions

3.1.2.1 Dual Flip System

3.1.2.1.1 Orientation and Error Definitions

The dual flip system is designed to operate in two modes during every orbit:

(1) Immediately following occultation, the system is to cause the vehicle to turn 180° about an axis orthogonal to the symmetrical axis; the symmetrical axis being defined as the axis passing through the center of the patterns and the center of gravity. Another flip maneuver of 180° is to take place when the vehicle is nearest the sun. The maneuvers are designed to cause one side of the vehicle to face the sun during the solar approach half of the orbit and the opposite side to face the sun during the recession half of the orbit.

(2) At all other times the vehicle symmetrical axis is to be kept pointing along the sunline. It is kept from spinning about this axis by means of torques generated in response to error signals derived from the difference between programmed and measured magnetic field data.

Figure 3.1-1 illustrates the sunline-ecliptic axes (X,Y,Z) and corresponding body axes (x,y,z). Since the error functions used to derive the coil currents must utilize sun sensor and magnetometer signals, the definition of the errors must correspond to the information obtainable from these sensors. In general, the magnetometer information will consist of axial components of the earth's field, each probe metering the field along one of the three orthogonal major axes. The sun sensors can be designed to measure the cosine between the sunline and the symmetrical axis of the sensor, which would correspond to the directional cosine for sun sensors mounted along the major axes of the vehicle. Therefore, any system design must utilize the magnetometer and sunline data thus generated.

Figure 3.1-2 illustrates the definition of the sunline error for the routine mode, where α represents the error angle between the symmetrical x-axis and the desired pointing direction for this axis, the sunline. The computation of this

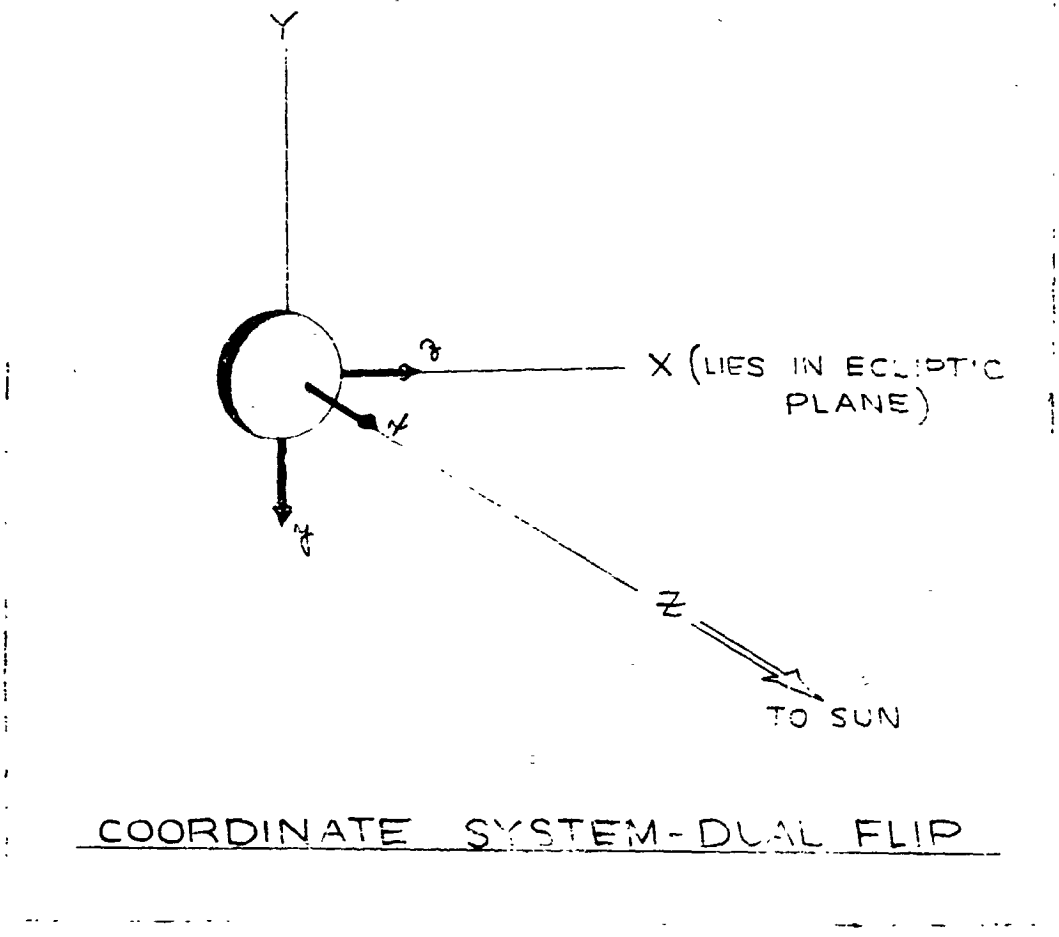

Figure 3.1-1

angle would be complex and would not provide a direction in which to apply the correction torque. A function which would supply nearly all the necessary information is given by the cross product of a unit x-axis vector and the unit sunline vector expressed in vehicle coordinates. This vector ($\bar{i} \times \bar{S}$) has a magnitude proportional to sine α and is in a direction which would correspond to the desired direction of restoring torque. If the commanded restoring torque is made proportional to the sine of the error angle, an undamped second-order system will result. The addition of the damping will be discussed in section 3.1.2.1.2.

To prevent spinning about the symmetrical axis, which would degrade flip performance, the system must develop an error proportional to motion about this axis. Figure 3.1-3 illustrates the method chosen for this error signal generation. The field components B_{ry} and B_{rz} represent the magnetic field readings along the y

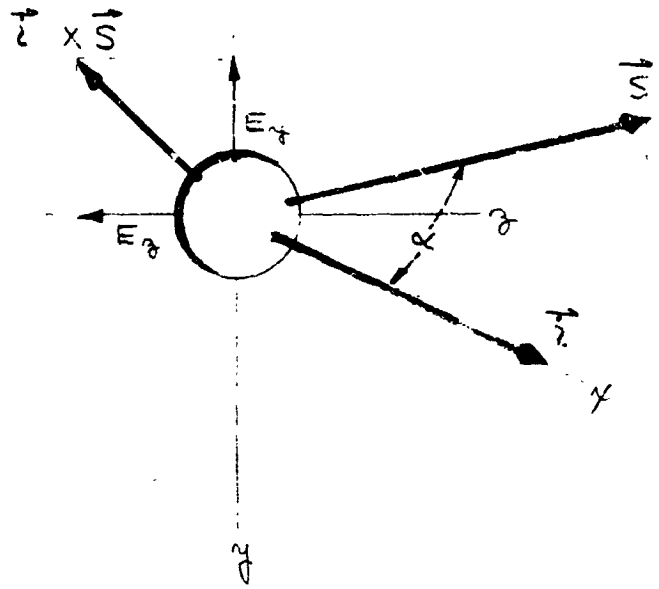

SUNLINE ERROR VECTORS - E_y & E_z

Figure 3.1-2

and z axes if the vehicle is properly aligned. The angle θ between the vector formed from these components ($\overline{B_r}$) and the vector ($\overline{B_a}$) formed from magnetometer readings in these axes (B_{ay} and B_{az}) indicates the error about the x-axis. In a manner similar to the generation of the sunline error, the error about the x-axis will be defined by the cross product of the $\overline{B_r}$ and $\overline{B_a}$ vectors. Since the magnetic field strength will vary, the stored data must be generated in normalized form (constant composite magnitude) and the result of the cross product divided by the magnitude of the composite vector formed from the magnetometer readings. This will yield a vector $\overline{E_x}$, which is a function only of the sine of the angle between the vectors $\overline{B_r}$ and $\overline{B_a}$. The utilization of the error functions derived from the sunline and magnetic field data are discussed in section 3.1.2.1.2.

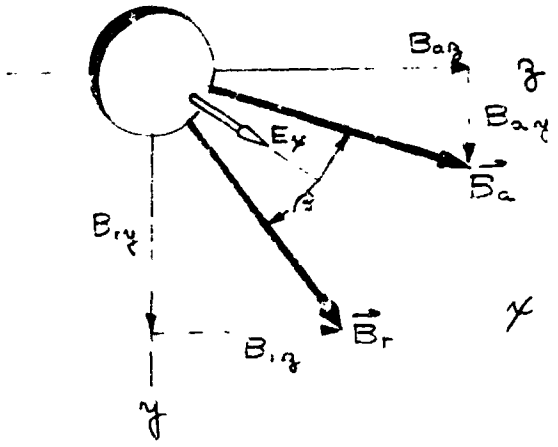

SPIN MOTION ERROR VECTOR - E_x

Figure 3.1-3

It was found during the study program that the loop gain during the routine mode could not be raised to a large enough value to permit closed loop operation during the flip mode. The flip then had to be performed in a manner which did not permit feedback control of the x-axis position during the flip operation. The details are contained in section 3.1.2.1.3.

3.1.2.1.2 Block Diagram-Routine Mode

During the nonmaneuvering phase of the orbit, the system is to maintain the symmetrical axis of the vehicle pointed along the sunline while maintaining a nonspinning condition. Figure 3.1-4 illustrates the system in general form. The reference magnetic field data is stored on board during a pass over a ground station. At each point in the orbit, the reference data and the magnetometer data are made to form a cross product, which is then normalized by dividing by the absolute value

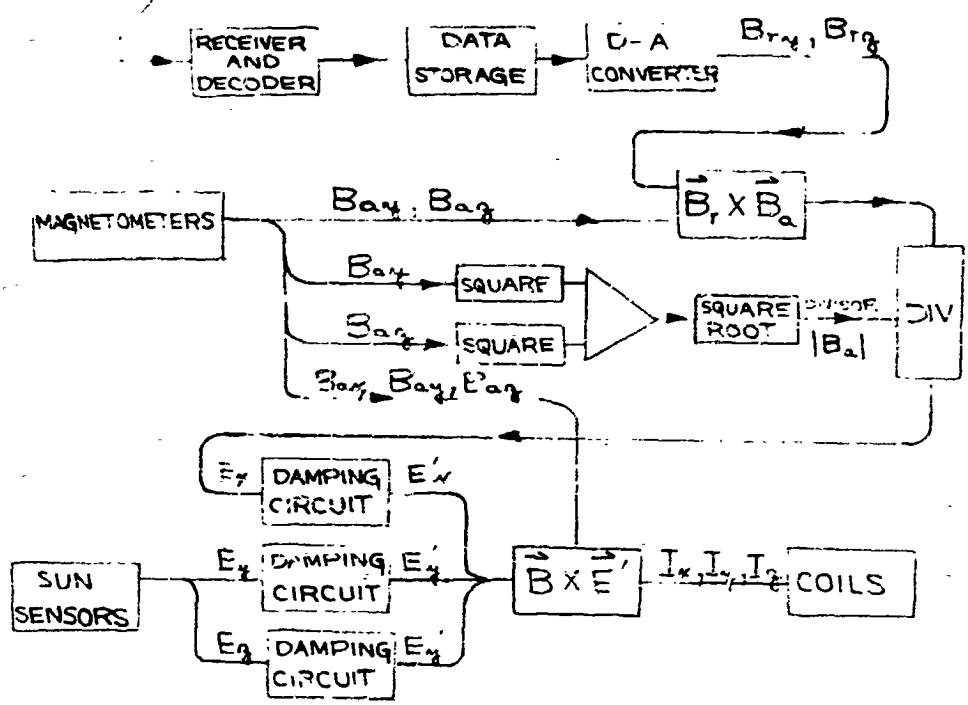

Figure 3.1.4

of the field component in the y-z plane. The resultant signal is E_x, a measure of the error around the sunline. The E_y and E_z signals are derived from the sun sensors and are equal to $+ S_z$ and $- S_y$ respectively, which are the directional cosines between the sunline and the z and y axes. These signals form the sunline error vector where from section 3.1.2.1.1

$$\overline{E_s} = \overline{i_x} \times \overline{S}$$

and $E_y = jS_z$, $E_z = -kS_y$ } { where j and k are unit vectors along the y and z axes

The only portion of the composite error ($iE_x + jE_y + k E_z$) which can be corrected is that which is orthogonal to the magnetic field. Since the coil field vector must itself lie orthogonal to both the magnetic field and the correctable portion of the error, the coil current is computed as the cross product of the error

signal and the magnetic field vector in vehicle coordinates. Since the resulting system, with corrective torque proportional to error, is unstable, some means had to be introduced to provide a signal approximately proportional to $\dot{E}$. This was carried out by detecting the signal rate direction of the absolute value of each component (E_x, E_y and E_z) and attenuating the contribution to the cross-product by that component if its absolute value was decreasing. With reference to figure 3.1-4:

$$E'_x = k_x E_x, \quad \text{where } k_x = 1 \text{ when } |\dot{E}_x| > 0$$

$$\text{and} \quad k_x < 1 \text{ when } |\dot{E}_x| < 0$$

The logic for E'_y and E'_z is similar.

3.1.2.1.3 Block Diagram - Flip Mode

The flip mode operation was basically designed as an optimum open loop controller. Since, in the routine pointing mode, the symmetrical axis of the vehicle is maintained along the sunline, it should only be necessary to develop a fixed torque orthogonal to both the magnetic field and the sunline to flip the vehicle 180° with no residual rate. This would involve reversing the required torque direction in the middle of the flip. Figure 3.1-5 illustrates the sequence of the desired flip. At step 1, the vehicle symmetrical axis is pointing at the sunline and the rates about the three vehicle axes are assumed to be minimal. Point "a" represents the intersection of the symmetrical axis with the vehicle surface. A fixed torque orthogonal to both the $\bar{B}$ (field) and $\bar{S}$ (sunline) vectors is applied (into the paper on figure 3.1-5) and the vehicle accelerates until it reaches point 4, where the torque vector is reversed, so that from point 4A to point 7 the vehicle is decelerating. At point 7 the commanded torque is reduced to zero.

Figure 3.1-6 illustrates the mechanization. The reference torque vector, which is orthogonal to both the magnetic field and the sunline, is generated by taking the cross product of the measured magnetic and sunline coordinates, and normalized by dividing by the absolute value of the resultant vector. The computed signals represent the command-torque components and are used to form the coil

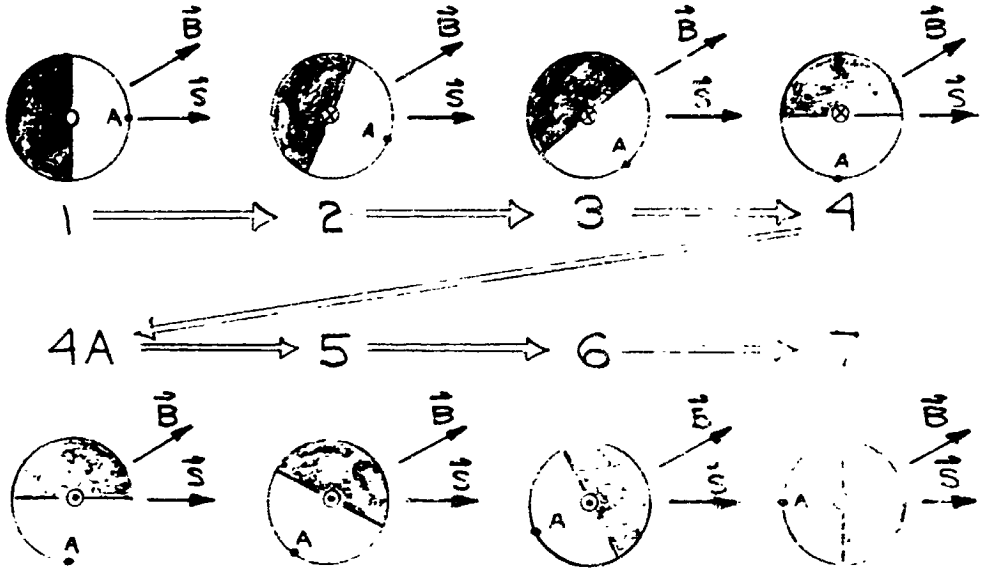

FLIP OPERATION - DUAL FLIP SYSTEM

Figure 3.1-5

currents by taking the cross-product $\bar{T} \times \bar{B}$. Since the coil field will then be orthogonal to both $\bar{T}$ and $\bar{B}$, the actual torque vector produced by interaction with the earth's field will be colinear with the $\bar{T}$ vector, since it is formed by the cross product $\bar{I} \times \bar{B}$. The torque reversal operation and the reversion to the routine pointing mode are carried out in response to one bit commands from the data storage element.

3.1.2.2 Vertical System

The vertically oriented system is designed to maintain the vehicle symmetrical axis along the velocity vector of the orbit. In addition, the vehicle motion about the velocity vector is maintained at an average of zero to minimize the destabilizing effect of rate buildup about the velocity vector.

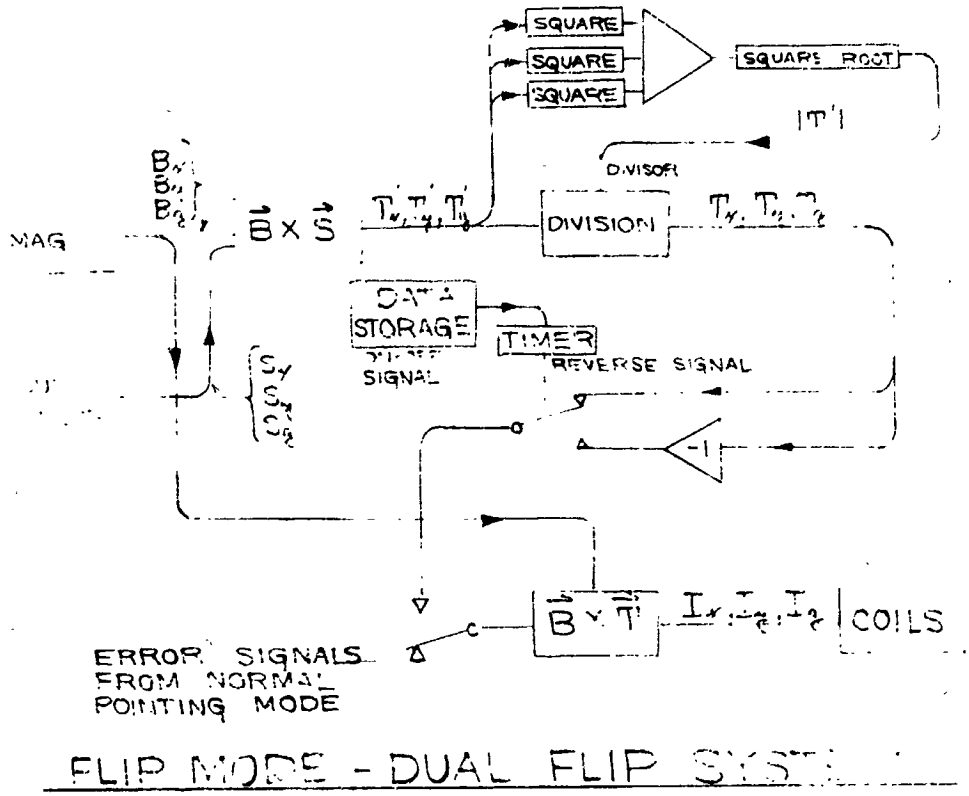

Figure 3.1-6

3.1.2.2.1 Orientation and Error Definitions

Figure 3.1-7 illustrates the orbit coordinates (X,Y,Z) and the body axes (x,y,z) as shown for a condition of perfect alignment. For imperfect alignment, the error signals should, as in the dual flip system, correspond to the direction in which a restoring torque is to be applied. In addition, the error signals must be computed from available sensor information. The development of pointing error vectors and the spin motion error vector is carried out in a fashion similar to the error computations for the dual flip routine pointing mode. The error generation for the vertical configuration is shown on figures 3.1-8 and 3.1-9. The major difference is in the use of the velocity direction unit vector ($\bar{X}$) in place of the sunline and the employment of the vertical direction unit vector ($\bar{Z}$) in place of the difference between two magnetic field vectors.

COORDINATE SYSTEM - VERTICAL CONFIG.

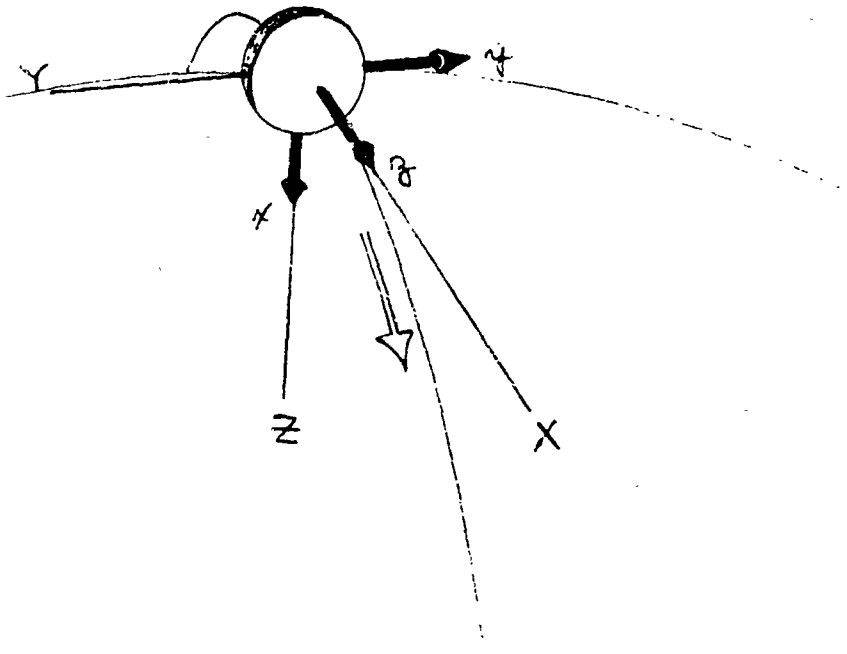

Figure 3.1-7

The major difference between the dual flip and vertical configurations lies in the availability of signals which could be readily processed to yield the errors with respect to the external coordinate system. Since the sunline and magnetic field vectors will not, in the general case, lie along any of the orbit axes, it becomes necessary to compute the direction cosines between the orbit axes and the vehicle axes for the vertical system. The computation must be carried out utilizing four sources of information:

(1) The predicted magnetic field vector for each point in the orbit, expressed in orbital coordinates.

(2) The predicted sunline vector for each point in the orbit, expressed in orbital coordinates.

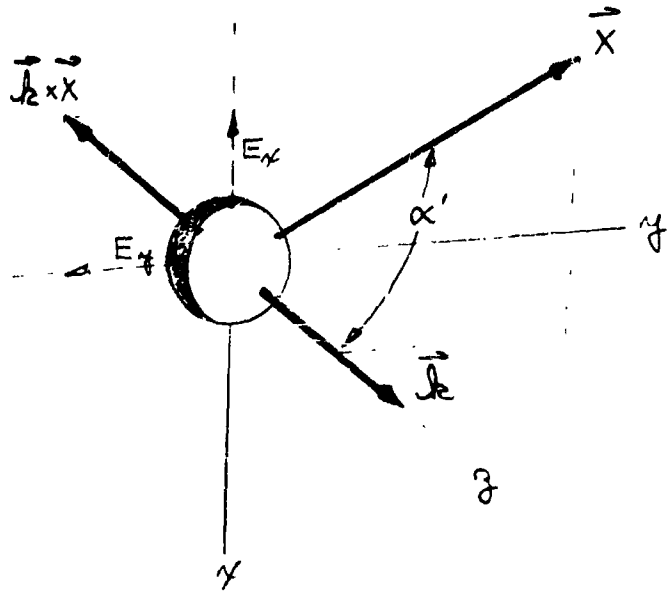

POINTING ERROR VECTORS - E_x & E_y

Figure 3.1-8

(3) The magnetic field vector, expressed in vehicle coordinates, from magnetometer readings.

(4) The sunline vector, expressed in vehicle coordinates, from sun sensor readings.

The cross product definitions of errors shown on figures 3.1-8 and 3.1-9 can be expressed as direction cosines, which is equivalent to expressing them as elements of the transformation matrix relating orbital to vehicle coordinates. The problem then becomes one of computing the matrix elements in terms of the four available parameters, two of which are stored in a memory on board the vehicle.

The first step is to form the cross product $\bar{B} \times \bar{S} = \bar{L}$ which yields two vectors, one in each coordinate system, which can be used in addition to the four

SPIN MOTION ERROR VECTOR - E_γ

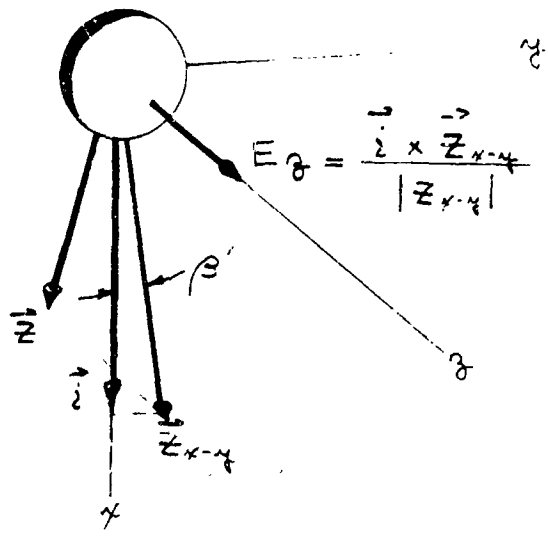

Figure 3.1-9

others to provide the solution for the matrix elements. There will then be nine equations with nine unknowns:

$$L_x = a_{11} L_X + a_{12} L_Y + a_{13} L_Z$$
$$B_x = a_{11} B_X + a_{12} B_Y + a_{13} B_Z$$
$$S_x = a_{11} S_X + a_{12} S_Y + a_{13} S_Z$$
$$L_y = a_{21} L_X + a_{22} L_Y + a_{23} L_Z$$
$$B_y = a_{21} B_X + a_{22} B_Y + a_{23} B_Z$$
$$S_y = a_{21} S_X + a_{22} S_Y + a_{23} S_Z$$
$$L_z = a_{31} L_X + a_{32} L_Y + a_{33} L_Z$$
$$B_z = a_{31} B_X + a_{32} B_Y + a_{33} B_Z$$
$$S_z = a_{31} S_X + a_{32} S_Y + a_{33} S_Z$$

Four of the matrix elements are required to generate the error components E_x, E_y, E_z. These elements are: a_{11}, a_{21}, a_{23} and a_{13}. The first three equations can be used to solve for a_{11} nd a_{31} while the second three equations will yield solutions for a_{21} and a_{23}.

The solutions for the equations are:

$$a_{11} = \frac{L_x(B_Y S_Z - B_Z S_Y) - B_x (L_Y S_Z - L_Z S_Y) + S_x(L_Y B_Z - L_Z B_Y)}{|L|^2}$$

$$a_{21} = \frac{L_y(B_Y S_Z - B_Z S_Y) - B_y (L_Y S_Z - L_Z S_Y) + S_y(L_Y B_Z - L_Z B_Y)}{|L|^2}$$

$$a_{13} = \frac{L_x(B_X S_Y - B_Y S_X) - B_x (L_X S_Y - L_Y S_X) + S_x(L_X B_Y - L_Y B_X)}{|L|^2}$$

$$a_{23} = \frac{L_y(B_X S_Y - B_Y S_X) - B_y (L_X S_Y - L_Y S_X) + S_y(L_X B_R - L_Y B_X)}{|L|^2}$$

which will then be used to solve for E:

$$E_x = -a_{21}$$

$$E_y = +a_{11}$$

$$E_z = \frac{+a_{23}}{\sqrt{a_{23}^2 + a_{13}^2}}$$

The analog computer study program utilizes the matrix elements directly to reduce complexity, since the computations involved are straightforward.

3.1.2.2.2 Block Diagram

Figure 3.1-10 illustrates the block diagram of the vertical system. The reference data for the magnetic field and sunline is stored in the data storage unit during a pass over the ground station. This reference data is continually made available in analog form as the orbit angle progresses, and is used in conjunction with the magnetometer and sun sensor information to provide a solution to the matrix element equations described in section 3.1.2.2.1. When the error components are computed, the system (damping circuits, $\bar{B} \times \bar{E}$ current computation) becomes the same as the routine mode of the dual flip system, described in section

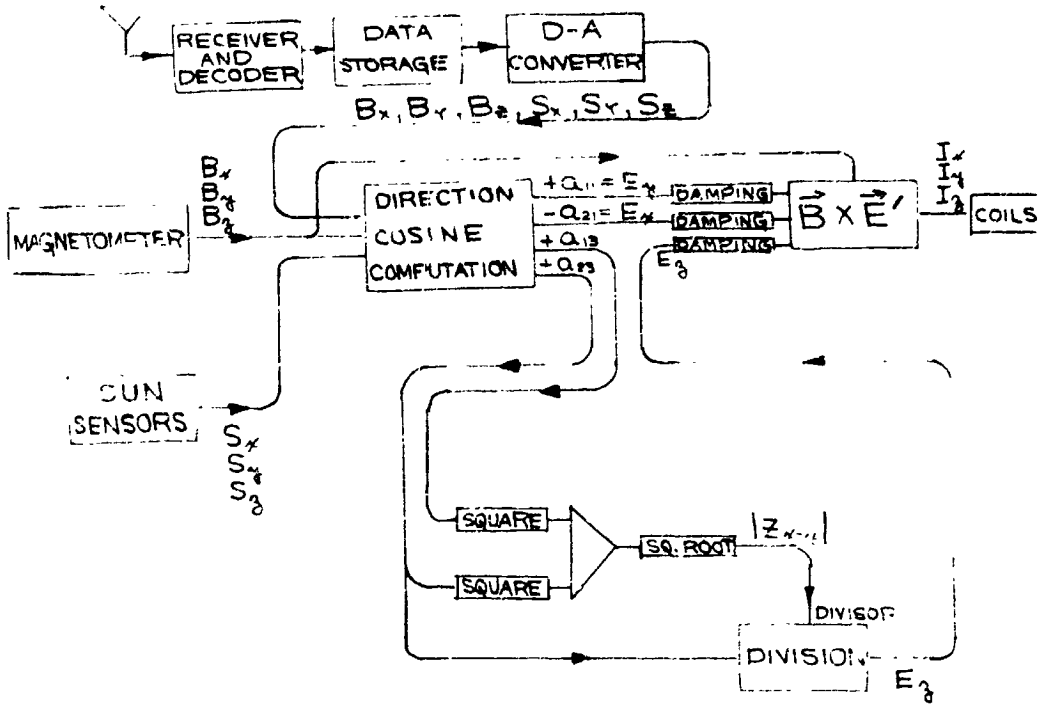

BLOCK DIAGRAM - VERTICAL SYSTEM

Figure 3.1-10

3.1.2.1.2.

When it becomes necessary to reverse the direction of the symmetrical axis along the velocity vector, the reference coordinates of the magnetic field and sunline are changed to correspond to a constant angular velocity of the reference (orbit) coordinates about the vertical Z axis. At the end of this maneuver, the X axis points in the direction the vehicle has come from. At all times the vehicle remains under closed loop control.

3.1.2.3 Sun Orientation Comparison

Figure 3.1-11 gives direct radiation force vs orbit angle for the two systems. This force was multiplied by the sine of the orbit angle and integrated over the orbit to obtain the net force due to direct radiation for each system.

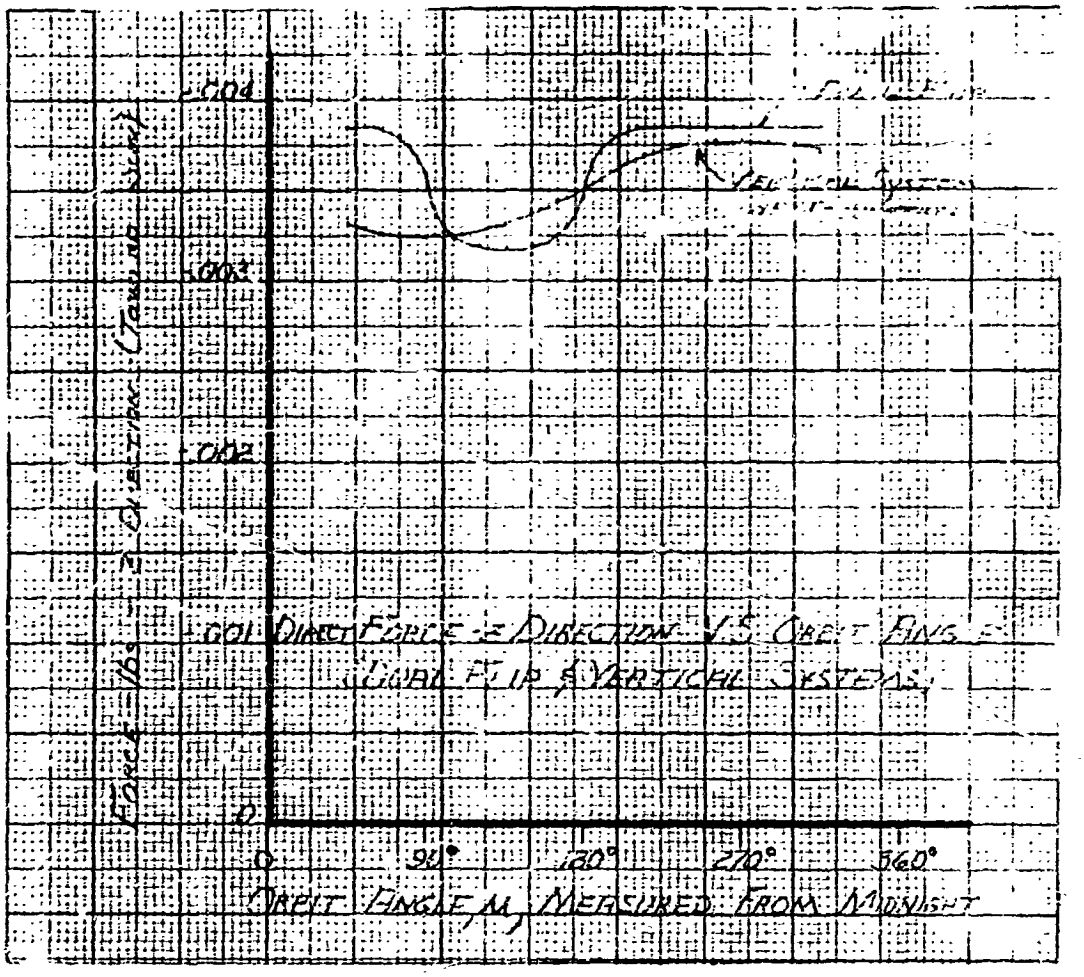

Figure 3.1-11 Direct Z Force vs Orbit Angle for Two Systems

This was done graphically - multiplying each value of F_z by sine μ and measuring the area under the resultant function with a planometer - and analytically - approximating variations in F_z with sinusoids and integrating between the proper limits. The results of this study were found to be .044 #-deg per orbit for the vertical system and 0.036 #-deg per orbit for the dual flip system.

This study was done for direct solar force only since the forces due to reradiation, albedo, and earth are not known at this time for a 45° inclined orbit to the ecliptic.

3.1.2.4 Complexity Comparison

Utilizing the diagrams of the detailed system blocks, figures 3.1-12,13, 14 and 15, the total system complexities of both the dual flip and vertical

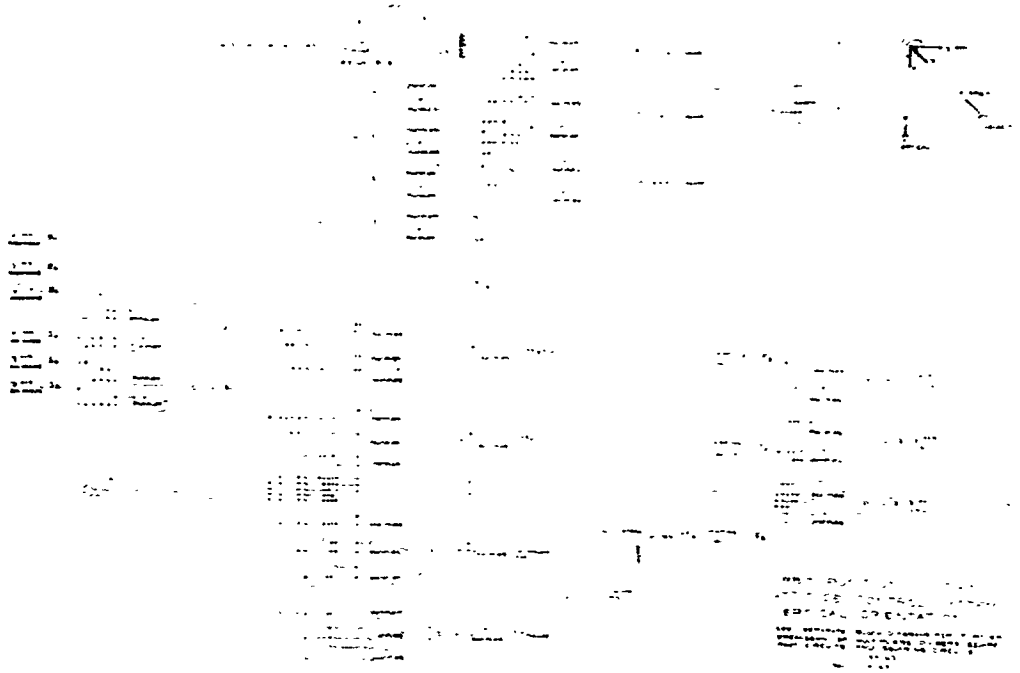

Figure 3.1-12 Detailed Block Diagram, Vertical System

configurations were estimated.

Each of the system blocks was broken down into a probable number of equivalent electronic blocks, components, or comparable number of bits to be stored or converted:

	Dual Flip	Vertical
Multipliers (4)*	54	123
Damping Cir. (16)	48	48
Square and Square Root (1)	3	7
Division (3)	3	6
Power Amplifiers (9)	27	27
Summing Amplifier (1)	6	16
	141	227
Data Storage	72,000 bits	189,000 bits

*Numbers in parentheses are equivalent functional electronic blocks or components required/unit.

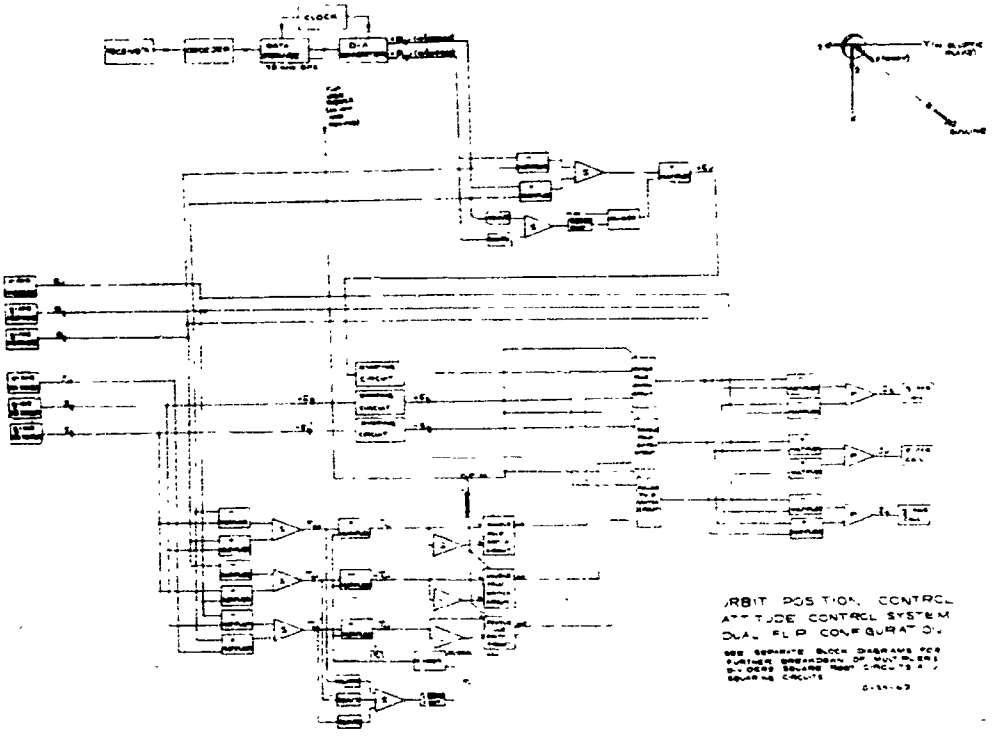

Figure 3.1-13 Detailed Block Diagram, Dual Flip System

Since single or even multiple failures in the data storage elements will probably not result in catastrophic failure, and since the same type receiver, decoder, power supply and clock could be used for either system, the complexity of the vertical system relative to that of the dual flip system will not be much in excess of that for the analog stages (a factor of 1.61) which would make it in the order of 1.75.

3.1.2.5 Gain Definition

In subsequent sections which describe the performance results, one of the parameters is gain. For convenience in analysis, two definitions were used, one for the dual flip system where it was necessary to relate closed loop performance to flip operation capability, the other for the vertical system where a more general gain definition is desired. A constant relates the two gains.

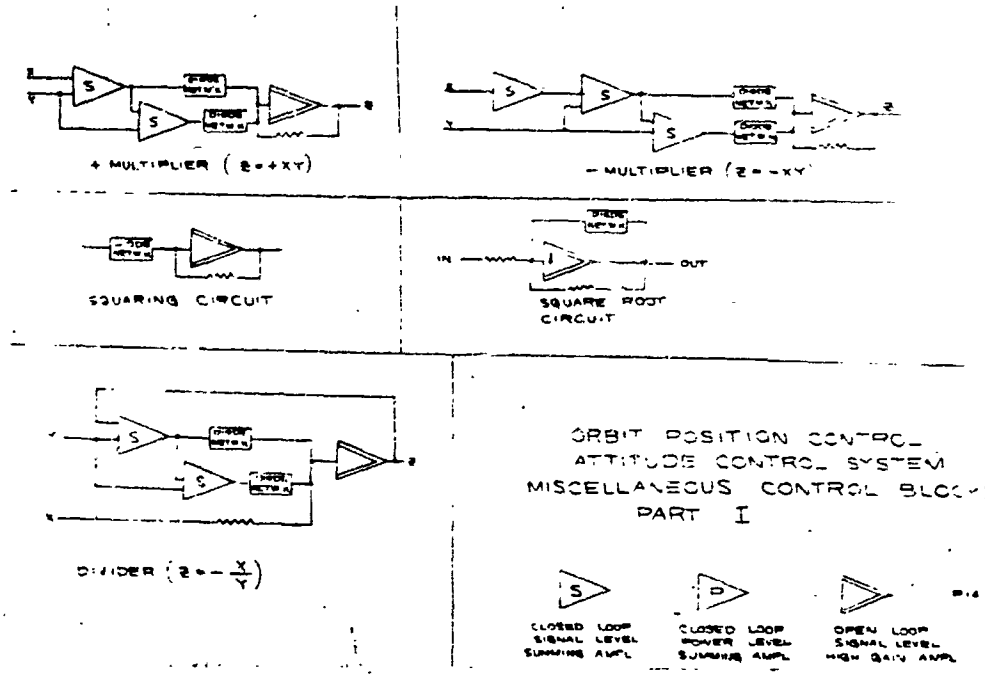

Figure 3.1-14

Dual Flip Gain Definition - See figure 3.1-16

Vertical System Gain Definition - The output torque generated per unit field strength orthogonal to the coil axis, divided by the axial component of the error which is normal to the field.

In addition to the parameter gain, a gain ratio parameter is also used. This is defined as the ratio of the gain when the absolute value of the error is decreasing to the gain when the absolute error is increasing.

3.1.3 Routine Mode Performance Comparison

In sections 3.1.3, 4 and 5, the results of an analog computer simulation of vehicle performance are detailed. Section 3.1.3 is concerned with routine (nonmaneuver) performance of the two systems. All runs were made at 1500 statute miles altitude, 30° inclination, with a uniform distributed spherical vehicle

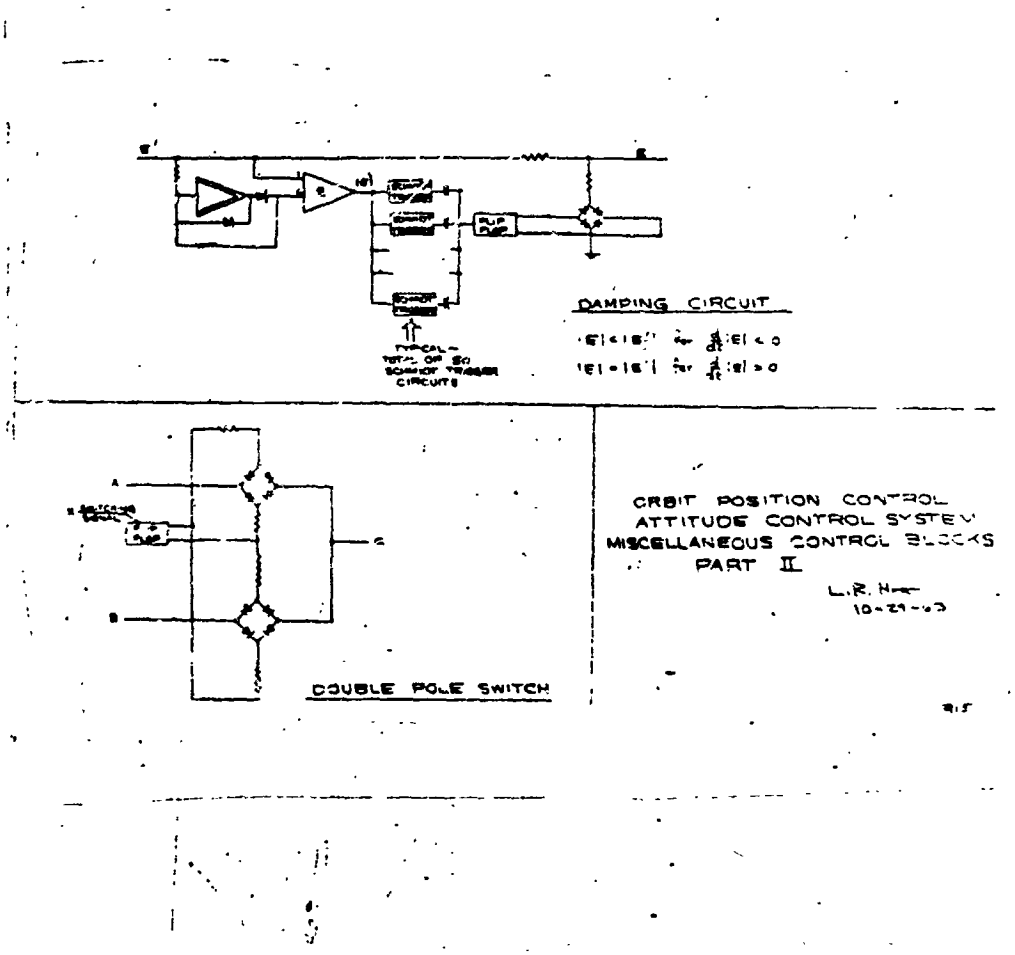

Figure 3.1-15

having a moment of inertia about each of the three axes of 4.5×10^5 slug-ft.^{2}.

3.1.3.1 Peak Error

The complex nonlinearities of the two systems preclude an analytic solution for performance evaluation. For this reason, it was necessary to make long computer runs to determine the peak and average values of parameters such as errors, torque and current.

The relative position of the vehicle symmetrical axis with respect to the required pointing direction formed the measure of error used in evaluating performance. Since three directional cosines can relate the position of a line (symmetrical axis) with respect to an external coordinate system, they were recorded on all runs and also used to compute the sine of the angular error. The peak arc-sine was then calculated and tabulated as a function of system parameter variation.

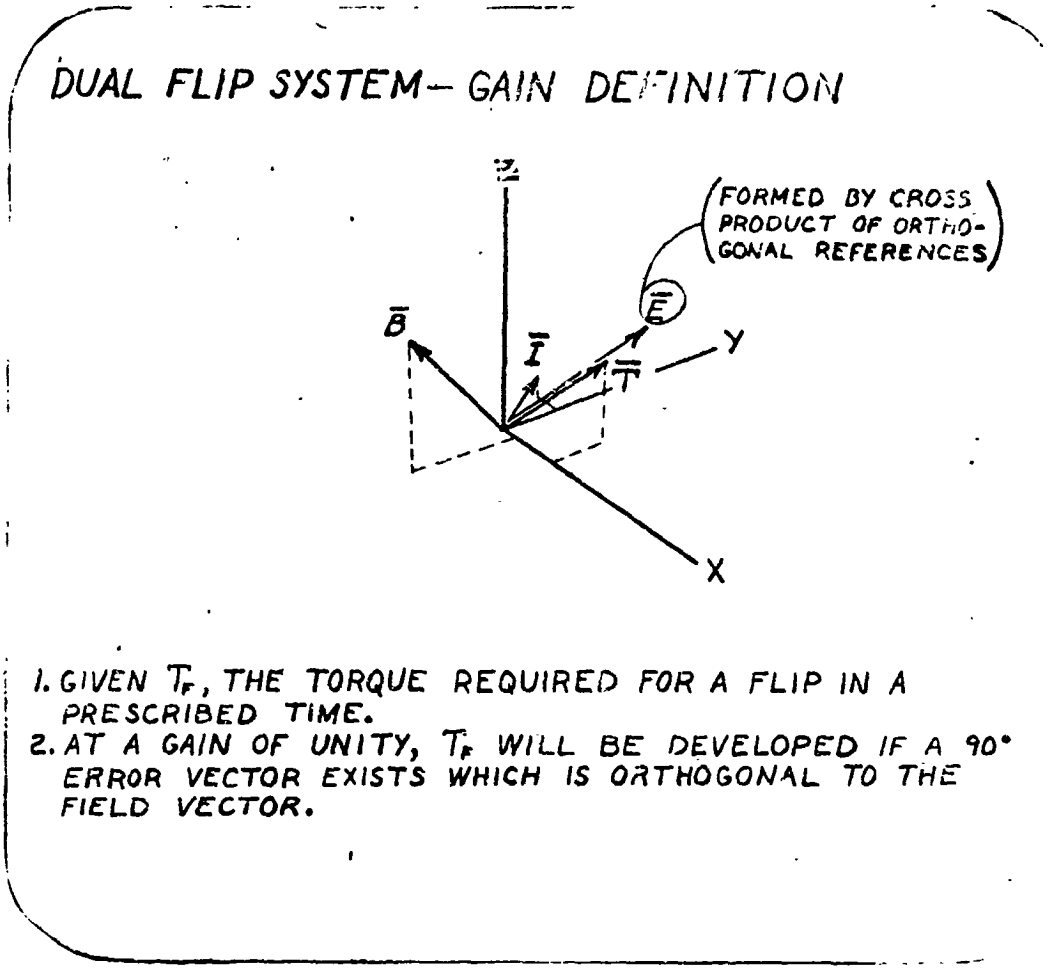

Figure 3.1-16

3.1.3.1.1 Dual Flip System

The dual flip system routine pointing mode was evaluated using no maneuvers. It therefore corresponded to a sun-pointing vehicle. This was done to establish a relative performance criteria for comparing it with the vertical system and to establish optimum loop parameters prior to attempting a flip operation. Figure 3.1-17 (solid line) illustrates the performance with no disturbance torque and a fixed gained ratio. With a minimum peak error of 3 degrees, it has a better optimum performance than the vertical system (comparable curve shown by dotted lines) but the sharper slopes for other than optimum gain makes the system much more gain sensitive.

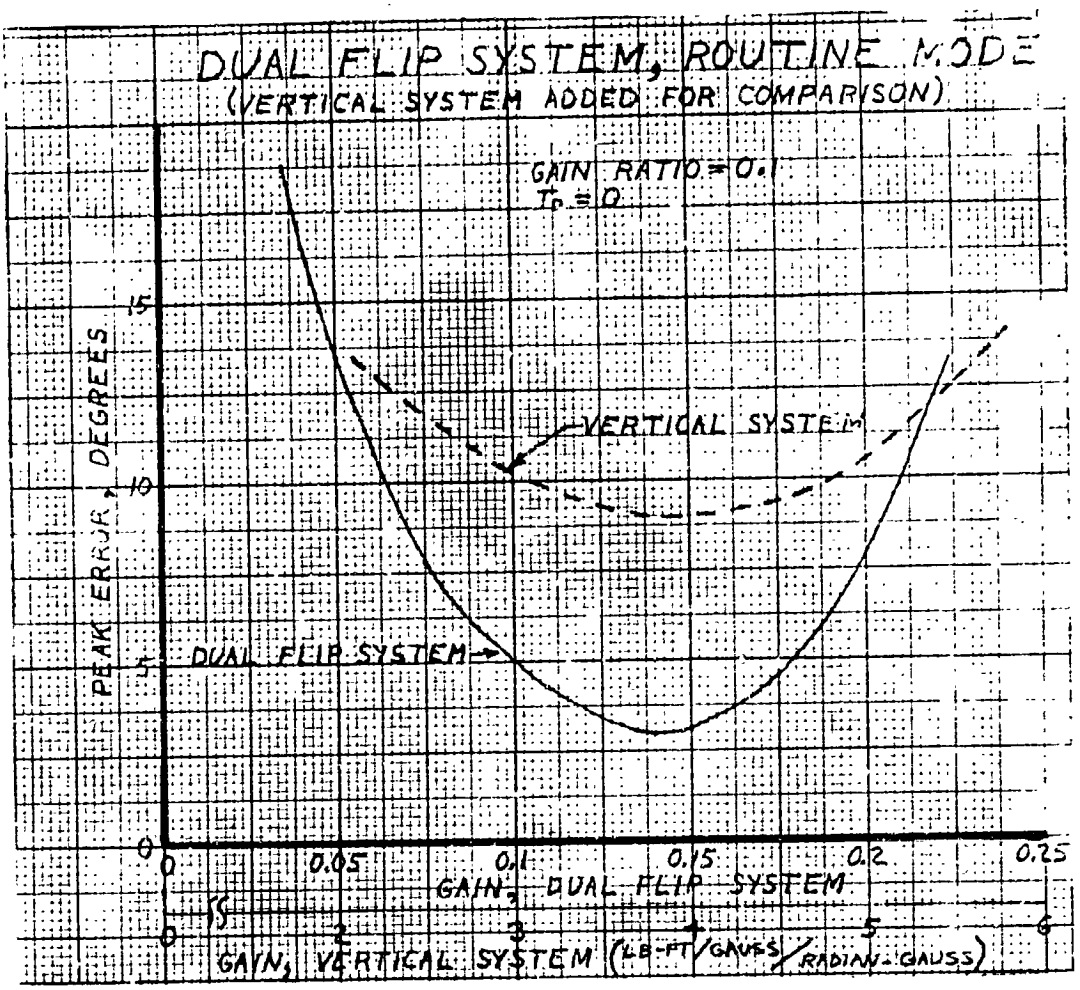

Figure 3.1-17 Peak Error vs Gain, Both Systems, Routine Mode, $T_D = 0$

3.1.3.1.2 Vertical System

As noted above, the vertical system has higher errors for optimum gain settings. This results from the generation of inertial reference torques to correct errors which are functions of a moving (orbital) coordinate system. Figure 3.1-18 illustrates vertical system performance for a family of disturbance torques. For purposes of analysis, it was assumed that the principal disturbance torque would result from dissimilar surface coatings on the two sides of the vehicle and would generate a torque whose vector would be orthogonal to both the sunline and the symmetrical axis and whose magnitude would be proportional to the sine of the angle between the sunline and symmetrical axis. It can therefore be expressed conveniently as a cross-product and, consequently, readily mechanized. The disturbance torque is rated in terms of its peak value which would occur with

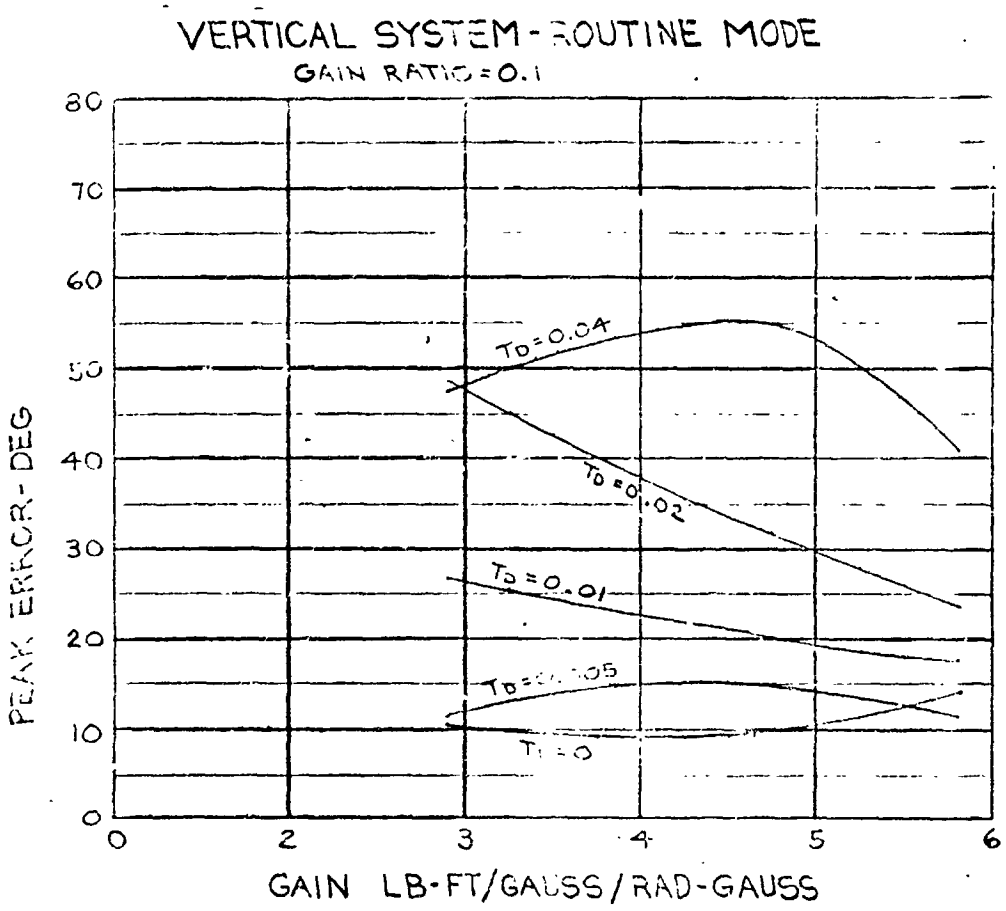

Figure 3.1-18 Peak Error vs Gain, Vertical System, Routine Mode

the sunline normal to the symmetrical axis. The curves of figure 3.1-18 indicate a substantial rise in peak error as the disturbance torque rises. The character of the curves indicates that the optimum gain varies as a function of disturbance torque and lies off the scale for some of the disturbance values used. Figure 3.1-19 shows a brush record of a sample run.

3.1.3.2 Settling Time

This is defined as the number of orbits required to stabilize from an initial 45° error to the point where the error is equal to its maximum subsequent value.

3.1.3.2.1 Dual Flip System

Figure 3.1-20 illustrates the variation in settling time as a function of gain, both for a case of zero disturbance torque and disturbance torque equal

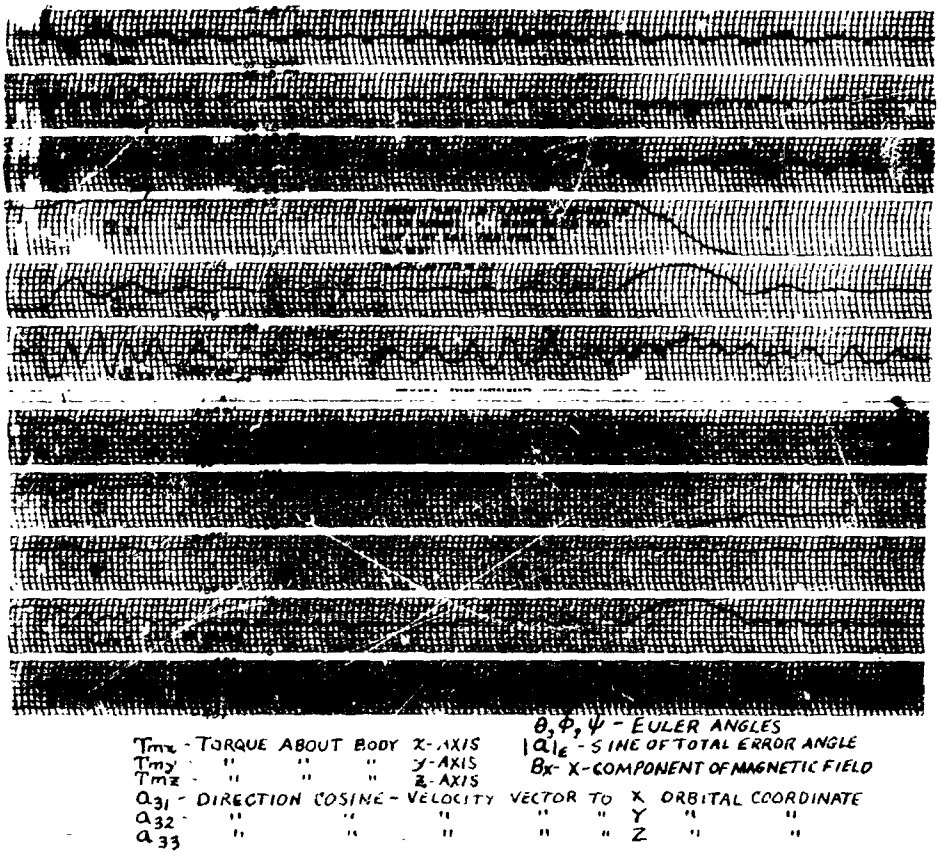

Figure 3.1-19 Typical Computer Run, Vertical System

to 0.005 lb.-ft. The results of similar runs with the vertical system are also shown. A comparison with figure 3.1-17 would indicate that the point of minimum error does not quite correspond to the point of minimum settling time but since the difference is not very great (gain = 0.14 for ε_{min} vs gain = 0.15 for T_{s-min}) it would be easy to specify a compromise gain. The presence of the disturbance torque increases the settling time but has very little effect on the optimum gain point.

Figure 3.1-21 illustrates the variation in settling time as the gain ratio is changed. The increase in gain ratio has a destabilizing effect which results in longer settling times but does not tend to shift the optimum gain point.

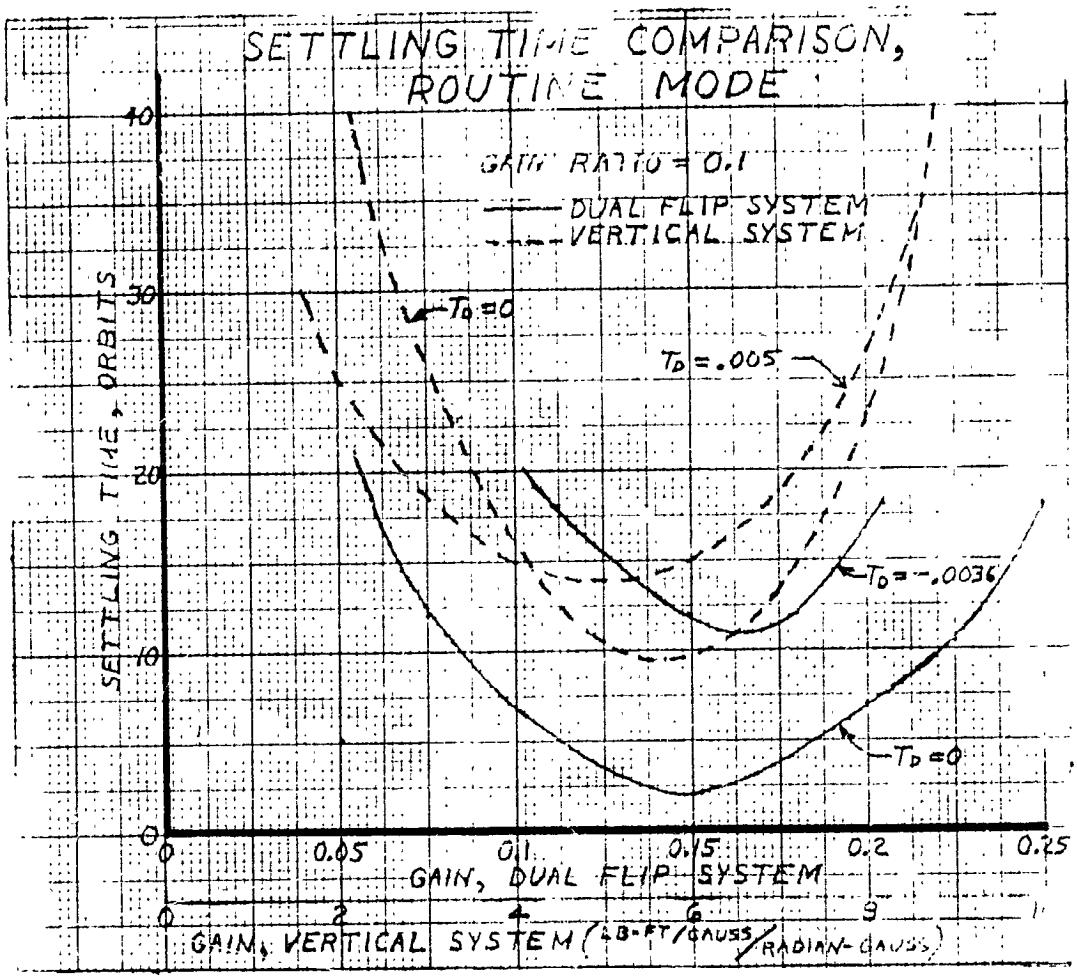

Figure 3.1-20

3.1.3.2.2 Vertical System

A comparison of figures 3.1-22 and 3.1-17 indicates a difference between optimum gain for minimum error (gain = 4) and optimum gain for minimum settling time (gain = 5.7), both cases for zero disturbance torque. Since the resultant difference is not substantial, and since figure 3.1-22 indicates a shift toward a lower optimum gain for settling as the disturbance is increased, the compromise gain will probably lie in the region of 4 lb/ft per gauss/radian-gauss.

The variation of settling time as a function of disturbance torque would indicate that the larger normal pointing errors associated with increased disturbance torques permit an apparent decrease in the settling time with increased disturbance torque. As the disturbance torque is increased past 0.020 lb-ft, however, the effect of the low initial slope associated with a more lightly damped system will become

UNCLASSIFIED

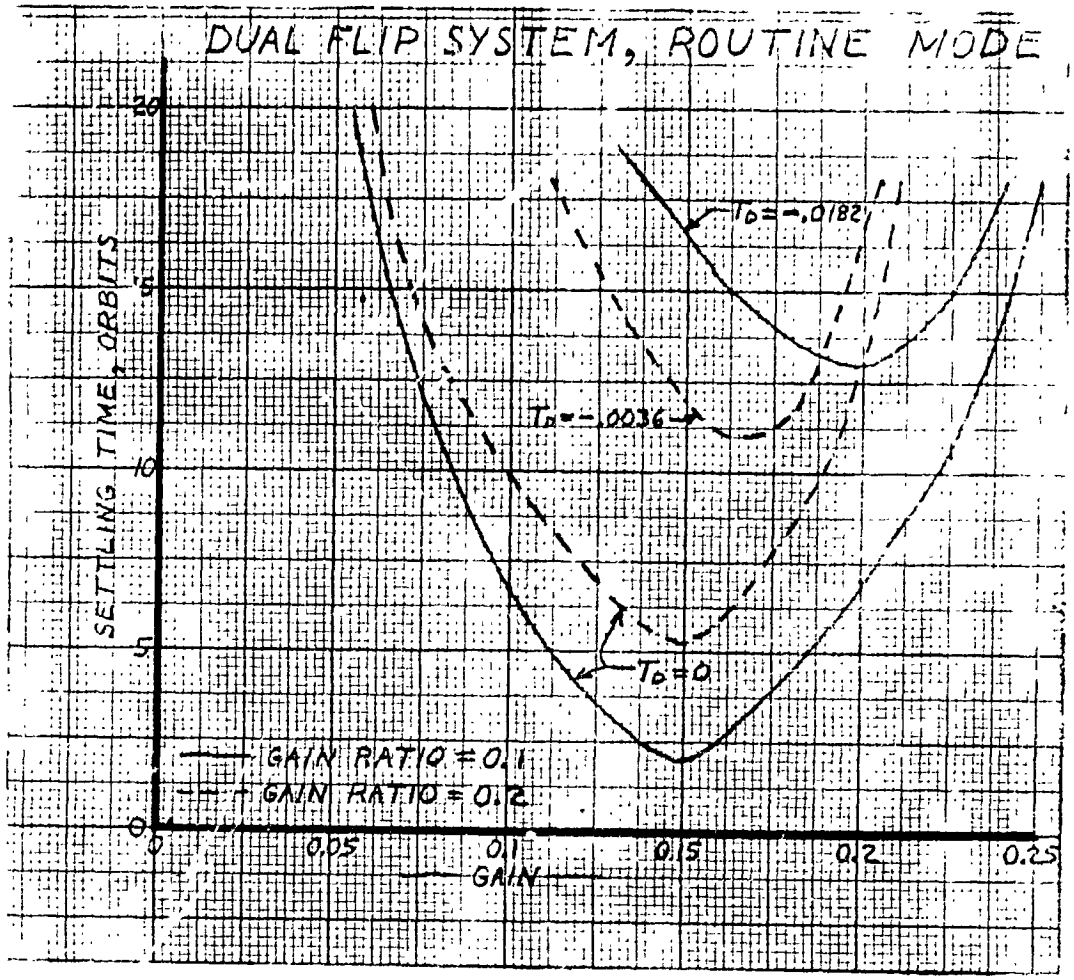

Figure 3.1-21 Settling Time vs Gain, Dual Flip System, Routine Mode

more effective. This is shown by the rise in the settling time with T_D = 0.040 lb-ft. The differences in the optimum gains will probably be caused by the same effect which produced the variation in optimum gain point for minimum error; a modulation effect induced by the approximately sinusoidal variation in disturbance torque acting on the vehicle.

Figure 3.1-23 indicates the variation of settling time as a function of gain ratio. The optimum gain ratio would appear to be in the region of 0.1, although the variation is not very pronounced. At lower than this ratio, the individual error components (E_x, E_y and E_z) are not corrected rapidly enough due to too low a gain and the composite error (approximately = $\sqrt{E_x^2 + E_y^2}$) remains at a high level. At higher ratios the effective phase margin, introduced by the variation in gain, is substantially reduced and results in longer settling times.

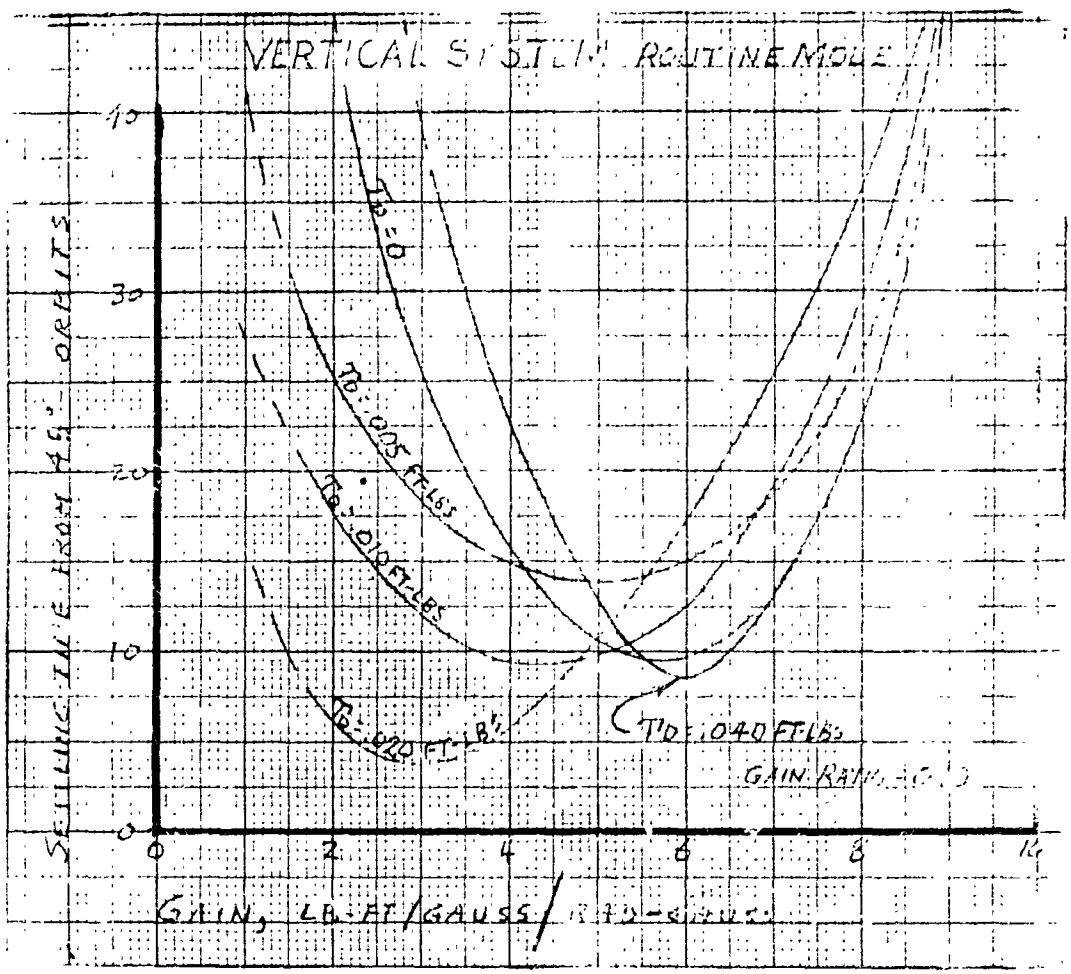

Figure 3.1-22 Settling Time vs Gain, Vertical System, Various T_D's

3.1.4 Flip Mode Performance Comparison

3.1.4.1 Dual Flip Mode

The dual flip operation was set up on the analog computer but at no time could it be made to maintain any semblance of sunline pointing during the flip pointing mode of the orbit. It is therefore concluded that the dual flip system is not feasible.

An examination of figure 3.1-24 shows that even for a low gain ratio, it was not possible to raise the loop gain beyond 0.24 during closed loop operation. Since this means that a 90° error (yields maximum $\bar{E}$ signal) would only result in 24% of the torque required to accomplish the flip in the specified time, it is impossible to accomplish the flip with a closed loop control system. This result dictated the attempt at using the open loop system described in section 3.1.2.1.3.

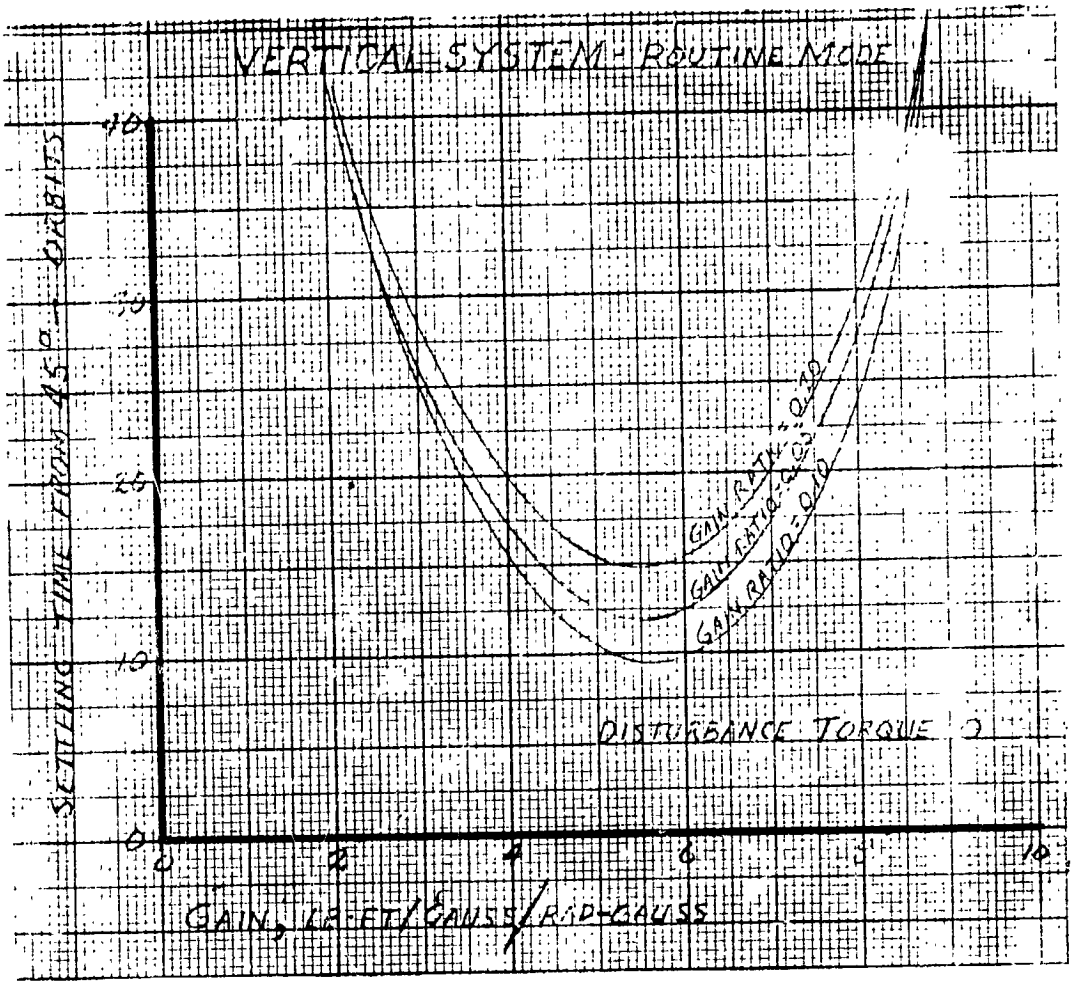

Figure 3.1-23 Settling Time vs Gain, Vertical System Various Gain Ratios

The open loop system, as described in section 3.1.2.1.3, depends on developing a torque vector orthogonal to both the sunline and magnetic field. Since the magnetic field changes direction rather sharply during the 90° of orbit angle that the flip is to be accomplished in, the result will be that the nose of the vehicle will trace out an angle whose integral length is 180° but which yields a great circle displacement of less than 180°. The error effect during the reverse flip which immediately follows the first flip will tend to be cumulative, developing a large error to be eliminated in the remainder of the orbit. Since it takes several orbits to settle out from any error, the net effect will be to produce large amplitude random motion in the vehicle due to the two required flips per orbit.

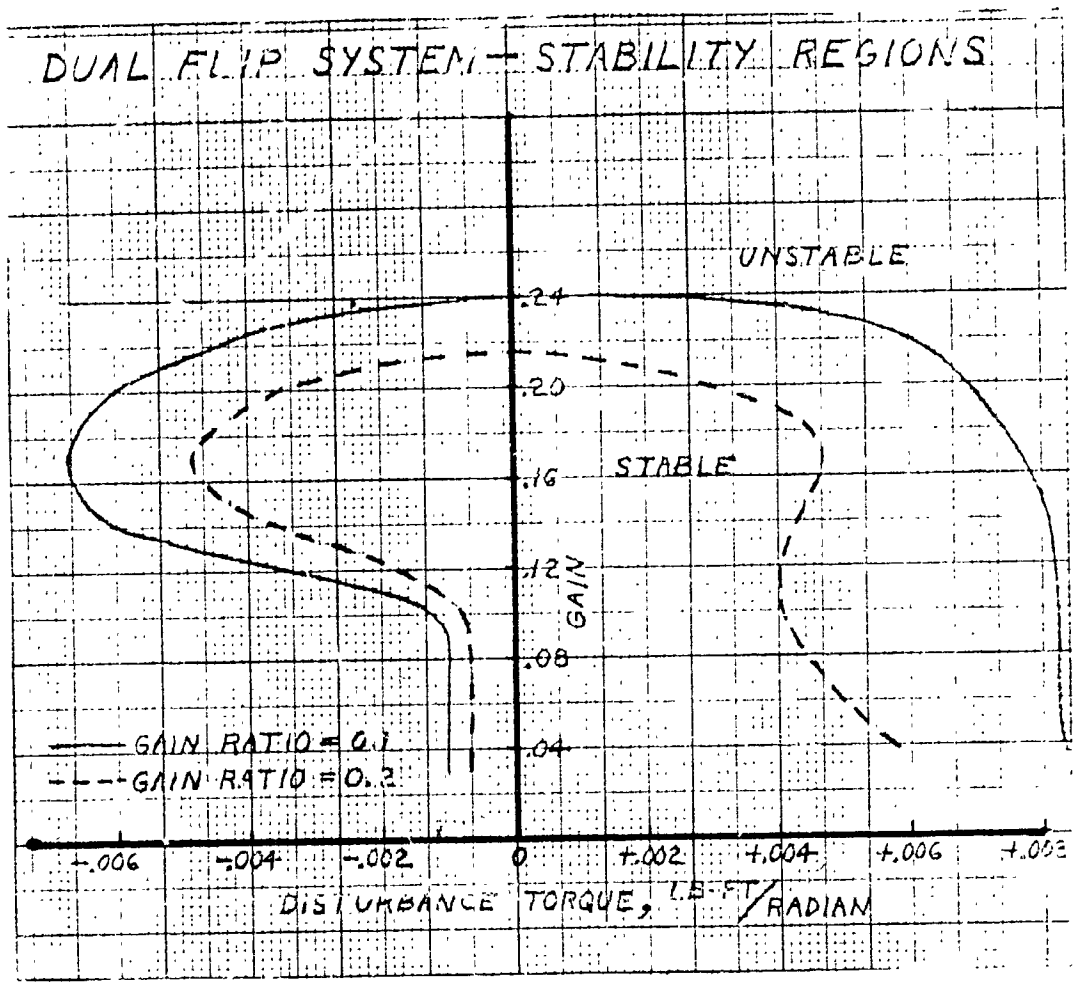

Figure 3.1-24

3.1.4.2 Vertical System

For the vertical system, the flip operation is carried out over many orbits, which permits continuous closed loop control. In evaluating the system, two new parameters must be introduced: flip time reference and flip time. The flip time reference is the number of orbits required to swing the pointing reference (X axis) around at a constant rate through 180°. The flip time is defined as the number of orbits from initiation of flip operation until the time that the angle between the symmetrical axis and the velocity vector falls, without re-emerging, to the maximum level which it reaches during the subsequent routine pointing mode.

UNCLASSIFIED

Figure 3.1-25 illustrates the variation of flip time vs flip time reference for several gain values. The three curves tend to approach one another for longer flip times, which is to be expected since loop gains tend to mean less as it takes longer and longer to reverse the reference direction. As the flip times become less, however, the gain factor becomes more important. This is due to the increased importance of short settling times. Therefore as the gain increases up to optimum value for settling time (see figure 3.1-22), the total flip time becomes lower and lower. At flip time references below 8-11 orbits, the control system tended to produce large Euler angle errors which made the simulation invalid and, consequently, limited the region of investigation.

Further investigation will deal with a flip reference other than the constant velocity type represented here, possibly showing that shorter flip times are possible.

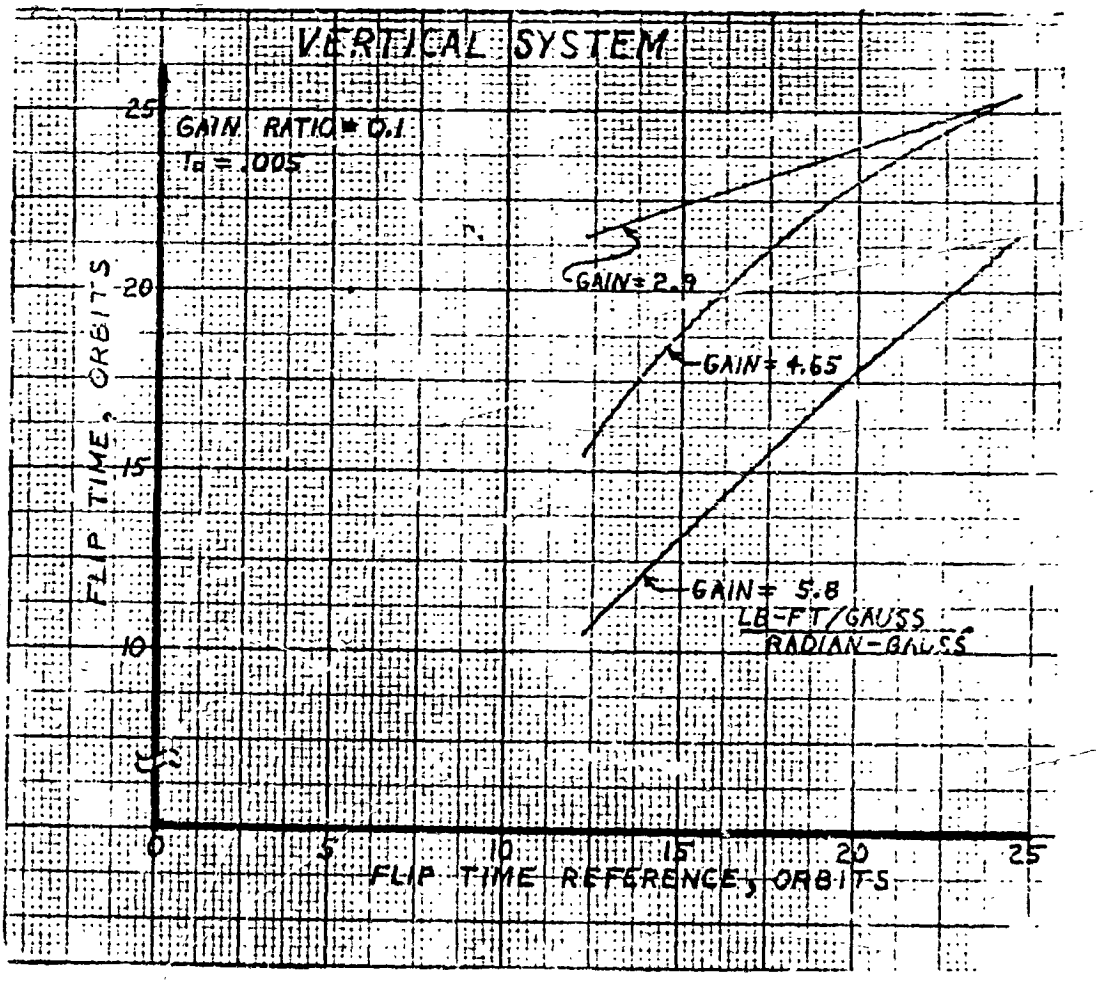

Figure 3.1-25 Flip Time vs Reference, Vertical System

Figure 3.1-26 illustrates the ability of the system to maintain its vertical pointing reference during the flip operation. The curves do not indicate any great change in performance during a flip operation as a function of T_D. The minimizing of errors for gains between 5 and 6 are consistent with results using other performance criteria.

3.1.5 Torque Comparison

3.1.5.1 Normal Mode

Since the peak torque for flip operation (1.36 lb-ft) will be applied to the vehicle over a 180° orbit angle, the average torque will be at least 0.68 lb-ft for the dual flip system. The measurement of the lower level routine pointing mode torques will then mean little for the dual flip system.

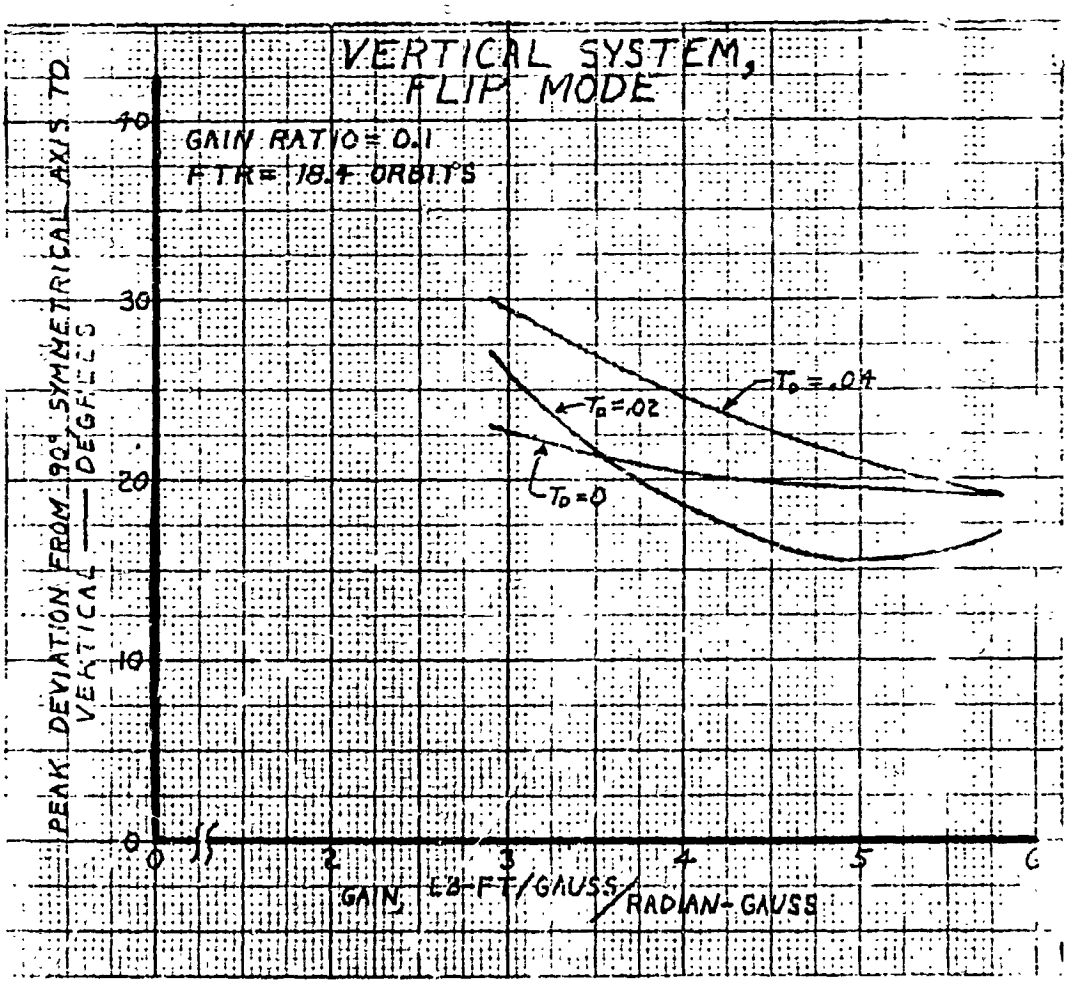

Figure 3.1-26 One Axis Error During Flip, Vertical System

The vertical system, however, always develops peak torques of a much lower amplitude. The routine pointing torques then become meaningful, since the higher flip mode torques only occur occasionally and the average level is much lower. This is indicative of a much lower power drain.

Figures 3.1-27,28 and 29 illustrate the variation of peak torque with gain for the three axes of the vehicle when controlled by the vertical system. The variations indicate the general trend of higher magnetic torques for greater disturbance torques, which is expected. The general shape of the expected curve would be a positive slope starting from the origin (no current commanded for zero gain), followed by a decrease in the vicinity of optimum gain, and finally a steep ascent due to increased error amplitude and torque per unit error increase as the gain becomes higher than optimum. The presence of curves with either maxima or minima points is indicative of the wide range of disturbance torque sensitive optimum gain points. The range of gain chosen was based on the $T_D = 0$ case.

3.1.5.2 Flip Mode

For the dual flip system, the peak torque is present during the entire flip operation, although the torque on any one coil will never exceed this peak value and will average less.

The vertical system performance is given on figures 3.1-30,31 & 32 for the three vehicle axes. The results are shown for two levels of disturbance torque and two flip time references. The results are consistent with runs for the routine pointing mode at similar disturbance levels. It is quite apparent that the optimum gain lies at a higher value for $T_D \neq 0$ than for the $T_D = 0$ case. For gains greater than 5, the decrease in torque reflects the lower level of reference following error as the gain approaches an optimum for the T_D levels shown. The lower torque rates for higher flip time reference (FTR) is indicative of the shallower position ramp which the symmetrical axis must follow as the time to make the flip increases.

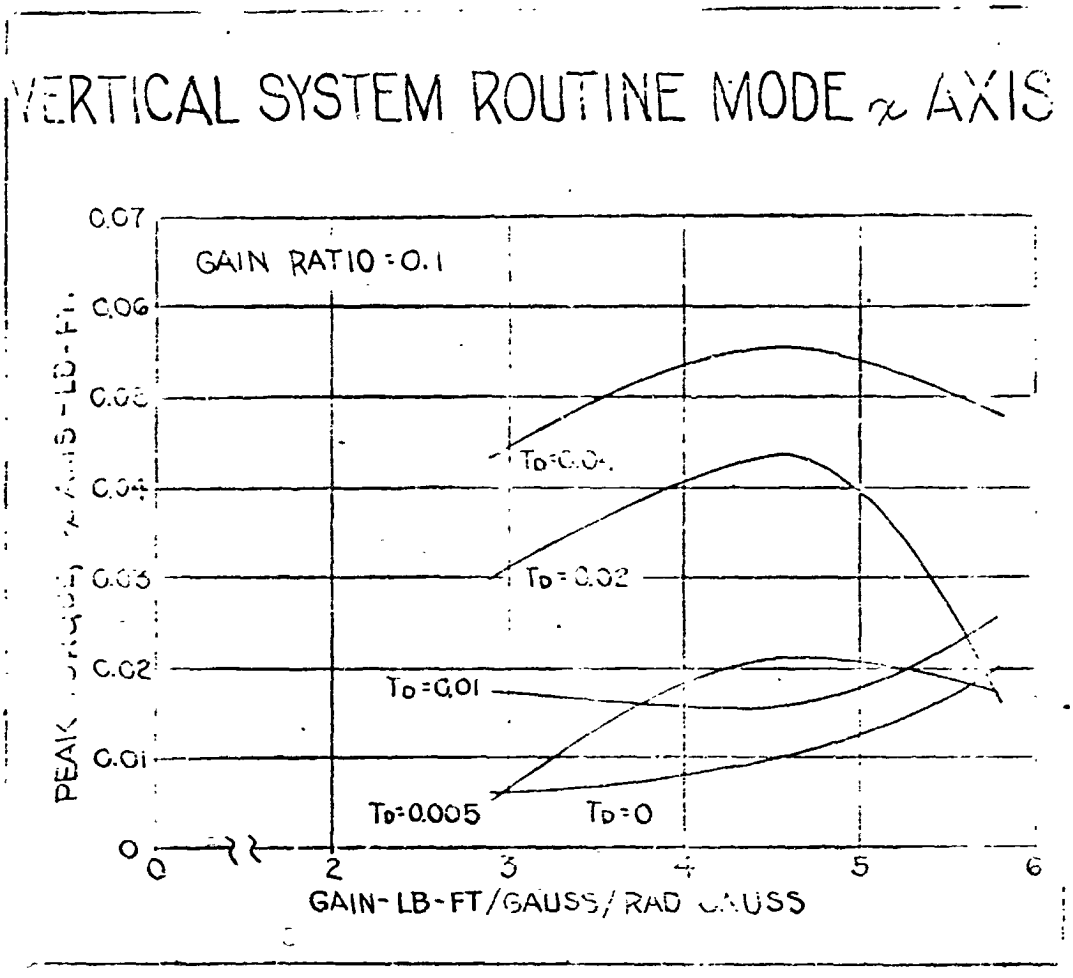

Figure 3.1-27 x-Axis Peak Torque, Vertical System, Routine Mode

3.1.5.3 Magnetic Torquer Requirements

The magnetic torquers for the dual flip system must be capable of generating the full flip torque under conditions of minimum field magnitude, which dictates a requirement for a torquer capable of 6 lb-ft per gauss for each of the three torquers.

The peak torques generated by the vertical system are much lower, which is reflected in the lower peak coil excitation (torque/gauss) required in the torquers. The variation in peak torque per gauss required during a typical flip operation (FTR = 18.4 orbits) is shown in figures 3.1-33, 34 & 35. Since the gain will be set in the range of 4 to 4.5 to minimize settling time and peak routine error, the torquer size will be the largest of the values read from three axial curves shown at a gain of 4.5. This would dictate (from the x-axis coil curve)

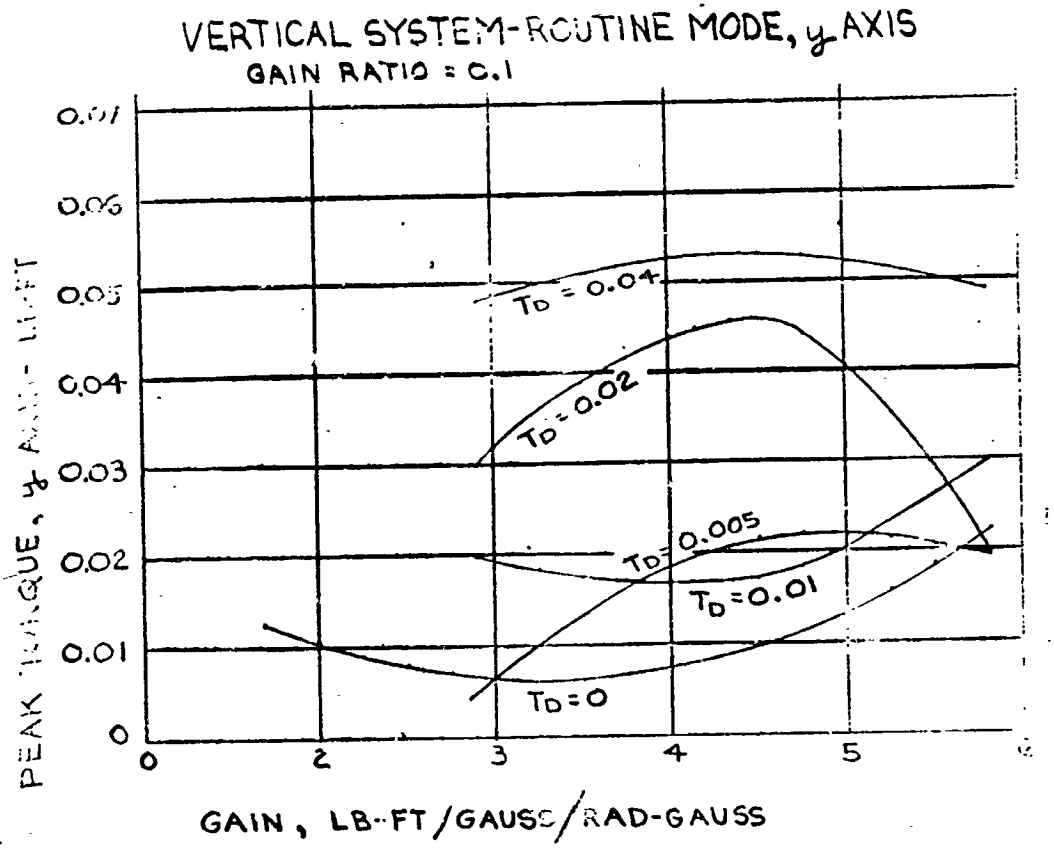

Figure 3.1-28 y-Axis Peak Torque, Vertical System, Routine Mode

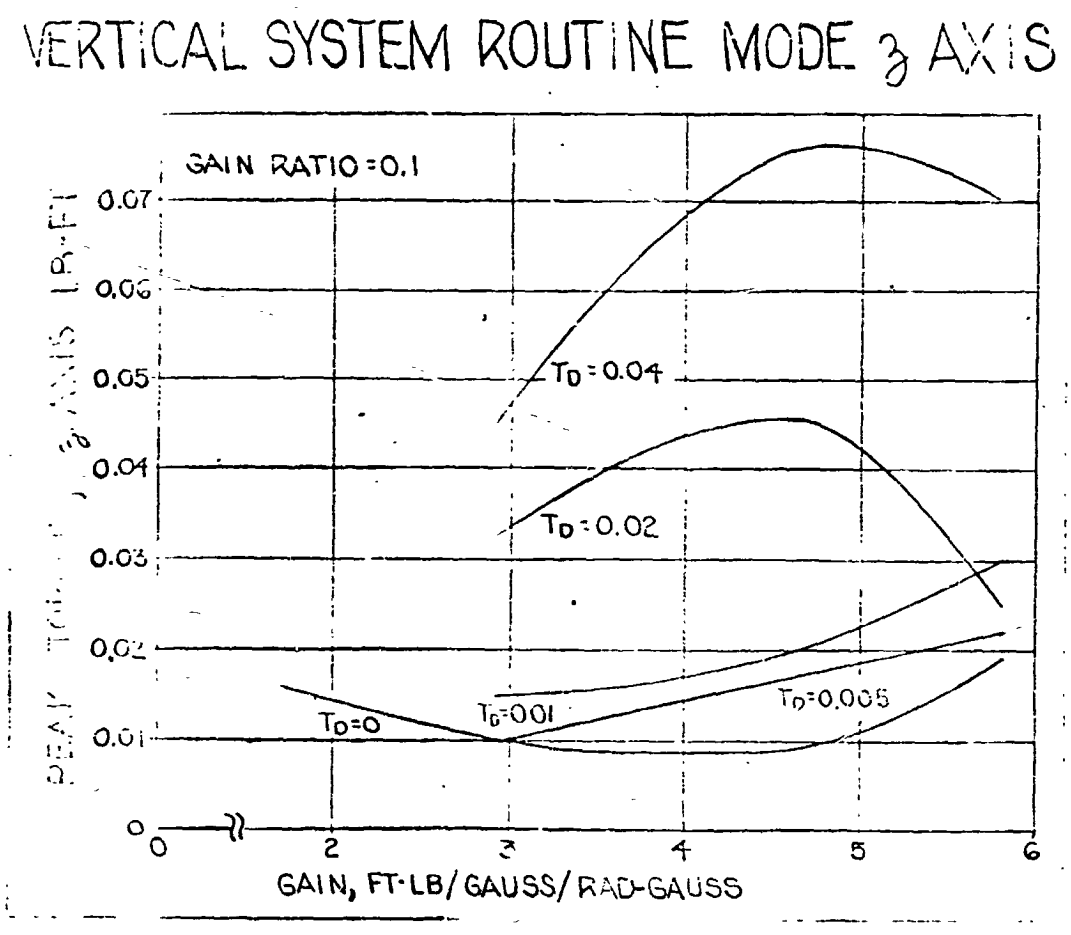

Figure 3.1-29 z - Axis Peak Torque, Vertical System, Routine Mode

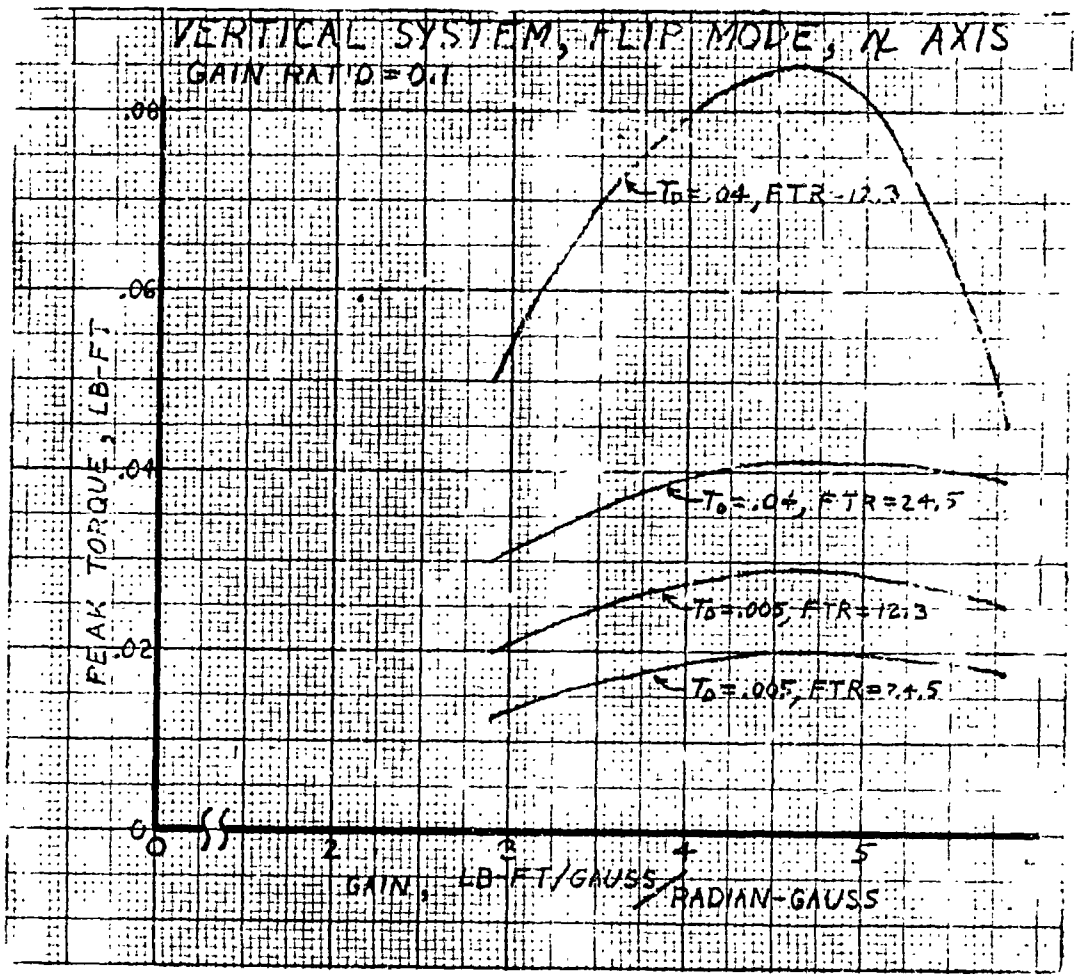

Figure 3.1-30 x-Axis Peak Torque, Vertical System, Flip Mode

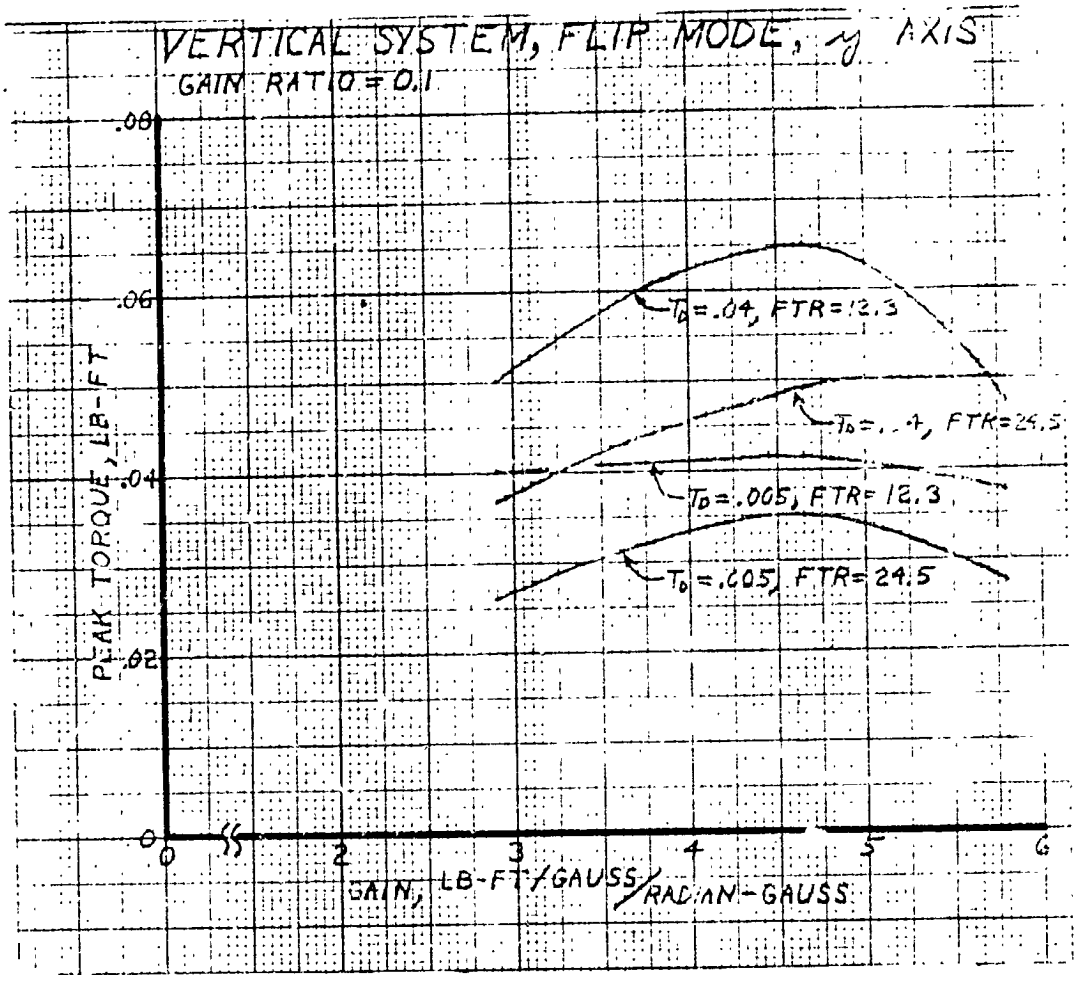

Figure 3.1-31 y - Axis Peak Torque, Vertical System, Flip Mode

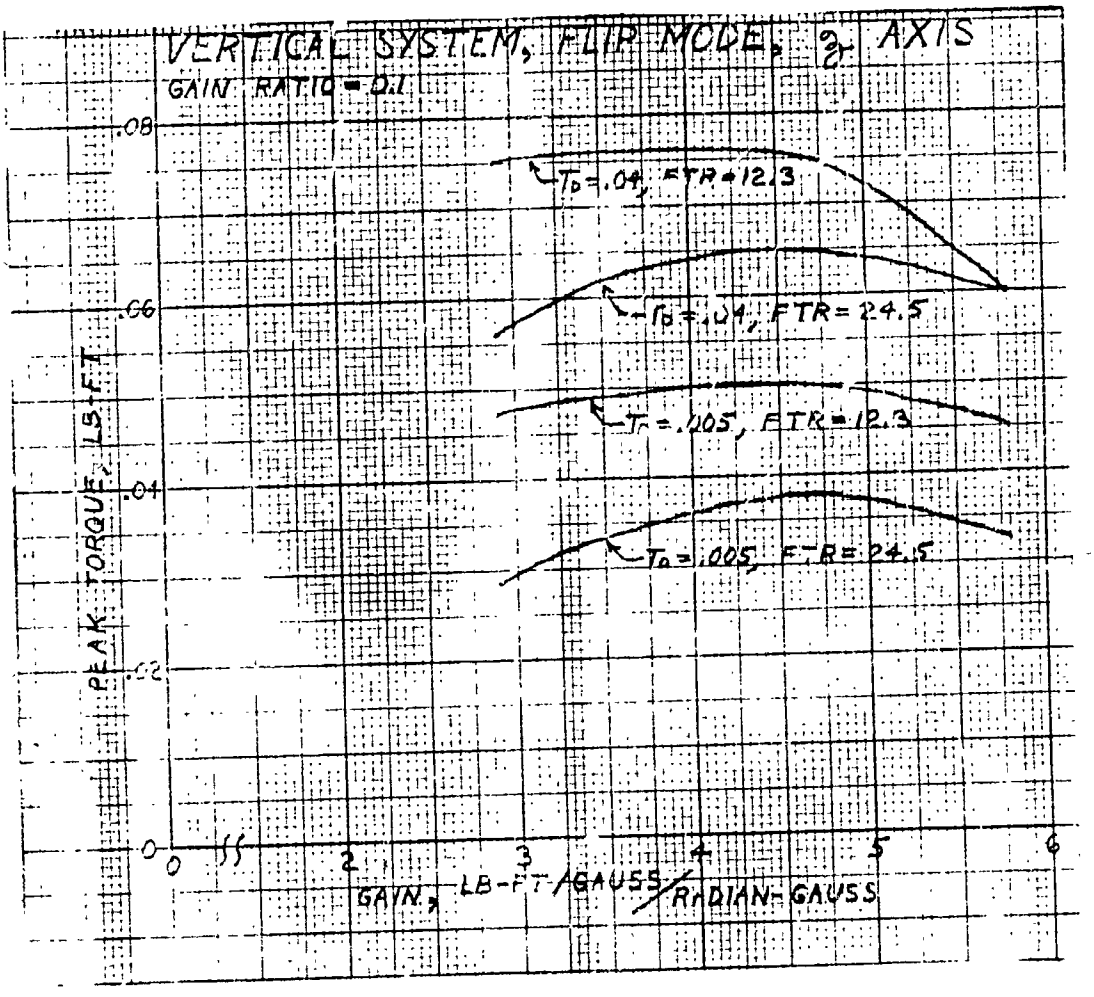

Figure 3.1-32 z - Axis Peak Torque, Vertical System, Flip Mode

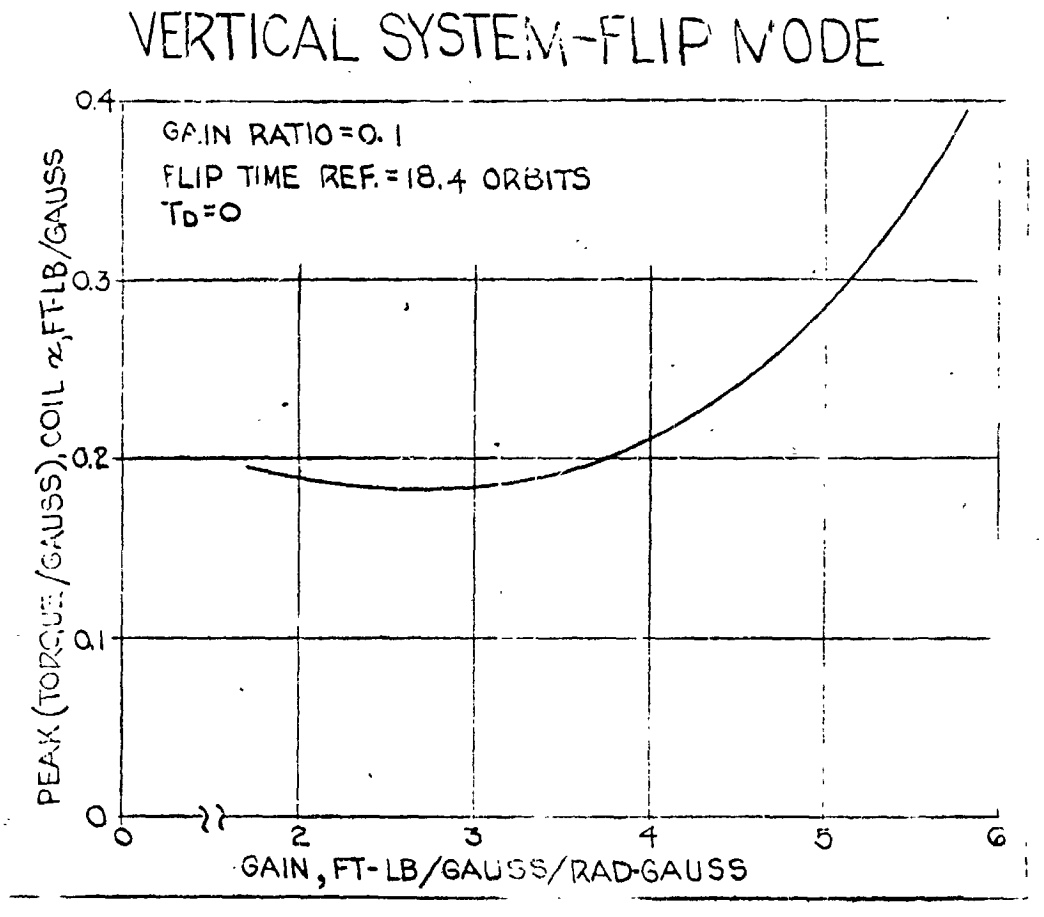

Figure 3.1-33 Coil x Peak Requirement, Vertical System

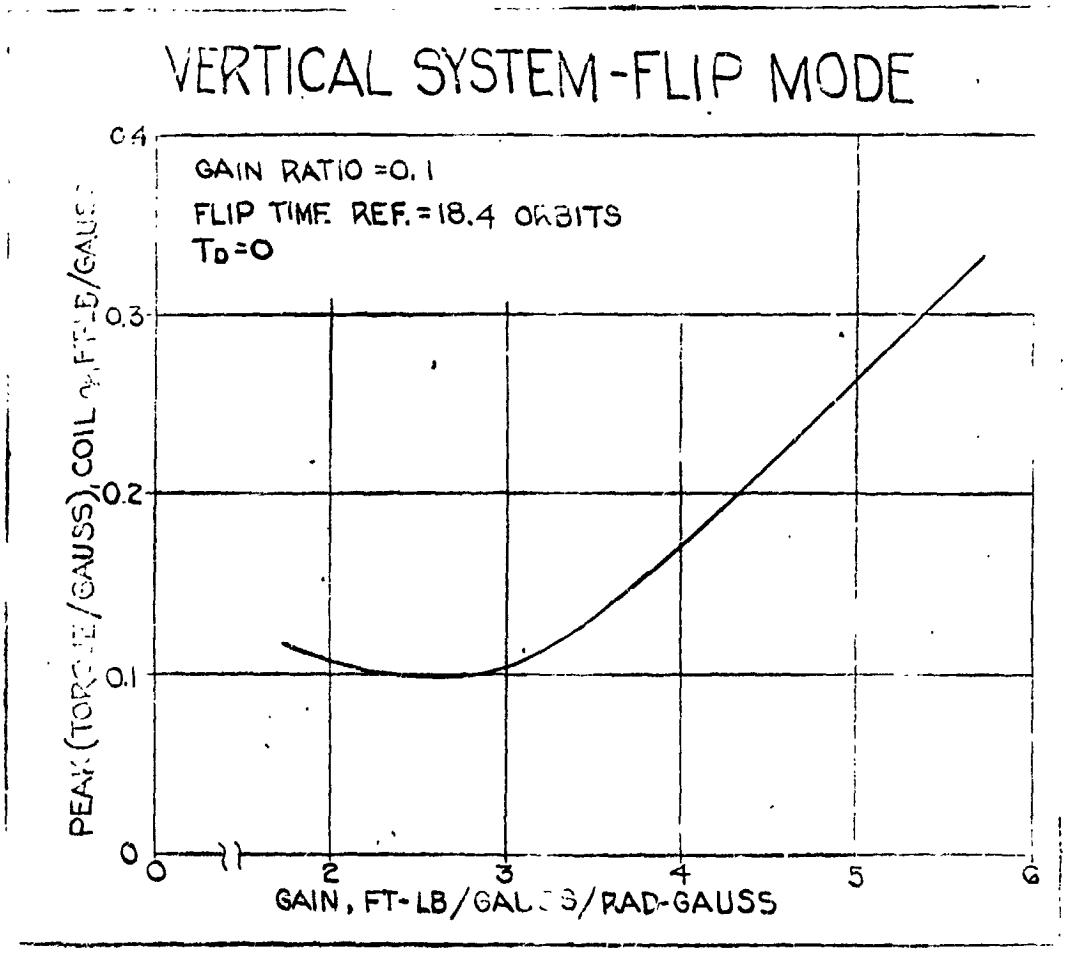

Figure 3.1-34 Coil y Peak Requirement, Vertical System

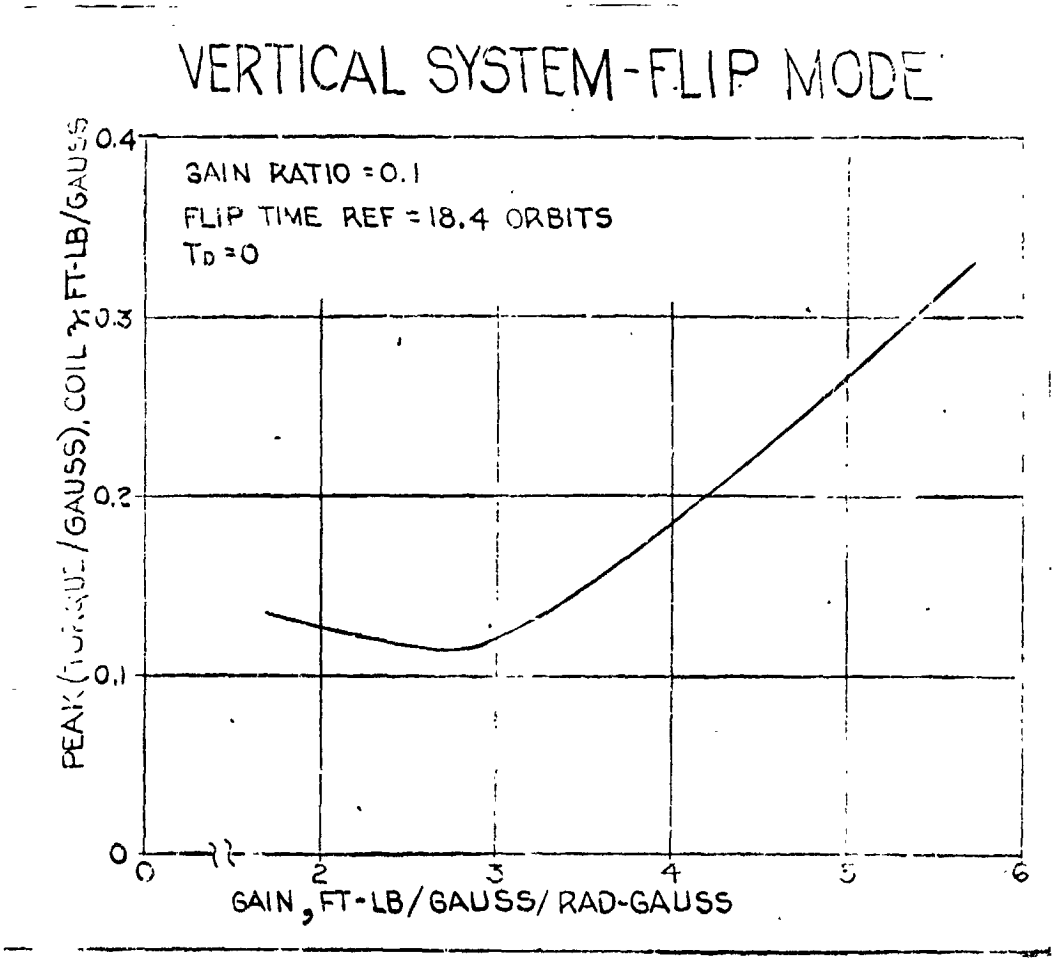

Figure 3.1-35 Coil z Peak Requirement, Vertical System

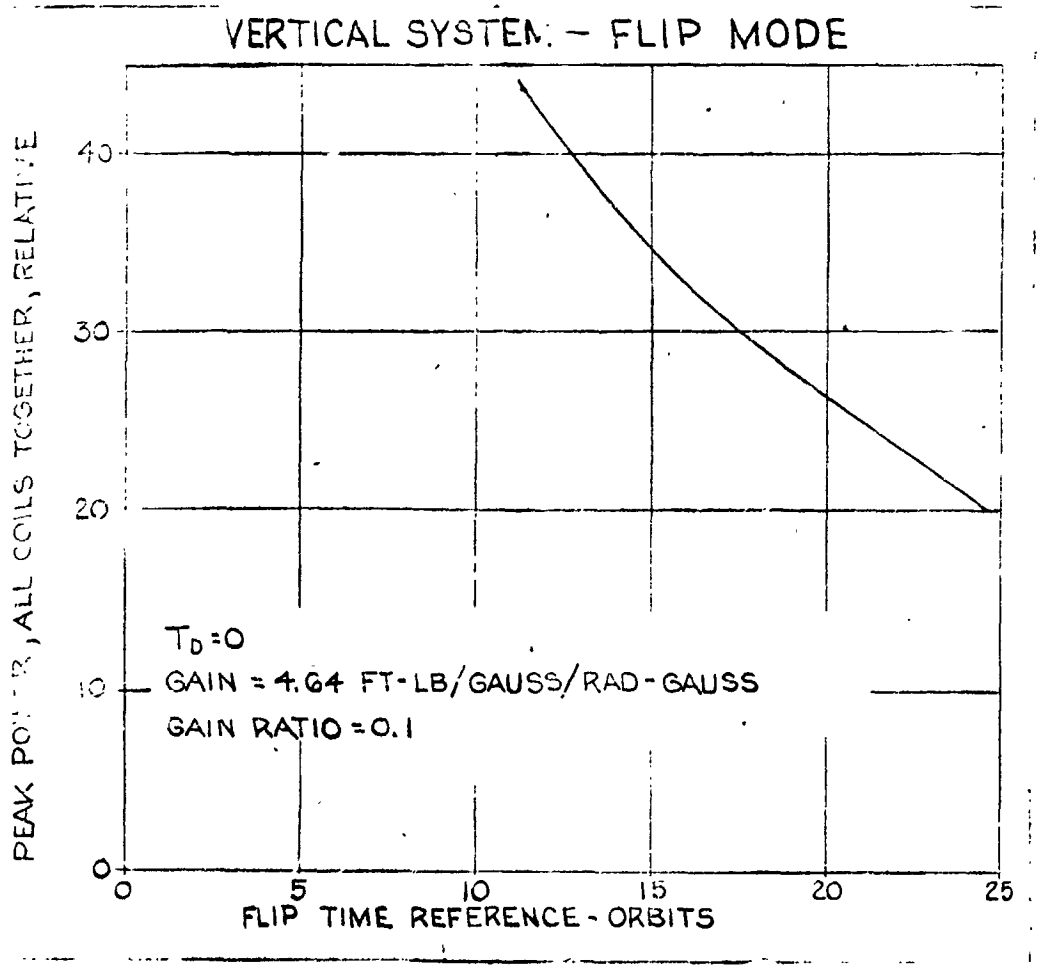

Figure 3.1-36 Relative Peak Total Coil Power, Vertical System, Flip Mode

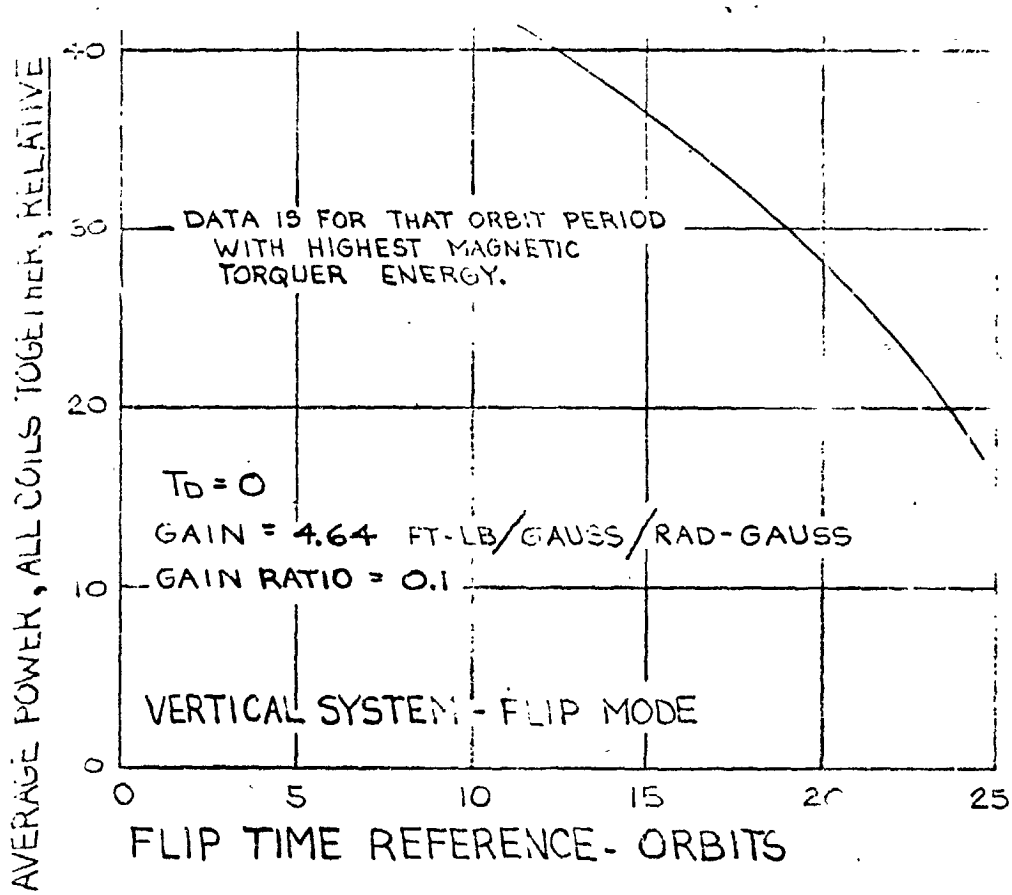

Figure 3.1-37 Relative Average Total Coil Power, Vertical System, Flip Mode

a torquer size of 0.25 lb-ft/gauss.

3.1.6 Power Drain Comparison

3.1.6.1 Normal Mode

The dual flip system operates with the full torque on 50% of the time. The average power could thus be closely estimated using the average power taken during the flip mode only. Counting the power used by the electronics, the total average drain for routine operation will be 250 W.

The vertical system power drain is a function of coil design, which can be optimized for the lower level torques generated by this system. It is estimated that the average power taken during routine operation will be 54.9W.

3.1.6.2 Flip Mode

The peak power drain for the dual flip system will occur if all three coils are used at some point in the flip to develop the required torque. At this time the most inefficient point of operation would occur and the power drain would be approximately 70% higher than if the torque was generated using a single coil. With the average power during a flip taken as 400 W, the peak (worst case) will approach 700 W.

The vertical system will require only a minor increase in power for average flip mode drain compared to the routine mode drain, the difference being 56.0 (including electronics) vs 54.9W. The peak power drain will be 66.0 watts. Figures 3.1-36 and 37 indicate the relative peak and average power drawn by the coils alone as a function of flip time reference. The longer the flip time is extended, the lower the power taken by the coils. This result is consistent with the results of previous runs which show peak torque and current drain as a function of the same variable.

3.1.7 Summary

The results of the point-by-point comparison are shown on figure 3.1-38. The system with the advantage on any particular point is outlined in a heavy shade of black. It is quite obvious that the unfeasibility of the flip operation twice in each orbit precludes the use of the dual flip system. The lower power drain

ITEM OF COMPARISON	DUAL FLIP SYSTEM	VERTICAL SYSTEM
SUN ORIENTATION	.036 LB-DEG	0.044 LB-DEG
RELATIVE COMPLEXITY	1	1-3/4
ROUTINE MODE PEAK ERROR	*3 DEGREES	9 DEGREES
SETTLING TIME	2 - 12 ORBITS	9-1/2 - 12 ORBITS
FLIP MODE PERFORMANCE	NOT FEASIBLE	FEASIBLE
PEAK TORQUE ON STRUCTURE	1,360 FT-LB	0,085 FT-LB
MAGNETIC TORQUER REQUIREMENT	6 FT-LB/GAUSS	1/4 FT-LB/GAUSS
RELATIVE SYSTEM POWER DRAIN	6	1

* WITHOUT FLIP OPERATION

Figure 3.1-38 Comparison Summary for the Two Systems

and smaller torquer size required by the vertical system tend to offset the increased complexity. The apparent advantage in accuracy of the dual flip system is offset by the fact that the data is representative of runs with no flips performed. Even if a system were designed to offset the effects of the varying field, there would be residual rates resulting from total system imperfections amounting to only 2% full output which could yield body rates in excess of those developed in stabilizing from a 45° initial error (approximately 12 deg/hr).

3.2 Power Supply and Torquer Weights

3.2.1 Dual Flip System

The dual flip system is sun oriented, and therefore requires an array of solar cells capable of developing satellite power on two opposite sides of the sphere. The total area of solar cell array is determined from a consideration of satellite orientation, time spent in eclipse, power loss during flip, and total power required per orbit. The degradation of solar cell output due to artificial and Van Allen belt radiation must also be considered. It is anticipated that at an altitude of 500 miles and inclination of 60°, the use of blue shifted N or P solar cells with a 10 mil synthetic quartz cover slide will prove adequate for 5-10 year life. To insure completion of the mission, a 25% over-capacity will be designed into the solar panels.

For purposes of control system comparison, a 200 foot diameter satellite operating at an altitude of 1500 miles, with an orbit resulting in a maximum period of darkness per orbit is considerered. With an attainable solar cell output of 10 watts per square foot of projected area, an array of 79 ft^2 is required per hemisphere or a total of 158 ft^2 at a weight of 1 $lb./ft^2$.

A battery capacity equal to 50% of the flip power plus the total non-flip power during eclipse will be adequate for this mission. Available silver oxide-cadmium batteries can be discharged to a depth of 50% and recharged with high reliability over a large number of cycles. Providing a redundancy of two, the weight of batteries for this system is 32 pounds. The inclusion of a 2 pound battery charging circuit brings the total power supply weight to 192 pounds.

The torque coil design is determined by optimizing for minimum weight the combination of torque coil and torque coil power supply. Consider that a given current is required for torquing the satellite. If a coil of cross-sectional area A_1 is used, the power supply requirements and therefore power supply weight are determined. If the cross-sectional coil area changes to A_2, where $A_2 < A_1$, the coil weight decreases. However, the power required and power supply weights increase.

The design point, as previously stated, is that coil area which results in minimum total weight of coil-power supply combination. For the system being described, torque coil weights of 57 pounds per coil are required giving a total torquer weight of 171 pounds.

3.2.2 Vertically Oriented System

Since the vertical system is earth oriented, the satellite-sun line relationship is not constant as was the case for the dual flip system. A study of this relationship indicates that provision must be made for supplying power at any arbitrary balloon orientation. The optimum distribution of solar cells for an arbitrary balloon orientation has been determined to be six solar cell areas located at the ends of three mutually perpendicular diameters. The minimum projected area for such an array is equal to .167 of the total area, with a maximum projected area of .21 of the total area. The variation of power from maximum to minimum values is therefore only 21%. For the vertically oriented system, having the power requirements previously described, this will result in a total solar cell area of 56 ft^2, weighing 56 pounds. The battery requirements for this system, considering operation during orbital eclipse and peak torquing loads above solar cell capability, amount to 4 pounds including a redundant battery. The battery charging circuit raises the total power supply weight to 62 pounds.

The design of torque coils for the vertically oriented system is based on the same principle of optimization employed in the calculation of dual flip coils. There is, however, a slight difference due to the fact that the three vertical system coils are of varying weights. The total weight of torque coil required for this system is 10 pounds.

3.3 Forces and Torques

3.3.1 Torques

Correct orientation of the satellite in space is accomplished by the use of torques provided by the interaction of activated coils with the Earth's magnetic field. These torques may be calculated from the equation $T = NIAB_t$ where T = torque, N = number of coils, I = current, A = enclosed area, and B_t = magnetic flux density. For a given orbit altitude, balloon diameter, and required torque, a value for the product NI, ampere-turns, may be obtained. The peak torque requirements for a 200 foot diameter satellite, in a 1500 mile orbit, have been calculated to be 1.36 lb.-ft. for the dual flip system and .085 lb.-ft. for the vertically oriented system.

3.3.2 Forces

In addition to the desired torque forces described above, the activation of certain coils produces various undesired forces which must be carried by the satellite structure. These forces include hoop tensile forces, hoop compression, axial skin forces due to coil interaction, and scissors forces between perpendicular or crossed coils. An investigation of these forces indicates that the compressive or collapsing force is the only one of sufficient magnitude to be considered in the structural design of the satellite. This force is given by the equation $t = IB_tR$, where t = hoop compressive stress, I = current, B_t = magnetic flux density, and R = satellite radius.

The magnitude of the compressive load per coil can be controlled during detail design by varying the number of conductors in parallel carrying a given total current. The number of ampere turns is indicative of the total compressive loading. For the dual flip system, the total compressive load has been calculated to be 30×10^{-8} pounds per inch while the vertical system load is 2.3×10^{-8} pounds per inch.

3.4 Structural Weight

3.4.1 Definition of the Problem

The structural design analysis of a dynamically controlled, echo-type, spherical satellite is primarily concerned with the stability of an ultra-thin-walled vessel of large diameter subjected to loads which are both normal to and tangential to the surface and which are both distributed and localized in nature. A rather extensive literature search in the field of shell equations failed to yield any results which were considered to be even remotely applicable. The range of sphere diameter to wall thickness ratios considered in the literature was many orders of magnitude lower than the case considered here; the type of loading was not nearly as generalized as is required here; and in addition, all of the analyses made the tacit assumption that initial surface irregularities were not large compared to the skin or wall thickness. This is a primary consideration when buckling type loads are encountered.

3.4.2 Method of Analysis

In the absence of any suitable previous analyses, it was considered appropriate to analyze the balloon as if it were made up of many sections of curved beams. The loading applied to the beams comprises the force applied by torquing coils to impart rotational acceleration and the inertial loads applied by the various pieces of equipment and the structure itself in response to the acceleration. The limit of functional suitability is determined by the maximum allowable deflection of the structure which will not degrade the reflected communication signals beyond a tolerable level. This was taken as a ten per cent change in the large scale radius of curvature.

The curved beam equations were developed assuming semi-circular beams having pinned ends. The torque coil forces are applied at the ends of the beam so that the entire beam will tend to rotate about the center of the semi-circle (i.e. the center of the balloon) as indicated by Figure 3.4.1. The inertia forces of concentrated loads are applied tangentially at the mid-point of the arc, and inertia loads due to the beam structure are applied tangentially and distributed uniformly along the beam. This

CURVED BEAM LOADING AND EQUATIONS

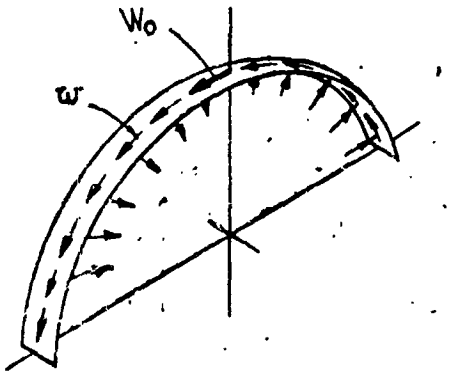

$$\delta = \frac{r^3}{EI_1 n_1}\left[.071\frac{W_o}{g} r\alpha + .037\frac{w}{g} r^2 \alpha\pi - \frac{.858 EI_2 n_2}{r^3}\right]$$

LETTING $I_1 = I_2$ AND $n_1 = n_2$

$$I = \frac{r^4\alpha}{1.858 gnE}\left[.071 W_o + .037 \omega r \pi\right]$$

I = SECTION INERTIA ONE RING, IN^4

n = NUMBER OF RINGS PER FT.

Figure 3.4-1 Curved Beam Loading and Equations

force and load distribution correlates well with three orthogonal major diameters of a sphere where each major diameter incorporates a torque coil and electronic equipment is located at each intersection of the coils. Bending moment equations were developed from this distribution of loads, and deflections were derived as general expressions by strain energy methods. In order to simplify the equations, it was assumed that the maximum radial deflection was equal to the tangential deflection at the center of the arc. This was found from geometry to be nearly true and thus justified the assumption.

Preliminary work quickly made two things apparent: (a) treating the curved beam as an isolated piece of structure led to results which were far too conservative, and (b) the section moment of inertia required to limit the deflection was many orders of magnitude larger than that attainable with a thin membrane skin alone.

This led to the concept of orthogonal sets of structural members attached to the inner surface of the balloon skin. These members increased the section inertia in the direction of the curved beam and also provided additional support by means of the orthogonal hoop members which resist deflection of the beam. This additional support was integrated into the strain energy equations and the results are shown in the equation shown on Figure 3.4.1. This equation becomes the prime design tool.

The exact geometry of the orthogonal structural members can take many forms and will be discussed later in this report. For purposes of further calculation and comparison it has been assumed that small diameter tubular members will be used. It has also been assumed that material of the Echo II type will be employed.

Several curves have been created from the design equation, and are shown in Figures 3.4.2 and 3.4.3. These curves indicate the section moment of inertia which is required in order to adequately limit the deflection for more or less arbitrarily chosen distributed and concentrated loads for various rotational accelerations. Since the required section inertia varies linearly with the load, the design section inertia can be found by proportioning the design loading to the arbitrary loading of the curves. It is to be noted that the section inertia required is a function of the third and fourth power of the balloon radius for concentrated and distributed loads respectively. This is an indication of the penalty to be paid for large diameter balloons.

The actual inertial loads applied to the balloon structure are a function of the angular accelerations and masses of the balloon structure, the torquing coils, the power supply, and the electronics. The electronics mass is relatively constant and in addition represents a relatively small fraction of the total weight; in the order of two or three percent for even the smaller balloons. The size and mass of the torquing coils and power supply is a function of the angular acceleration required, the balloon diameter, and the balloon mass. The mass of the balloon is a function of the structure which in turn is a function of the loads to be supported. These relationships have been reduced to equation form and solved in terms of relative weight with the aid of the assumption that the coils and power supply

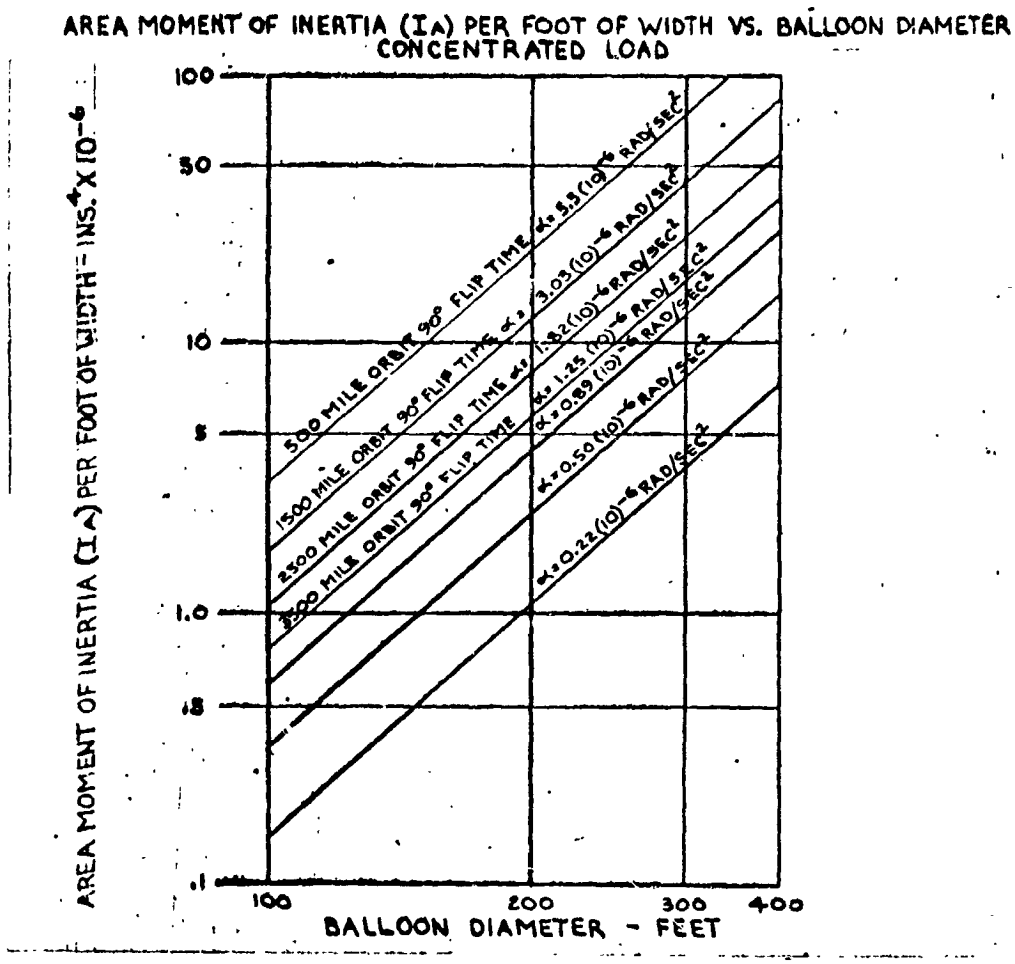

Figure 3.4-2 Required Section Inertia for Concentrated Loads

represent distributed loads. This assumption is correct for the coils and seems reasonably true for the power supply because most of the power supply mass is contributed by the solar cell array which is fairly spread out. The results of this analysis are presented by Figure 3.4.4, which indicates the calculated balloon weight in terms of an equivalent diameter Echo II balloon weight as a function of rotational acceleration and balloon diameter. The rapid increase of weight with diameter is again evident.

The dual flip system requires angular accelerations between 1.25 and 5.5 radians per second squared for orbit altitudes ranging from 3500 to 500 miles. It can be seen that large diameter and low altitude balloons are structurally prohibitive, and low altitude medium size balloons are marginal for this system.

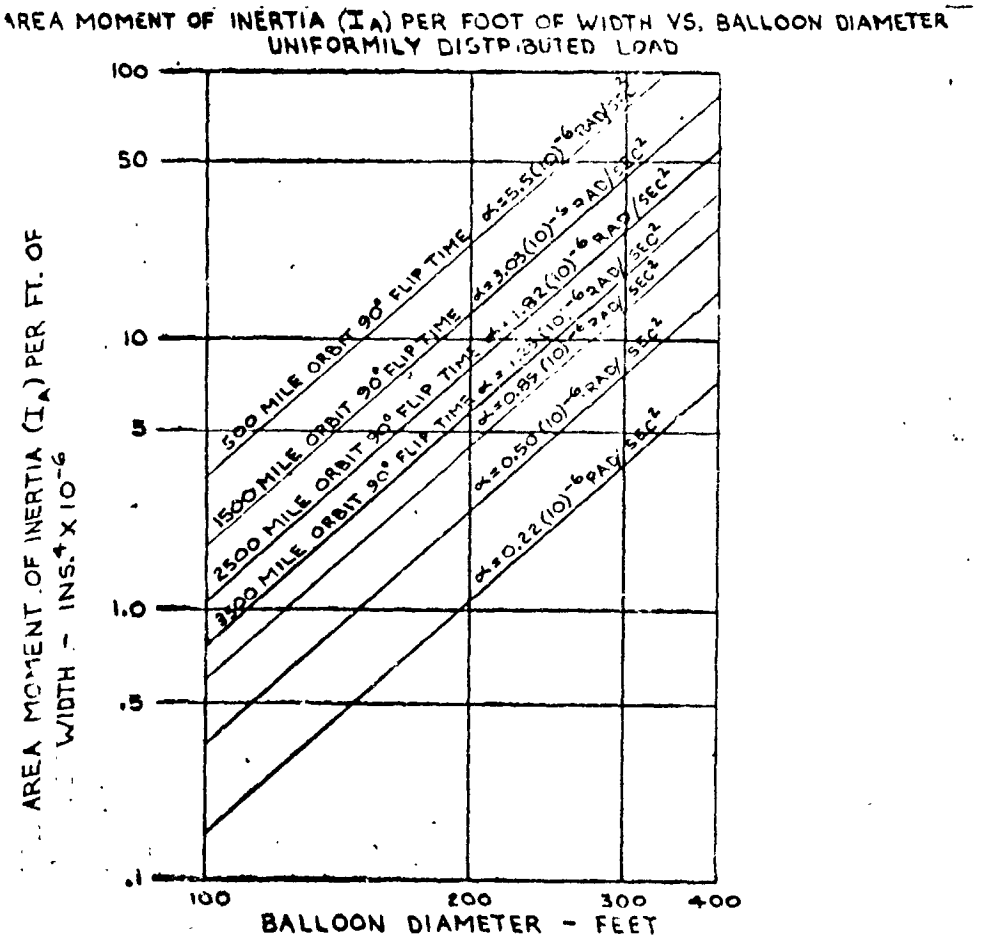

Figure 3.4-3 Required Section Inertia for Distributed Loads

3.4.3 Results

The earth oriented system has angular accelerations which are not intimately tied in with orbit altitude and can therefore be much less than the dual flip system. Example accelerations are indicated by the lower curves of Figure 3.4.4. It is to be noted that the weight to be expected is generally less than twice Echo weight for equivalent diameters. Slightly lower accelerations can keep the expected weight less than 1.5 times Echo II.

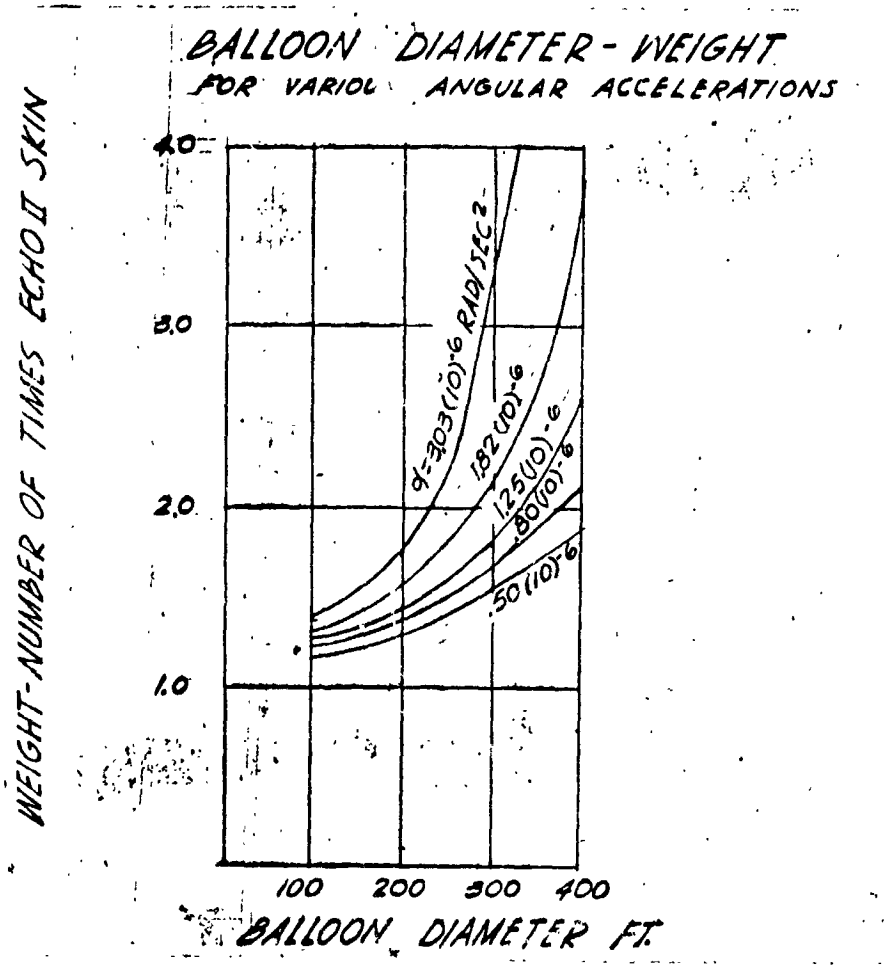

Figure 3.4-4 Balloon Weight

4.0 THE FEASIBILITY STUDIES

This section discusses feasibility items which are common to the passive communication satellite regardless of the exact orientation control system which is employed. These items are mainly concerned with the ability of the satellite system to provide and make use of differential solar forces and to provide hardware which will reliably survive the space environment.

The topics which are discussed are listed below:

(a) Solar forces

(b) Materials and structural concepts

(c) Surface finishes

(d) Thermal feasibility

(e) Equipment location and packaging

(f) Radiation and meteorite shielding

(g) Reliability

(h) Orbital computations

UNCLASSIFIED

4.1 SOLAR FORCES AND TORQUES

There are four sources of radiation which cause forces and torques on the vehicle. These forces are as follows:

(1) Direct solar forces - caused by direct solar energy impinging upon the vehicle.

(2) Albedo forces - produced by the direct sun energy reflecting off the earth and striking the vehicle.

(3) Direct earth forces - produced by direct earth energy impinging upon the vehicle.

(4) Reradiation forces - caused by the vehicle being a source of radiation due to its own temperature.

The radiation impingement (or emission) on the vehicle produces forces and torques which depend upon the surfaces of the vehicle. The surfaces of the vehicle can be either diffuse and specular and absorptive or reflective.

Four different patterns were studied to find the forces and torques on the vehicle. Configurations A, B and C of figure 4.1-1 are combinations of surfaces ranging from all specular to combinations of specular and diffuse surface. Configuration D of this illustration has a pattern which is half diffuse absorptive and half diffuse reflective.

For the first portion of this study program configuration D has been investigated more completely than has A, B, and C, and configuration D is the subject of the data herein. This pattern has the advantage, since its surface is all diffuse or nearly so, of being the one which will produce the smallest torques on the vehicle. Derivations have been made for the other patterns, but the computer runs to establish all of the needed relationships will not be complete until later.

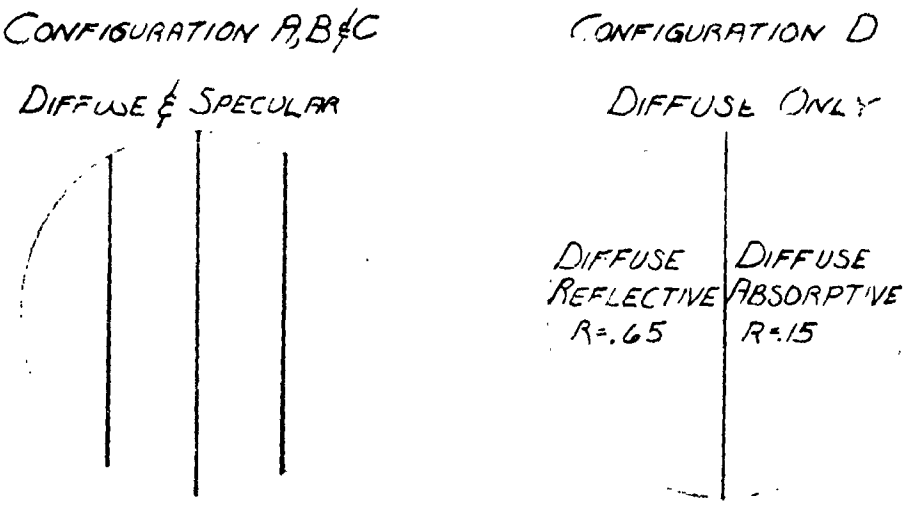

Figure 4.1-1 Patterns Studied

The forces produced on a 200-foot diameter vehicle for configuration D with a vertical system at 1500 miles altitude are presented on the illustrations to follow. The Z direction on the following curves is toward the sun, while the X direction is perpendicular to the Z. The orbit plane is assumed to include the sunline (except for figure 4.1-6), so that no Y -direction forces are produced. Admittedly, the data is incomplete until other orbit inclinations are added. In all of the graphs, the force in lbs is shown as a function of orbit angle measured from satellite midnight.

In figures 4.1-2 and 4.1-3, the X and Z forces are shown for the albedo, direct earth, and reradiation forces. The reradiation force is zero since the emissivities on the inside and outside of each surface have been made equal.

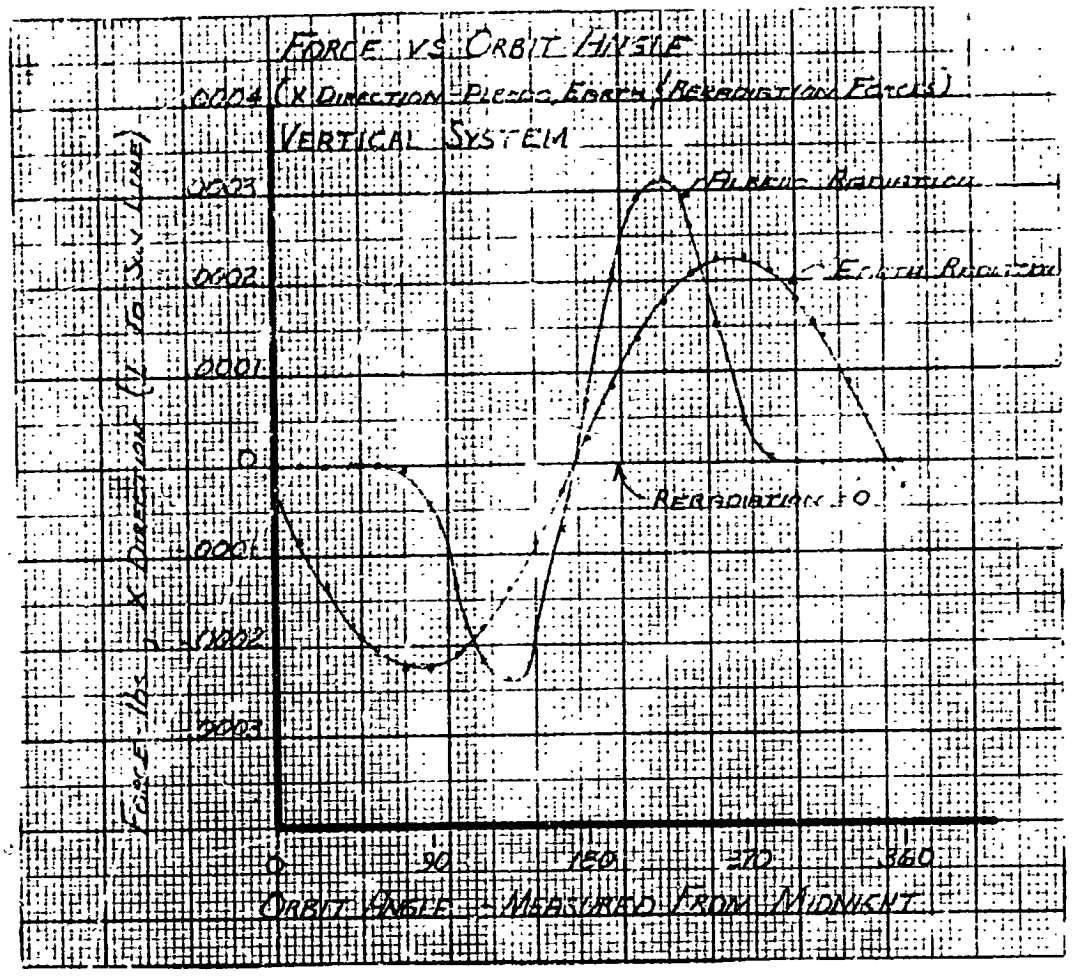

Figure 4.1-2 X Secondary Forces, Vertical System

The direct solar forces and the total of all four forces are shown for the X direction in figure 4.1-4 and for the Z direction in figure 4.1-5.

A study was made to determine the effect of having the orbital plane at one other inclination to the ecliptic plane. In figure 4.1-6 the results of this study are shown for the direct solar force in the Z direction only. From examination of the figure, there is little difference in the two curves. The programs developed to find the forces take the inclination into account when the forces are calculated.

In figure 3.1-11 the direct solar forces in the Z direction for the vertical and dual flip systems are shown for comparison. The orbit represented has a 1500-mile altitude and is inclined at 45° to the ecliptic. As explained in

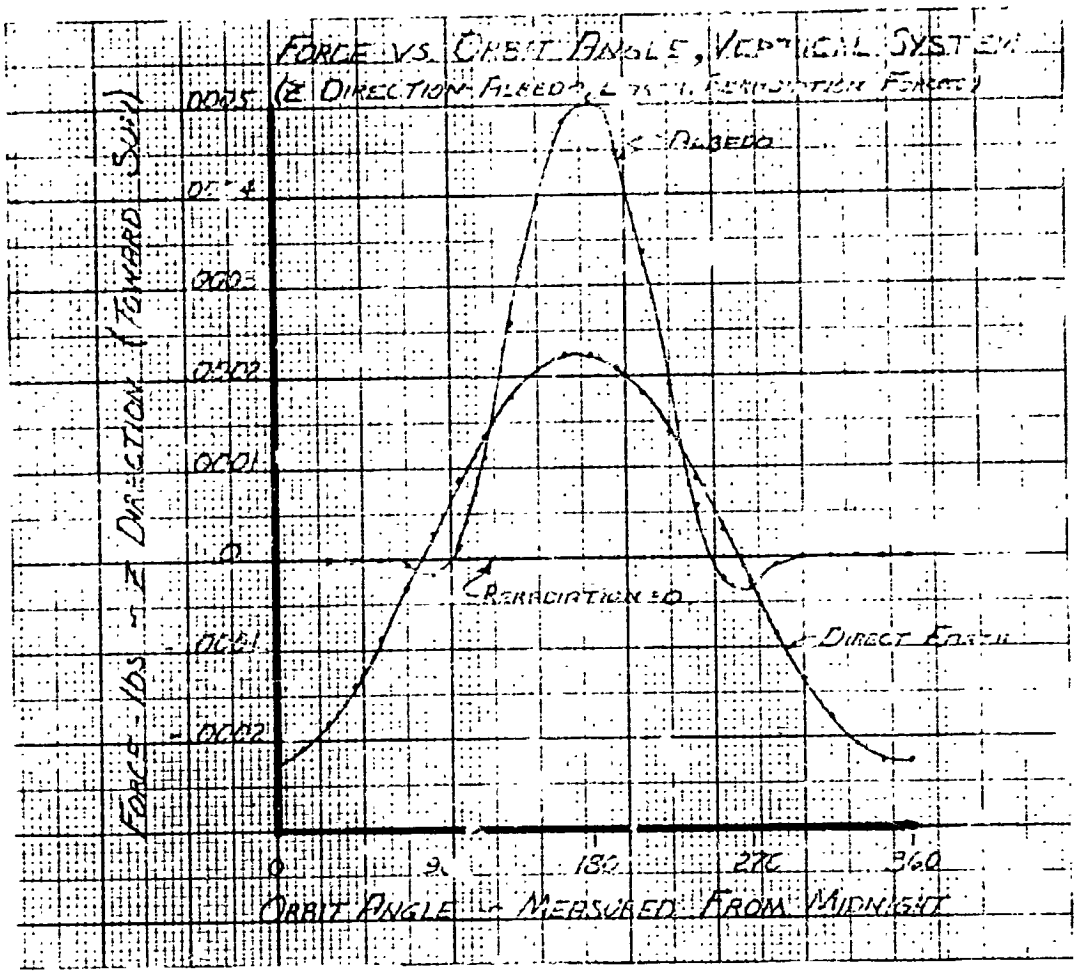

Figure 4.1-3 Z Secondary Forces, Vertical System

in section 3.1.2.3, the vertical system is actually superior at this inclination from the standpoint of differential Z force effectiveness.

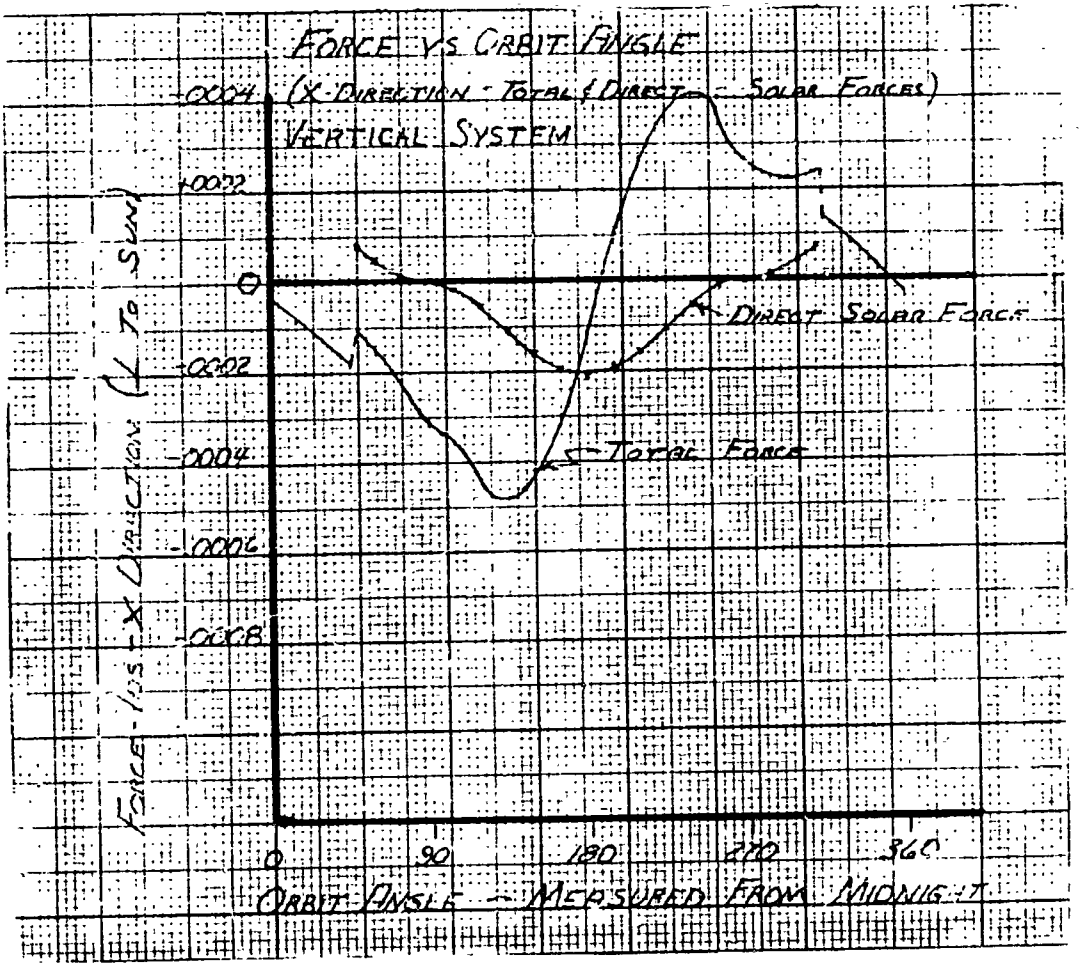

Figure 4.1-4 X Primary and Total Forces, Vertical System

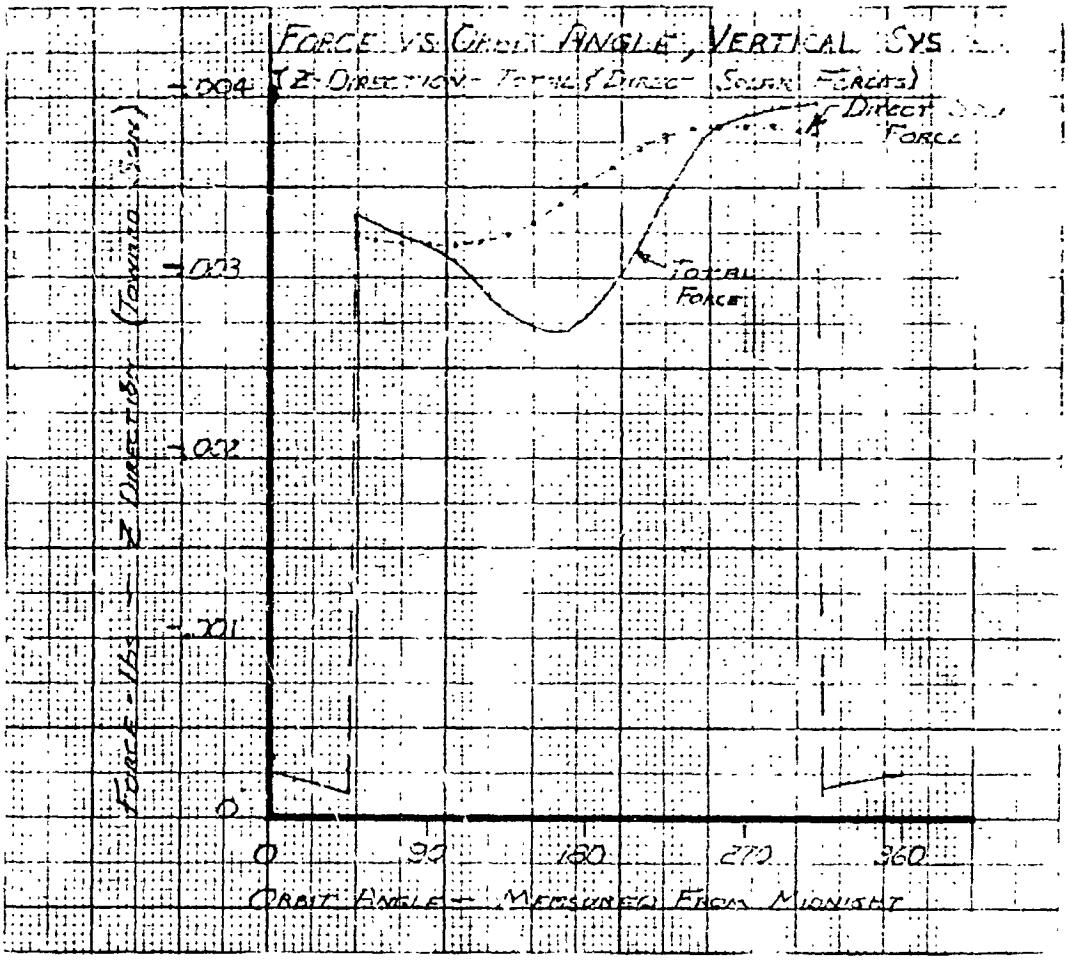

Figure 4.1-5 Z Primary and Total Forces, Vertical System

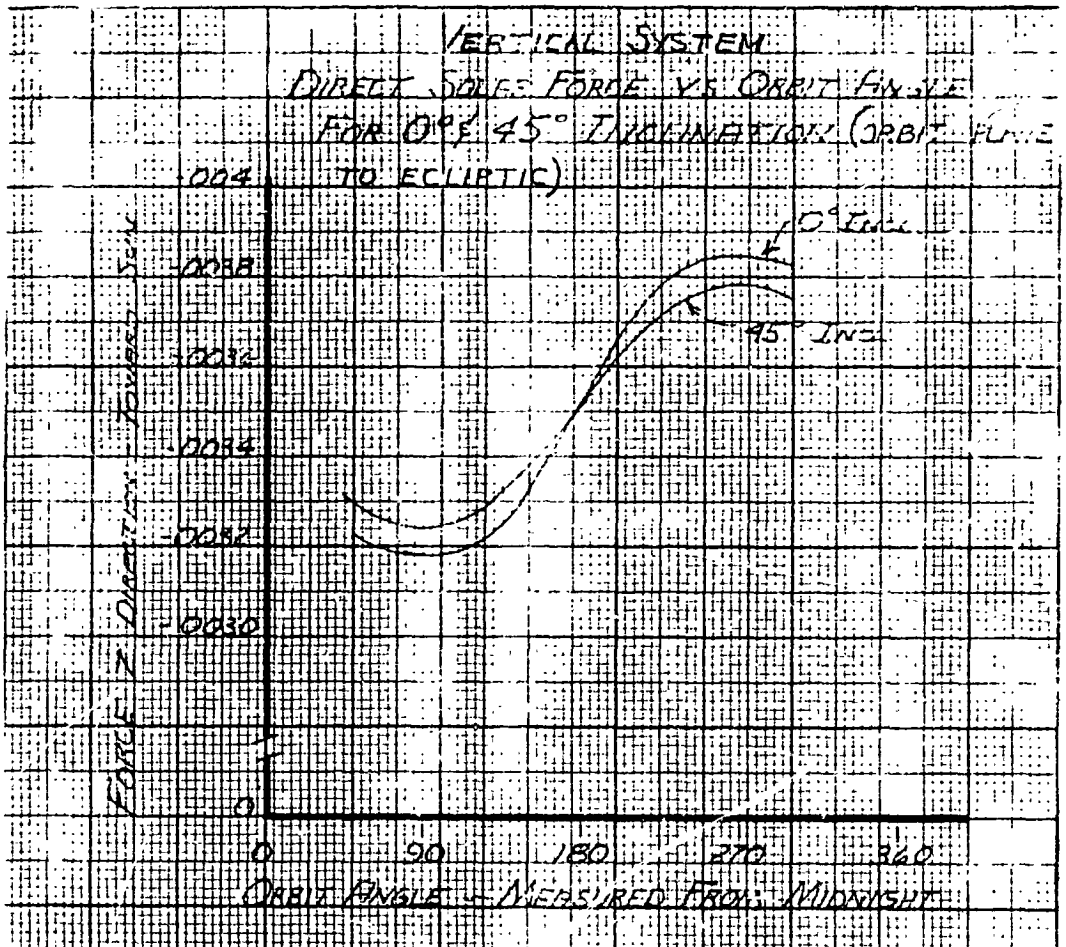

Figure 4.1-6 Z Primary Forces for Two Inclinations, Vertical System

4.2 Materials and Structural Concepts

4.2.1 Materials

The material choice for the balloon structure is limited to those materials which are highly flexible and are space proven to the extent that they do not require basic development. This limitation, combined with the requirement that large surface areas be provided for solar pressure forces, restricts the choice to a material either similar to, or identical with, the Echo II aluminum-mylar-aluminum laminate. This material appears to have all of the necessary characteristics. Other materials such as vacuum rigidizing fabrics, foams, fine wires, etc. are deficient with regard to the weight, volume requirements, certainty of space environment characteristics, stability, basic development, and similar items. The major improvement which could be expected from any material would be a significant increase in stiffness. The aluminum outer layers of the Echo II laminate provide bending stiffness which is difficult to approach with any other material of the same thickness. Increased material thickness has many undesirable characteristics such as bulkiness, poorer heat transfer, weight, and flexibility. Foaming materials offer some potential, but the present technology does not allow their immediate consideration.

Other characteristics which make the aluminum-mylar-aluminum sandwich particularly suitable are the good R.F. reflection reflectivity and the adaptability to desirable surface finish properties. These qualities are not inherent in other materials.

4.2.2 Structural Concepts

Several means for providing significant improvement in structural stiffness over the laminate alone have been considered on a preliminary basis. Figure 4.2-1 indicates some of the most promising possibilities. As shown by the illustration, they are basically tubular, U-channel, Z-channel, and box section configurations. The means of deployment varies with the type. The tubular form would require a secondary inflation system which would be activated after the balloon has taken overall shape. The U-channel scheme is intended to be self-forming during final yield stretching of the skin. Due to the skin curvature, the webs will form themselves toward the radial

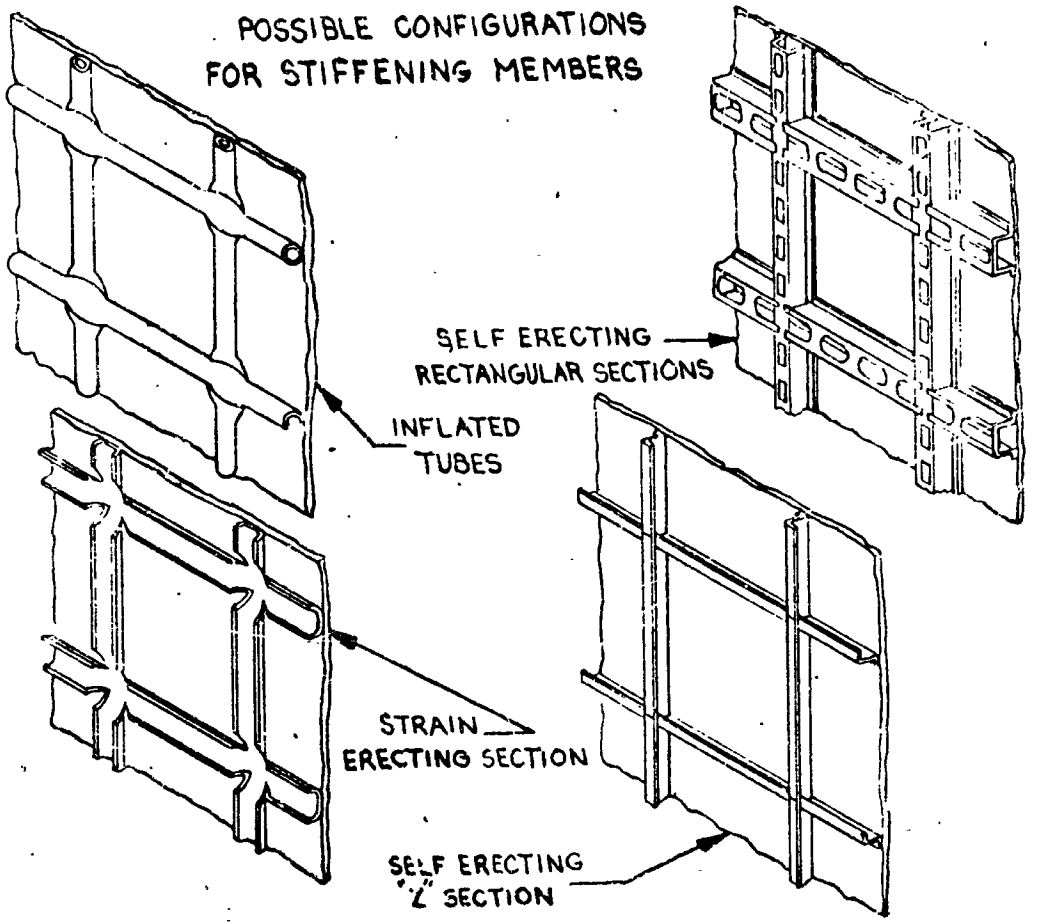

Figure 4.2-1 Structural Configurations

direction. The Z-section and box beam versions can be made and attached to the skin so that the unfolding of the balloon pleats forces them to erect. This method has been partially verified with paper and laminate models. Fabrication appears to be feasible but quite tedious.

The dynamic forces associated with the deployment of relatively large electronics masses during initial balloon inflation can best be minimized by keeping the inflation process as slow as possible. Residual air must be kept to a minimum. Once the initial shape has been attained, a second pressurizing phase is required to stretch the skin to remove fold lines and provide as smooth a spherical surface as possible.

4.3 Surface Finishes

The inner and outer finishes of the satellite are important for thermal and dynamic control. The finish properties that serve in these functions are solar absorbance (α_s), emittance (ϵ), and degree of specularity (ρ). For dynamic control, the types of finishes sought are shown below:

Class of Finish	Ideal Optical Properties
Diffuse Absorber	$\rho = 0$, $\alpha_s = 1$
Diffuse Reflector	$\rho = 0$, $\alpha_s = 0$
Specular Reflector	$\rho = 1$, $\alpha_s = 0$

To serve, as well, for thermal control, it was necessary that the diffuse absorber have a high emittance, the specular reflector have a low emittance, and the diffuse reflector, an emittance of intermediate value.

The choice of coating was limited, wherever possible, to aluminum "in situ" treatments as opposed to applied finishes. The benefits would be low weight penalty and maximum resistance to packaging and space environment stresses. The treatments considered were anodize (chromic and sulfuric acid types), chromate conversion coatings, chromate-phosphate conversion coatings, and chemical polishing. However, it was immediately apparent that these types of finishes could not provide a diffuse absorber sufficiently close to ideal to be useful. Therefore, an applied finish, India Ink, was also considered.

Values of α_s were taken from the literature and determinations made in the Aerospace Division laboratories. Emittance values were from the literature or personal communication with other laboratories.

Quantitative degrees of specularity for these finishes were given no consideration in the literature and had to be measured. Specularity was estimated by comparing the total hemispherical reflectance (R_{D+S}) with the hemispherical reflectance when the specular component is removed (R_D). The fraction of specularity (ρ) is calculated as:

$$\rho = 1 - \frac{R_D}{R_{D+S}}$$

For a highly diffuse surface where $\mathcal{S} \rightarrow 0$, then $R_D \rightarrow R_{D+S}$. For a highly specular surface where $\mathcal{S} \rightarrow 1$, then $R_D \rightarrow 0$.

On the Carey Model 14 spectrophotometer used for R_D and R_{D+S} measurements, the instrumental limitations were such that the specularity measurement could not be made at normal incidence over the spectrum range of 0.25 to 2.70 microns. Because these limitations, the measurements quantitatively established degrees of surface specularity in contrast to the subjective evaluation generally made for the finishes.

Values of α_s, ϵ, and $\mathcal{S}$ for practical treatments are shown in Table 4.3-1. In narrowing the choice for final selection of treatments, anodizing was rejected. The reasons were: (1) very light anodizing afforded values no different from chemical polishing. The only justification for use of anodizing would be as a means of preserving the polished finish. (2) Heavier coatings of anodize did not afford sufficiently high absorbence values before destroying the thin parent metal.

The final selection of coatings to serve both dynamic and thermal needs is indicated in Table 4.3-1. These are to be applied to satellite configurations for both external and internal locations. The coatings chosen marry practicality with a sufficiently close approach to the ideal to make the systems thermally and dynamically feasible.

Manufacturing and space environment resistance of these coatings are shown in Table 4.3-2.

OPTICAL PROPERTIES - ALUMINUM TREATMENTS

Aluminum Treatments	α_s	ϵ	% Specularity	Coating Density mg/100 ft.^{2}
Surface Alterations:				
Plain	0.25	0.07	61	
* Chemical Polished	0.2	0.04	90	0
Anodizing on Chem. Polish:				
Sulfuric Acid				
5 min. treatment	0.16	.08	68	
30 min. treatment	0.33	.20	48	
Chromic Acid				
30 min. treatment	0.52	-	24	
70 min. treatment	0.59	-	-	
Conversion Coatings:				
Chromate (Alodine 1200)	0.53	0.08	-	
Chromate-Phosphate				
* Alodine 401-41	0.35	0.5	-	450
Iridite 30	0.40-0.90	-	0-13	
Opaque Coatings:				
* India Ink	0.95	0.9	0	43,300

* Selected Treatments

Figure 4.3-1 Surface Finish Optical Properties

PROCESSABILITY - ALUMINUM TREATMENTS

	Ease	Cost	Adhesion	Folding Reaction	Effect on Parent
Chemically Polished	Fairly easy	high	no problem	none	none
Alodine 401 - 41	Very easy	medium	excellent	none	none
India Ink	Very easy	medium	excellent	none	none

STABILITY IN SPACE

	Vacuum/UV	Thermal Stability	Radiation	Micrometeorite
Chemically Polished	no effect	high	excellent	no unusual problem
Alodine 401 - 41	no effect known	high	no known effect	no unusual problem
India Ink	no effect	high	excellent	no unusual problem

Figure 4.3-2 Surface Finish Characteristics

4.4 Thermal Feasibility

The thermal feasibility of the passive communication satellite involves the following tasks.

a. Establishing the criterion for feasibility

b. Determining a method of analysis that indicates the relationship between the thermal design properties and the passive temperature control of the vehicle for various orbital environments.

c. Establishing the trade-offs between the dynamics requirements and thermal design.

4.4.1 The Criterion of Feasibility

The overall feasibility is associated with the life of the satellite which in turn is influenced by the temperature of the various components. Both the maximum and minimum temperatures are involved and the values selected are summarized below:

Skin temperature - - - - - - - - - - - - -	80°C max., -100°C min.
Electronics - - - - - - - - - - - - - - -	60°C max., - 10°C min.
Batteries - - - - - - - - - - - - - - - -	100°C max., 0°C min.
Solar Cells - - - - - - - - - - - - - - -	100°C max., - 75°C min

4.4.1.1 Skin Temperature

The values chosen for the skin temperature limits correspond to those previously set for other balloons. The maximum is very much lower than the upper limit for Echo II type material. The lower limit, however, is that imposed on Echo II material where the joints were concerned. Improvements in joining techniques have lowered this limit but sufficient data are not available to indicate how much.

4.4.1.2 Electronic Component Temperatures

The upper limit has been selected because it represents the point where the decrease in failure rates of most electronic components due to temperature effects becomes somewhat insignificant. The lower limit was chosen because it is a condition where the power supply stability becomes somewhat questionable.

4.4.1.3 Batteries

The temperature chosen here represents manufacture ratings.

4.4.1.4 Solar Cells

The upper limit provides an efficiency of 75 percent which is considered a good design value. The lower limit on the other hand represents a condition where the bonding of the cell to the balloon structure is impaired.

4.4.2 Method of Analysis

The method of analysis was to first determine the orbital environment that would influence the maximum and minimum temperatures. The internal and external conditions that would exist during the time periods associated with ground, launch, inflation, stabilization, and stabilized orbit operation were qualitatively evaluated to establish the orbital environment which would most likely yield the highest and lowest temperature. The ultimate objective was to provide a basis for the quantitative thermal analysis.

4.4.2.1 Qualitative Analysis

The thermal environments associated with ground cooling and launch periods do not offer any severe problems. In addition the period of time during inflation should be of small concern. During this period the expanding air and vapors will reach low temperatures because these gases will expand nearly adiabatically. However, since the mass of gas involved is small as compared to the total mass of the system, the effective temperature reduction of the entire system will be of small moment.

The tumbling of the satellite during the orientation stabilization period can produce the worst-worst space orientation. It appears then that the conditions when the satellite is oriented in a position so that it receives the greatest amount of solar and earth energy would provide the highest skin temperatures while a position where it receives the least energy from the surroundings would provide the lowest. The orbiting plane selected for analysis is the ecliptic plane where the satellite receives the maximum albedo when located on the earth sun line. The plane also provides a time in the earth's shadow which is maximum at all times for any given altitude. For the purpose of determining skin temperature, a steady-state heat transfer

was assumed to exist when the vehicle is located at either of the positions. Where the various component temperatures are involved, the phase lag and attenuation in temperature change during an orbiting condition as a result of the energy stored in the component was evaluated.

4.4.2.2 Thermal Analysis - Skin Temperature

A heat balance for a point on the skin of the vehicle is shown in Figure 4.1-1. The main concern here is the determination of "q_B". The outgrowth of the analysis to determine this quantity is a temperature or property defined as the Mean Radiant Temperature (MRT). The value of the MRT is influenced by the external surface properties, α_o and ϵ_o of the vehicle, altitude and position in orbit. It, in turn, influences the skin temperature and component temperature because it represents, along with the internal surface conditions, the radiation background to which any point inside the vehicle is exposed. Since it is influenced by the total energy received by the vehicle, a means of determining this for a spherical vehicle was provided. The model chosen for analysis is shown in Figure 4.4-2. It is well to note that aerodynamic energy was not considered in the analysis because at the altitudes involved, this would be of small concern. In addition, the work done on the satellite due to solar effects was not involved because this vehicle is a rigid body and the force cannot appreciably defect the boundaries, i.e. no energy can cross the boundaries of the balloon due to a difference in force. Only radiation heat transfer was considered in the analysis.

The model chosen for analysis was based on the work done in NASA Technical Note D-115. However, since the vehicle contains more than one surface absorptivity (α_s) and emissivity (ϵ) a method of integrating the energy over the surface of the sphere was provided. The sphere was considered to be made up of a number of flat-plates. The number of flat plates was determined by comparing the calculation of MRT for a sphere of uniform surface conditions with the calculation using the equation in the above reference. The model chosen contained 144 surfaces and provided a MRT within 2°C of that calculated using the equations from the referenced document.

4.5 Equipment Location and Packaging

4.5.1 Introduction

During Phase I of the satellite study, system tradeoffs and overall feasibility have been evaluated from a packaging standpoint. After determining potential problem areas, the feasibility of providing reliable means of overcoming these problems has been demonstrated. Differences in packaging concepts resulting from system characteristics have been determined to aid in the selection of a control system for Phase II of the study. The areas considered include: structural compatibility, weight and inertia control, thermal balance, radiation protection, meteorite damage, launch vibration and folding requirements.

4.5.2 Equipment Location

One of the first areas in which a tradeoff exists is that of equipment location. Due to satellite orientation and required inertia characteristics, the placement of power supply and electronic packages differs with the type of control system employed. Equipment locations for the dual flip and vertically oriented systems are shown in figure 4.5-1. The dual flip is a sun-oriented system with either of two hemispherical surfaces maintained normal to the sun line. The solar cells are placed, therefore, in two arrays, one per hemisphere. Structural considerations dictate placement of these arrays at the intersections of two stiffening tube belts. The remaining equipment is distributed to provide equal moments of inertia about any axis, consistent with structural and folding requirements. One method of accomplishing this is the placement of electronics and batteries at the remaining four stiffening tube intersections. The vertical system is earth-oriented and therefore results in a variable satellite-sunline relationship. To assure the availability of solar cell power assuming a random relationship, six groups of solar cells are required. These cells would be located at the six intersections of stiffening tubes. The electronic equipment and battery packages are located at the stiffening tube intersections on the vertical axis to obtain the benefit of gravity gradient effects.

DETERMINATION OF SKIN TEMPERATURE

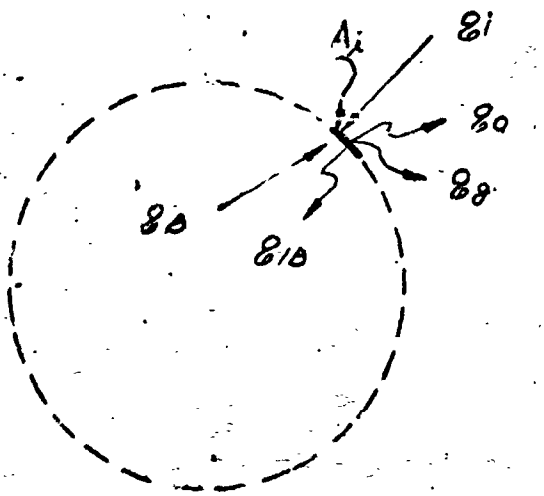

HEAT BALANCE

$$\alpha_{\lambda_i} \mathcal{E}_2'' A_2 + \alpha_{i_\theta} \mathcal{E}_b'' A_2 = 6 (\epsilon_2 + \epsilon_o) T_{s2}^4 A_2 \text{ WHERE } T_{s2} = T_{s3}$$

Figure 4.4-1 Determination of Skin Temperature

An analysis was provided for the various electrical components located inside the balloon. In order to determine the maximum and minimum temperatures, a typical electronic package was used for analysis and is shown in Figure 4.4-3. It is to be noted that there are two conditions that can exist where the thermal coupling of the components to the skin of the sphere is different. (1) Where gas conduction along with radiation heat transfer can exist, and (2) Where only radiation coupling is concerned. The former can exist during the early life of the vehicle while the latter will occur when little or no gas is present. The main concern here is to provide a thermal design where the watt density, package density, and isolation from the skin is sufficient to take care of both high and low temperatures whether gas is, or is not, present.

GEOMETRY USED FOR THE DETERMINATION OF ENERGY GAIN

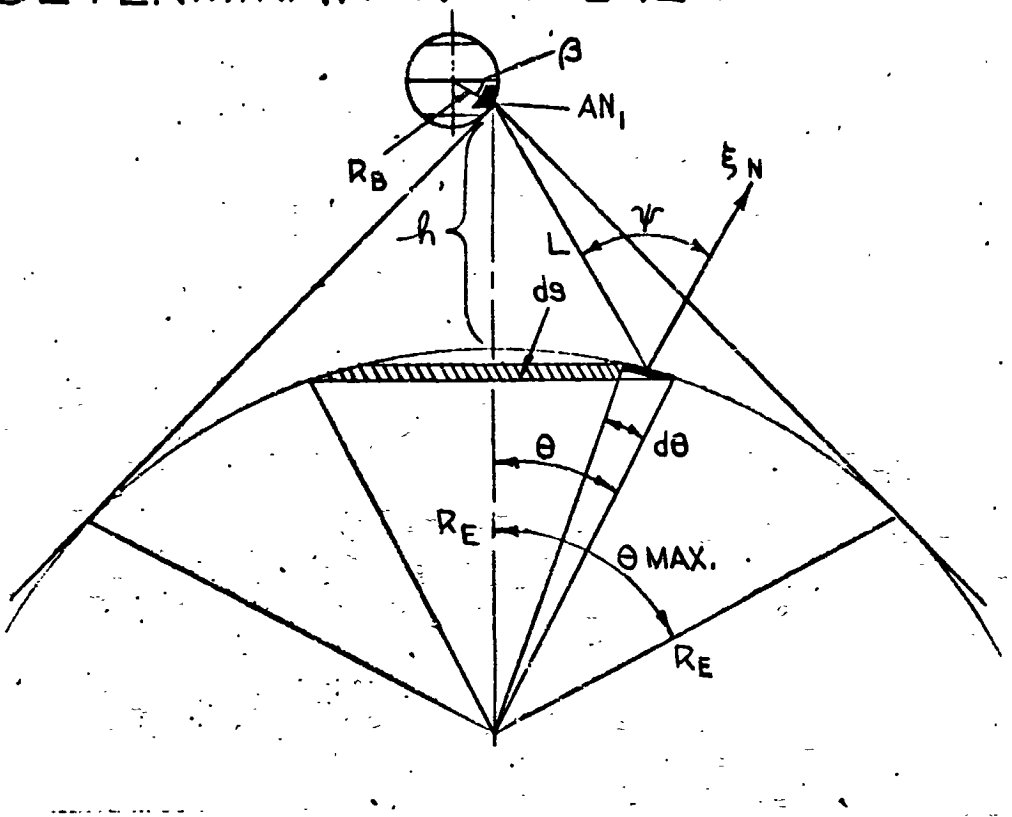

Figure 4.4-2 Geometry Used for Determination of Energy Gain

Three different situations must be evaluated with the vehicle in an orbiting condition, i.e.

(1) Random orientation of the vehicle where gas is present within the sphere

(2) Stabilized orbit with gas

(3) Stabilized orbit with no gas.

The former was considered to be similar to a dual flip system where no flip occurs while the latter was considered to be the earth oriented situation. The analysis provided a set of five equations in five unknowns. This was reduced to four equations by considering the MRT as a step-function. In order to make this evaluation, however, it was essential to first provide a vehicle with a design MRT. Because

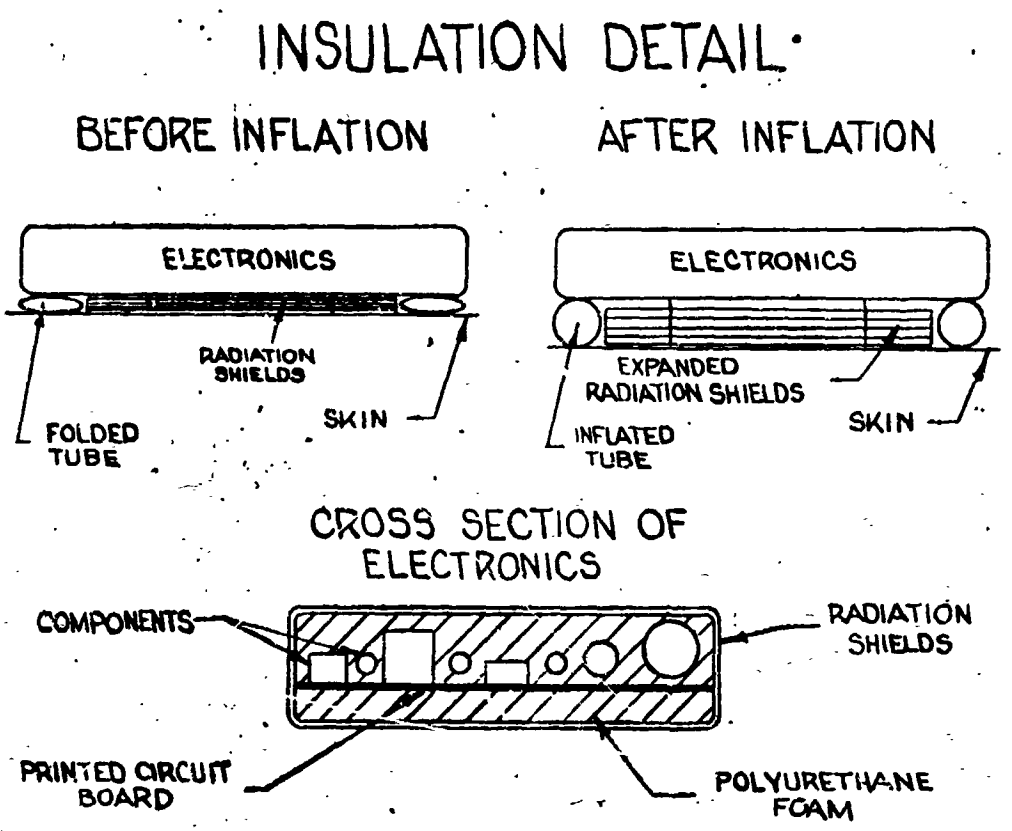

Figure 4.4-3 Typical Electronics Package

of the long time in the sun, a design goal of 10°C was established for this property, the value being selected on the basis of 500 watts of power and a package density of 20 pounds per ft.^{3}.

4.4.3 Selection of Thermal Properties of the Sphere

The properties that influence the MRT of the vehicle in most cases complement one another in such a fashion that anything that serves to change the MRT changes all other temperatures in the same direction. The exception are those associated with the area and internal coupling; that is to say, that internal emissivity can change the surface temperature without changing the MRT. In addition, the internal emissivity can reduce the hot spot temperature while at the same time, raise the cold spot. The thermal properties of the system, however, do not explicitly define any of the temperature

control points. Moreover, the competition between the high and low limits imposed on the various components coupled with the range of orbital requirements preclude any set of circumstances as design point. One then is confronted with the task of not only evaluating the magnitude and variation in temperature as influenced by the thermal design parameters, but at the same time, one must optimize these variables to values which are attainable in practice.

For this reason, a step-by-step evaluation of the various parameters was made beginning with an arbitrary vehicle with 4 surfaces. The external absorptivities and emissivities were fixed at what was considered to be practical values and the areas of each surface was set to be equal when projected normal to the sun's rays. The altitude was fixed at 1500 n. mi.

Step one - was to change the (ϵ_i) internal emissivity. The results, Figure 4.4-4, of this indicates that no great reduction in hot spot or increase in cold spot would occur when the ϵ_i was greater than .5, i.e. one can only expect marginal gains.

Step two - The area normal (B_1) to the sun was varied while that facing the earth, (B_2) remained fixed. The ϵ_i = .50. The results are shown in Figure 4.4-5a. Once again, only marginal gains were attained when "B_1" was reduced below 45°.

Step three - Two different conditions were evaluated, i.e. with B_1 = 15° and 45°, B_2 was varied. Figure 4.4-5b indicates that some large gains were available. The lowest temperature was attained when the vehicle approached a two-surfaced condition.

Step four - Vary outside emissivity. The desire for dynamics to use a two-surface vehicle where one side was a diffuse absorber (A), and the other side a diffuse reflector (R), led to abandoning the four-surface configuration ($B_1 = B_2 = 0$ for this case). Figure 4.4-6 shows the results of varying the emissivity of the diffuse absorber side. Figure 4.4-7 indicates the effect of varying the emissivity of the diffuse reflector side with ϵ_A = .90.

Step five - In order to ascertain the effect of orientation and to assure that the highest and lowest temperatures were evaluated, the vehicle was examined for all positions or angles to the earth sun line at the points defined as design condition. However, to reduce both hot spot and IRT to the goals designated, the ϵ_i was increased

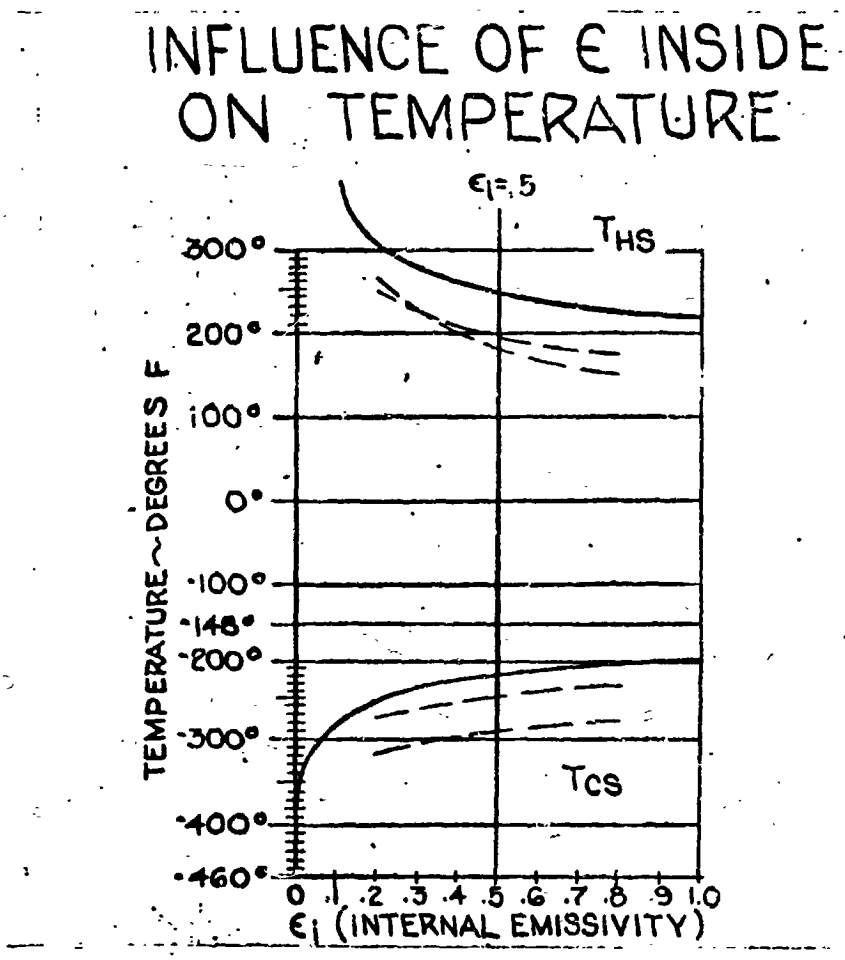

Figure 4.4-4 Influence of Inside Emissivity on Skin Temperature

to .90. In addition, the ϵ_R = .50. Figure 4.4-8 indicates these results. It will be noted that the position examined produces the highest temperature.

Step six - The design as selected above was examined for the effect of altitude. Figure 4.4-9 shows this effect.

The overall results indicate that with the best practical thermal surface, the hot spot can be satisfied under all conditions of orbit. The cold spot condition can only be satisfied at the lower altitude (500 N.M.). The MRT is always beyond the design conditions but never exceeds the maximum allowable component temperature; this of course merely infers a design condition. The cold spot condition then appears to be the only concern here. However, as indicated, improvements in both laminates and joints have been inferred by manufacturers of the laminate. The only factor in question is the reliability of the tests that have thus far been performed.

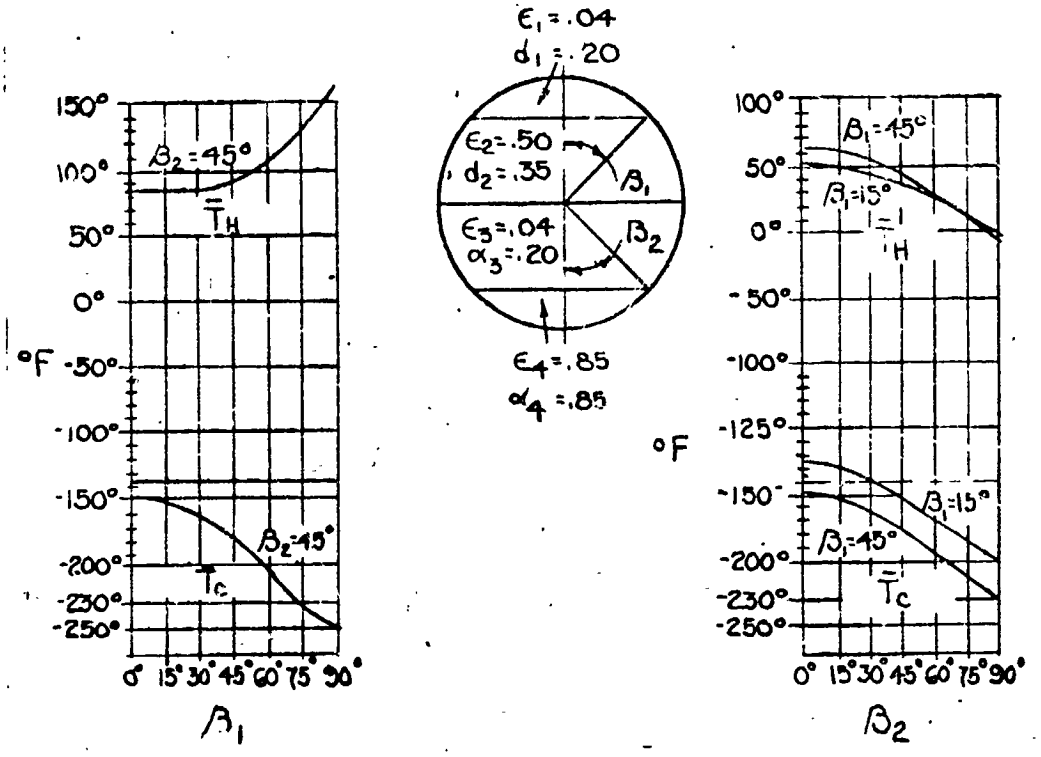

Figure 4.4-5 Influence of B_1 and B_2 on Mean Temperature

4.4.4 Evaluation of the Components

Several typical packages of the electronics and batteries were evaluated both in the operating and quiescent state. In addition, the solar cells were evaluated with different thermal coupling and masses. The results of this analysis are shown in Figures 4.4-10 and 4.4-11. This analysis was accomplished at 1500 n. mi. In order to compare the results of the analysis, a tabulation of the various goals and conclusions is shown in Figure 4.4-12.

4.4.5 Conclusion Regarding Feasibility

The results of the analysis indicate that the passive communication satellite is feasible in every respect except the low temperature at the higher altitudes. It does not appear that any thermal design can be achieved that satisfies all conditions, and at the same time raise the cold spot to the low temperature limit

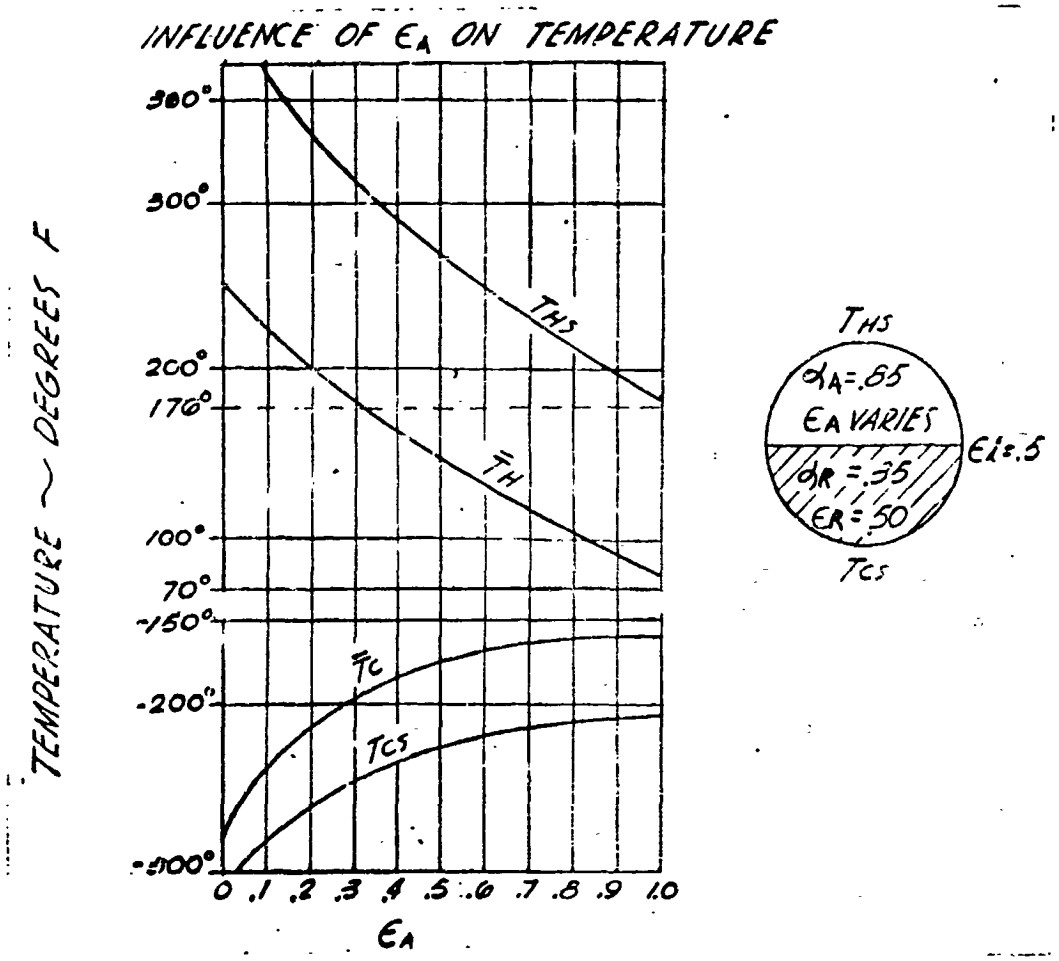

Figure 4.4-6 Influence of Emissivity of Absorbing Surface on Temperature

limit imposed on Echo II material. However, it is not a fundamental limit since newer laminate and joining procedures have shown up well at much lower temperatures. Some reliable tests under thermal fatigue conditions should be done to justify low temperature operation.

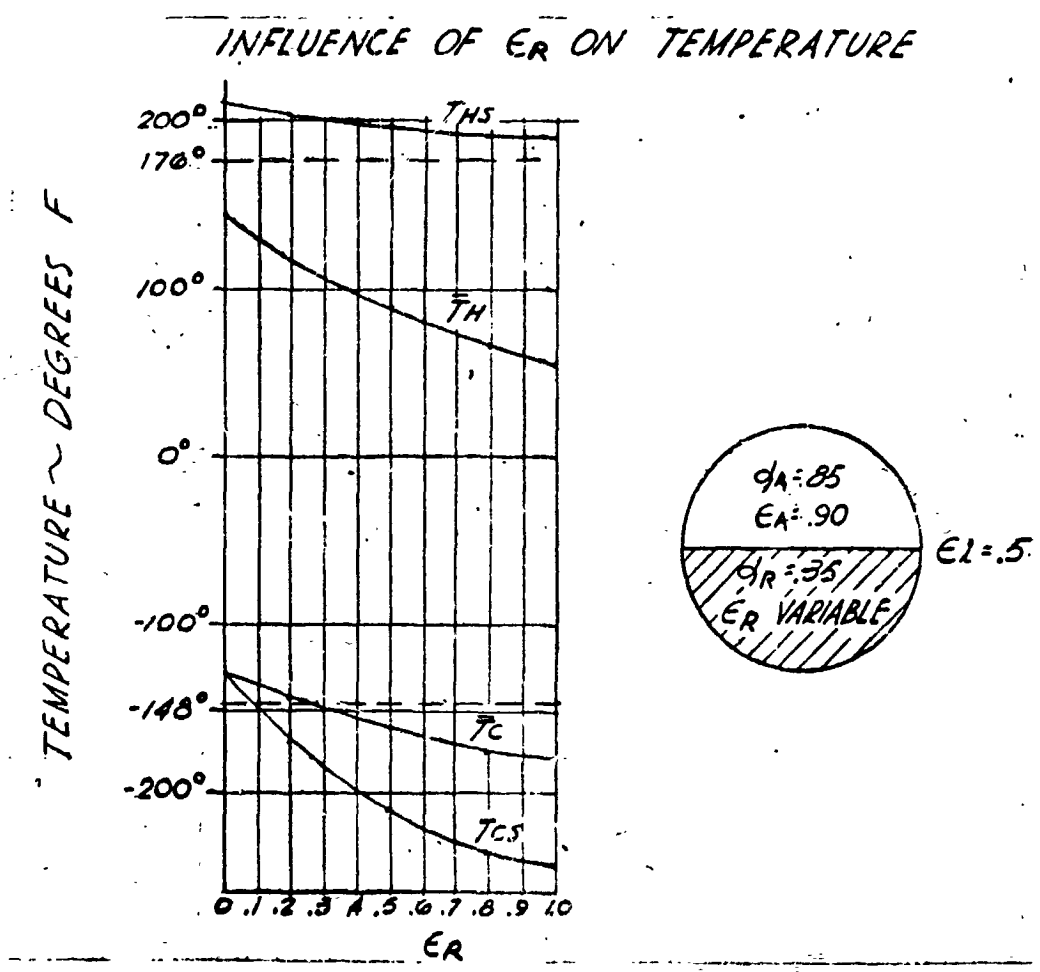

Figure 4.4-7 Influence of Emissivity of Reflecting Surface on Temperature

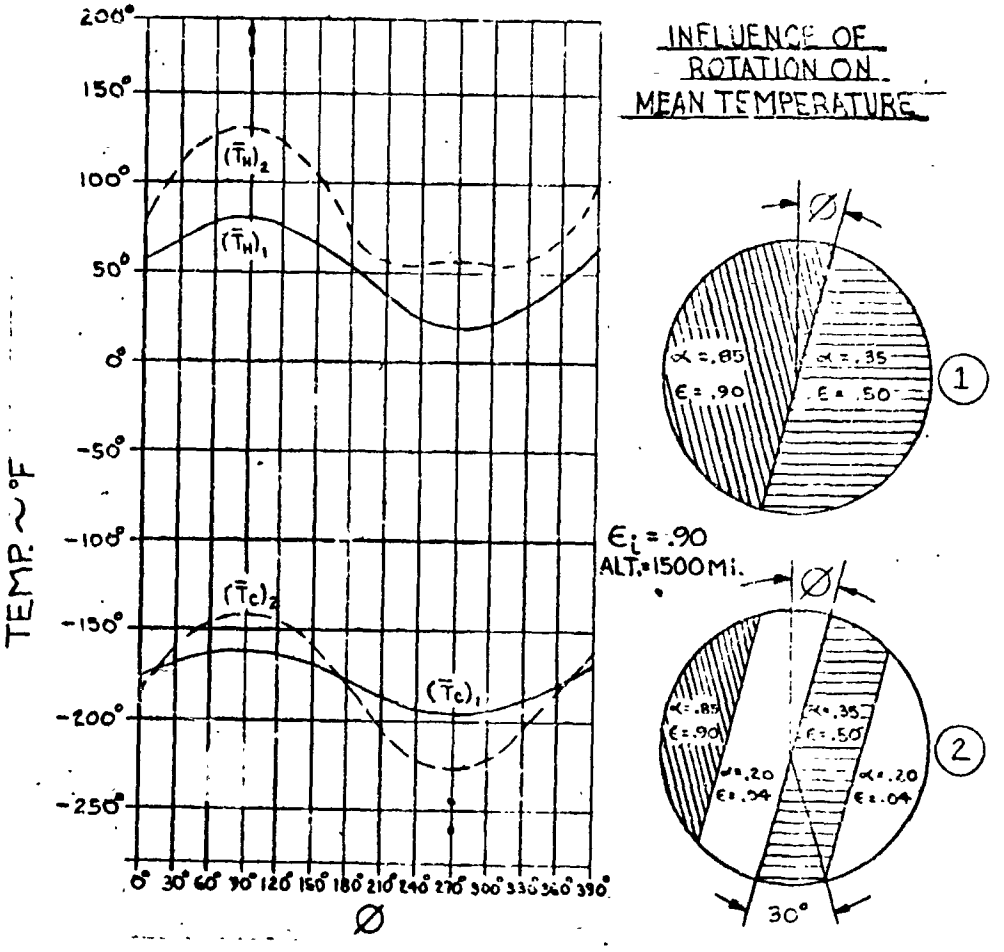

Figure 4.4-8 Influence of Rotation on Mean Temperature

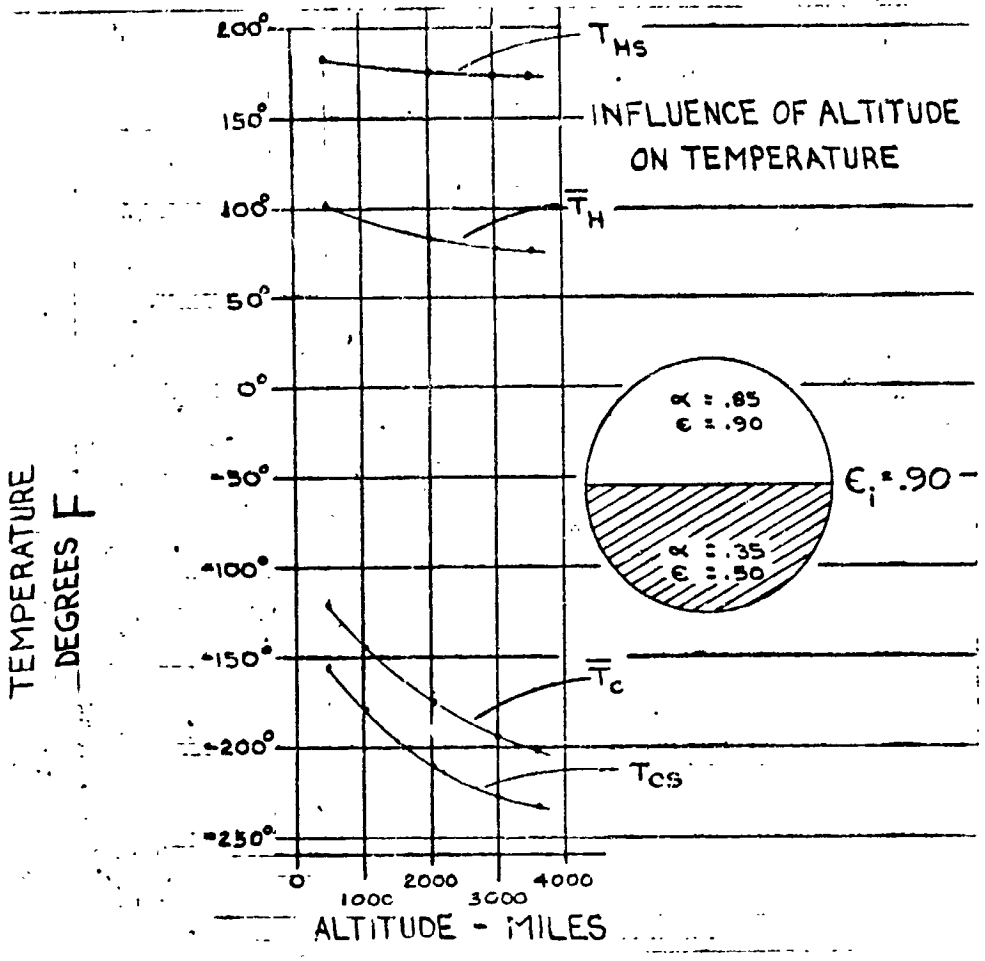

Figure 4.4-9 Influence of Altitude on Temperature

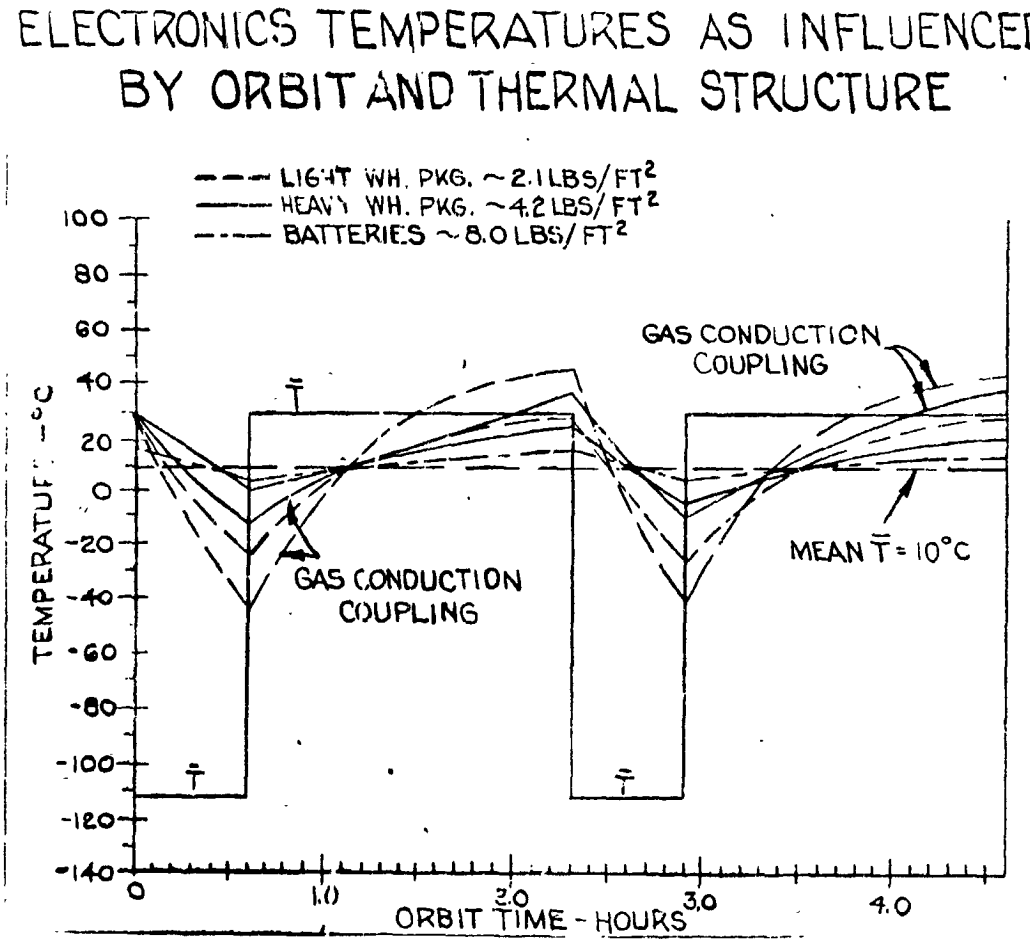

Figure 4.4-10 Effect of Package Density on Temperate of Components During 1500 SM Orbit

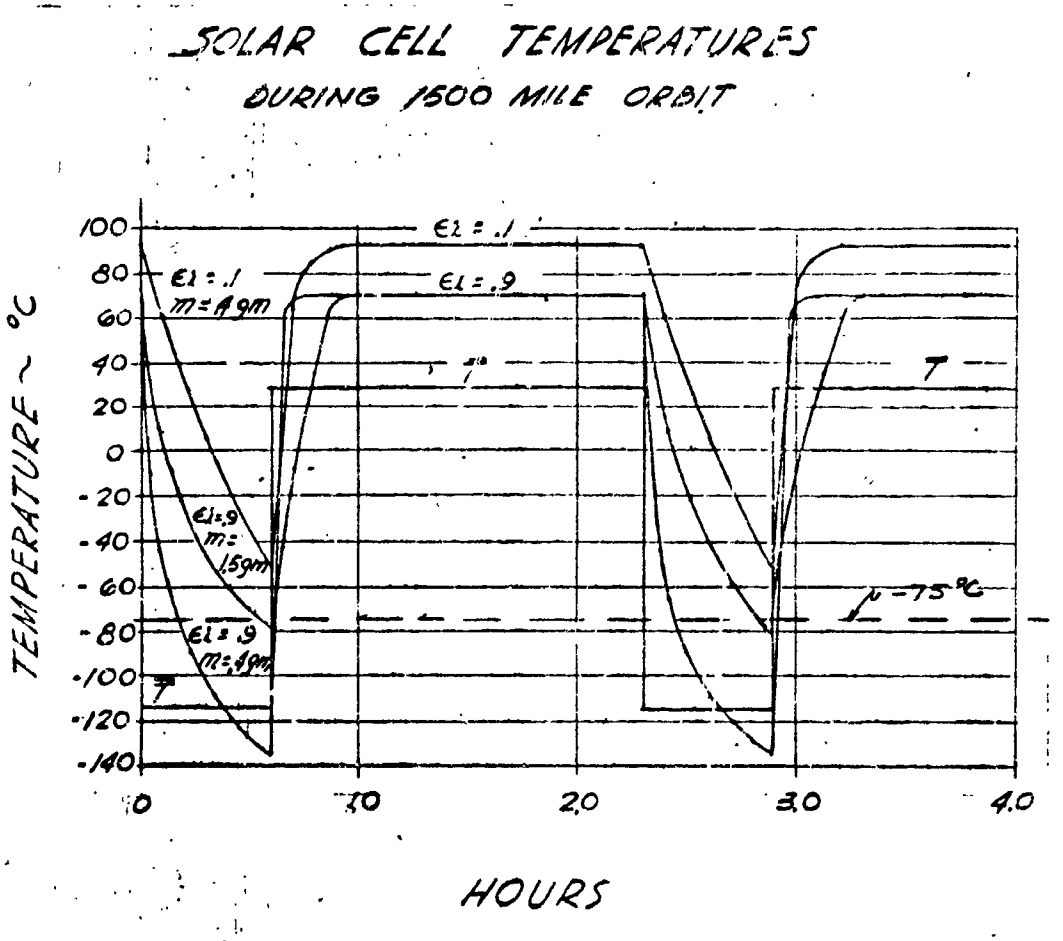

Figure 4.4-11 Solar Cell Temperature During 1500 NM Orbit

TABLE

SUMMARY OF THERMAL ANALYSIS

DESIRED GOALS			RESULTS	
Temperature °C	Maximum	Minimum	Maximum	Minimum
Skin	80	-100	85	-150
Components	60	-10°	38-60	0 to -4h
IRT	10	-	31	-
Battery	100	0	12-20	6
Solar Cells	100	-75	94	-55

Table 4.4.-12 Summary of thermal analysis

EQUIPMENT LOCATION

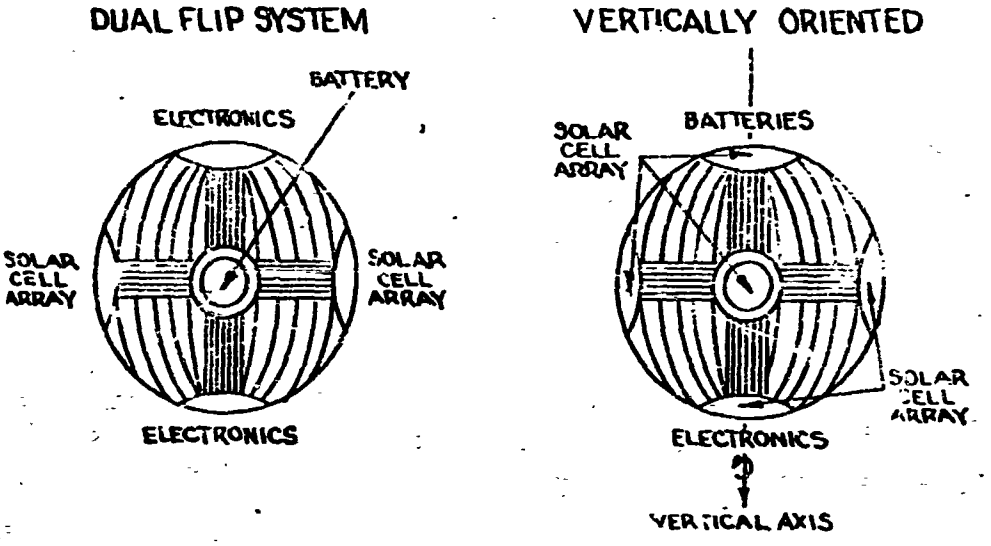

Figure 4.5-1 Equipment Location

4.5.3 Torque Coils

Materials and techniques for providing the necessary torque coils have been investigated during Phase I. To determine the most feasible method of mounting the coils to the satellite, various types of coil material have been evaluated, including limp wire, solid circular conductors, flexible printed circuitry, and the use of satellite structure for coil. The properties of common metals were also compared to determine the optimum coil material on a weight/conductivity basis. Results of these studies indicate that the coils should be constructed of aluminum for minimum weight. Connections to aluminum conductors appear feasible using laser and ultrasonic welding techniques; however, use of more conventional techniques would be allowed if copper coils, with their corresponding weight penalty, are used. The most feasible coil schemes are:

(1) Cementing $\frac{1}{2}$ mil thick flexible printed circuitry to the inside skin in the vicinity of the stiffening tubes.

(2) Utilizing the inner aluminum laminate of the stiffening tubes as conductor.

4.5.4 Size and Construction of Electronic Packages

The application of electronic equipment to the satellite can be accomplished by utilizing a number of small flat packages, interconnected as necessary with .5 mil thick flexible printed circuitry. The size and construction of the electronic packages appears to be restricted by structural and folding requirements and will be independent of the method of control. If the drop pleat method of folding is regarded as typical, permissible package sizes may vary from 12" x 12" x 1" to 18" x 18" x $1\frac{1}{2}$" with a maximum weight of approximately two pounds per package. As shown in Figure 4.4-3, the packages will consist of combinations of conventional and functional block components encapsulated in rigid polyurethane foam for structural support and environmental protection.

4.6 Radiation and Meteorite Shielding

4.6.1 Radiation Shielding

Both the vertically oriented and dual flip satellites contain a large number of semiconductor devices, which are inherently susceptible to radiation damage. The effect of Van Allen belt, atomic testing, and solar flare radiation on semiconductor life has been determined as a function of orbit altitude and is shown in Figure 4.6-1. From this data, required shield weights and thicknesses have been calculated for various orbits taking into consideration component derating to realize benefits of exponential performance degradation. The results, shown in Figure 4.6-2, indicate that shielding sufficient to provide a five year semiconductor lifetime is feasible. However, due to the high energy proton region of the Van Allen belt, orbits ranging from 800-3000 miles in altitude require radiation shields 5-10 times heavier than those required for a 500 or 3500 mile orbit. (For a shielded area of 4000 in^2, shield weight varies with altitude from 15 lbs. to 145 lbs.) The shielding problem for this project differs from that normally encountered in the design of satellite electronics in that thermal and structural requirements dictate a high ratio of shielded area to shielded mass. The unique situation develops in which shield weights may be many times the weight of the equipment shielded.

4.6.2 Meteorite Shielding

Regardless of control system, consideration must be given to the problem of meteorite damage. Failures caused by breakage of interconnecting wiring can easily be eliminated by redundant wiring. The electronic packages, however, must be examined in detail to determine the probability of penetration to component depth. Data from the Explorer XVI Satellite, presented in Figure 4.6-3, indicates that the number of penetrations observed is approximately 1/10 of that anticipated using the Whipple flux and Bjork penetration criteria. On the basis of this data, electronic components surrounded by a .040" aluminum radiation shield and embedded in a minimum of .31" polyurethane foam would be adequately protected against meteorite penetration for the required 5 year life.

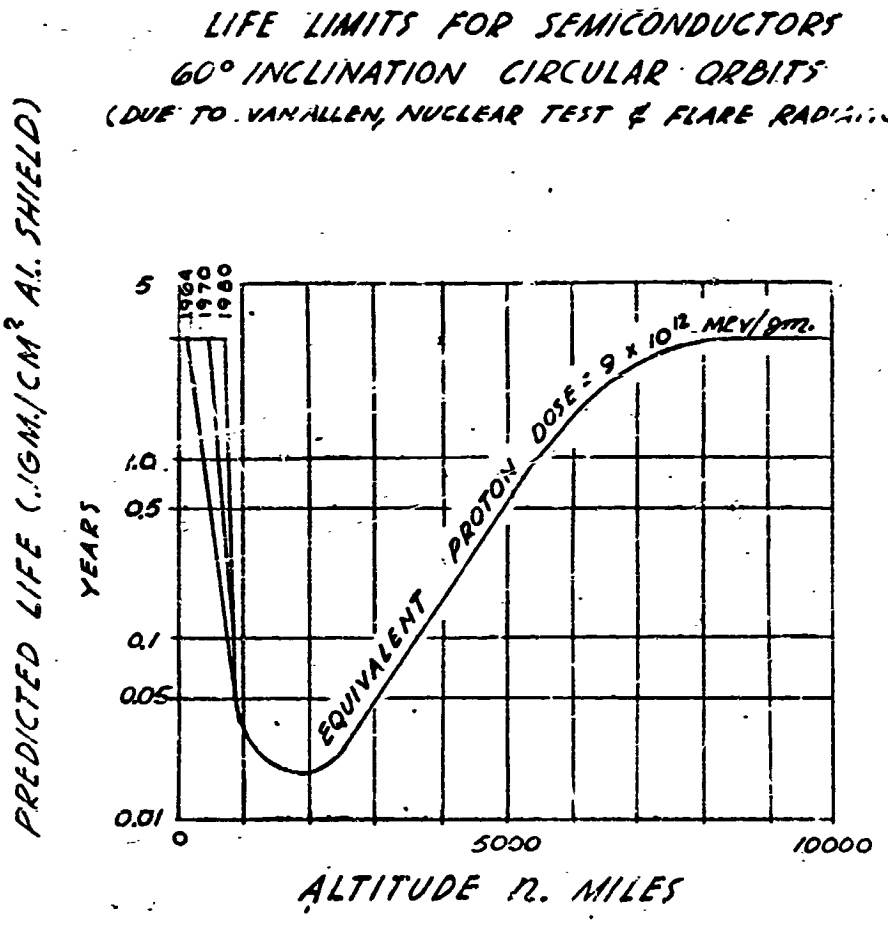

Figure 4.6-1 Semiconductor Life vs. Altitude

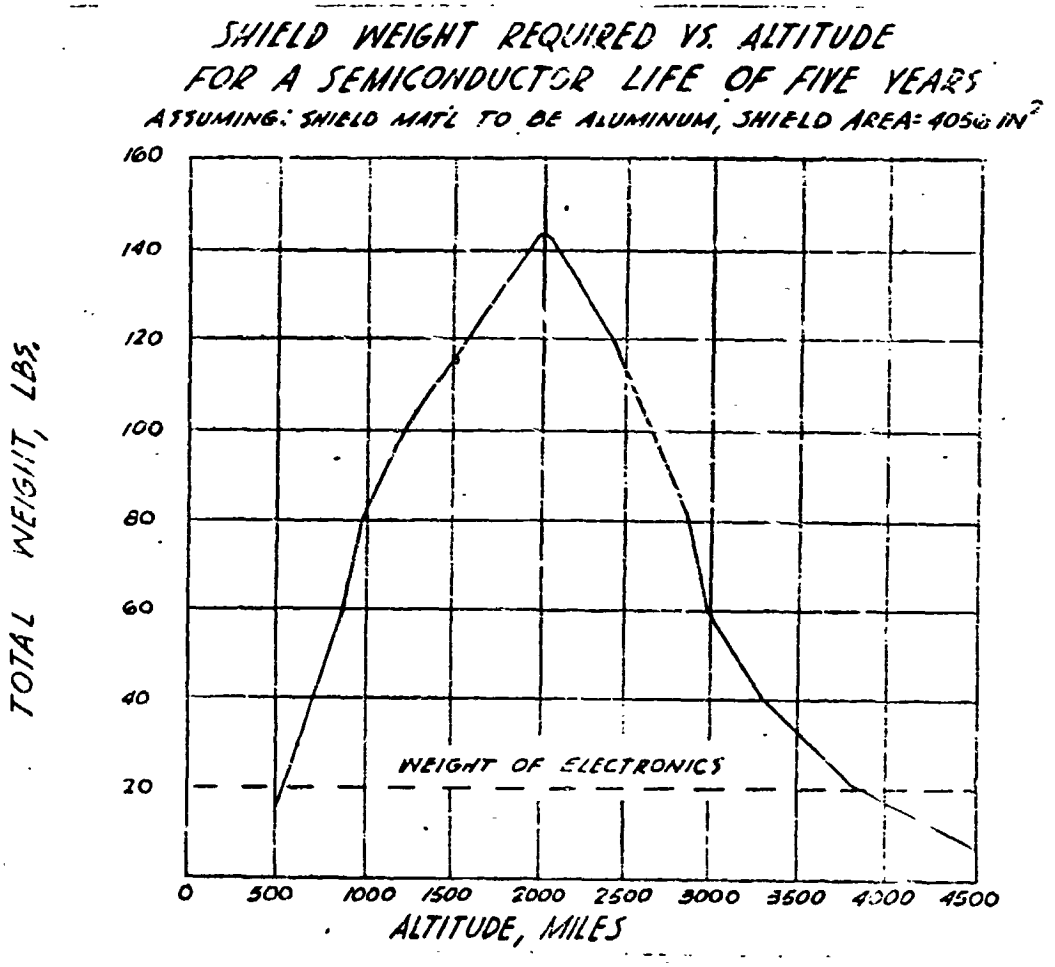

Figure 4.6-2 Shield Weight vs. Altitude for Five Year Life

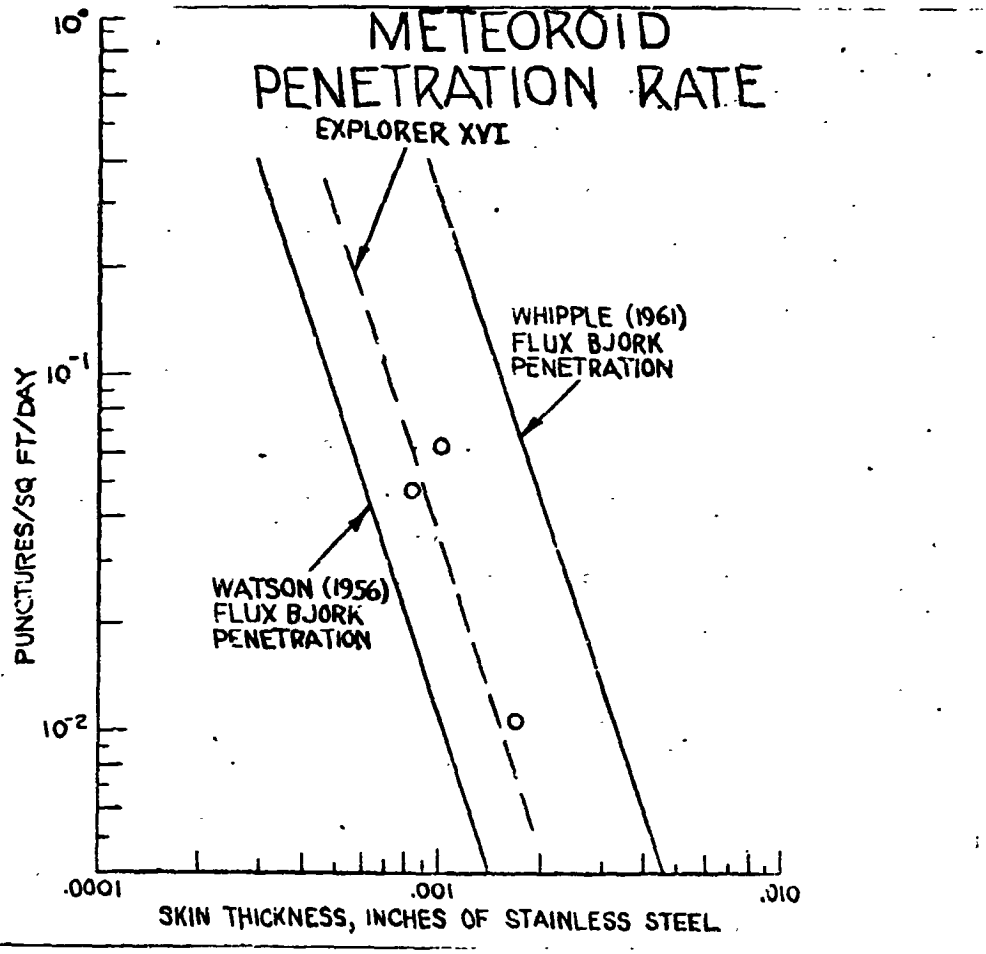

Figure 4.6-3 Meteorite Penetration Data

4.7 Reliability

4.7.1 Assumptions

This study was to compare the reliabilities of the two systems and also to determine the expected probability of mission success as compared to the desired probability of success. In order to do this some assumptions were required as being applicable to both systems. These included:

Use of Integrated Circuits - Because all of the circuit elements and interconnections are all contained on a single chip, it was assumed that an I.C. was one part and not the sum of the elements contained on it.

Each System is a Pure Series System - Thus the failure rates of individual subsystems were totaled to obtain the entire system failure rate. Failures were considered to occur at random so that the exponential distribution of failure could be applied.

Failure Rates - The failure rates used were those which were best substantiated. For conventional parts in the equipment, such as resistors and diodes, Mil-Handbook 217 rates were applied. The rates chosen were the average failure rate goal set by the manufacturer of Minuteman parts. Some of these goals have been achieved; all appear to be in the foreseeable future. The failure rate applied to Integrated Circuits was .01%/1000 hours per flat pack. This failure was based on one year's testing by the Signetic Corp. More optimistic rates were predicted but no substantiating data was found.

Launch Phase - For purposes of this study, the launch phase portion of the mission was not considered. The success of enduring this portion of flight is basically dependent on manufacturing and packaging techniques and has been successfully demonstrated many times.

4.7.2 Comparison of Systems

4.7.2.1 Method of Comparison

The desired mission was given to be a minimum of 5 year life with 90% probability of success. In order to achieve this goal, a system would be required to have a failure rate of .2397%/1000 hours. This is approximately $\frac{1}{2}$ the failure rate which can be expected in an airborne radar receiving tube or the failure

rate of a paper capacitor in a fire control radar.

A parts count was made of each subassembly of both systems. The relative complexity of each subassembly to the entire system was determined. Based on this degree of complexity, a required failure rate for each subassembly was then computed. These totaled to .2397% 1000 hours. These computed failure rates are the ones which each subassembly must have in order to meet the 5 year life requirement. This also implies that no redundancy or other improvement techniques are used.

To determine what could be expected, each part was assigned an optimistic, yet substantially realistic failure rate. These were summed and compared to the desired system requirements. As can be seen in Figure 4.7-1 the expected failure rate for the dual flip system is approximately 38 times, and the vertical system 48 times, greater than .2397%/1000 hours required. Figure 4.7-2 shows the total system failure rates which would be required for a life of 1 to 10 years with a 90% probability of success. It can be seen that for each added year of desired system life the failure rate is $\frac{1}{2}$ that of the preceding year. For a system to meet the goal of 5 year operation and $P_S = .9$ it would have to have an MTBF of 417,143 hours. Figure 4.7-3 indicates various MTBF required for 1 to 10 years operation.

4.7.2.2 Results of Comparison

Using the reliability equation, $R = e^{-\lambda t}$ where λ is system failure rate and t is the system mission time, the following probabilities of success were obtained.

	1 year	5 years
Dual Flip	R = 44%	R = 1.7%
Vertical	R = 36%	R = 0.6%

Using the same equation and assigning an R = 90% the life expectancy for the two systems are as follows:

Dual Flip = 1133 hours or 47 days

Vertical = 902 hours or 37 days

Figure 4.7-4 can be used to compare these results to other satellites. Figure 4.7-4 represents data from 49 satellites out of 184 attempted launchings. Thirty-three

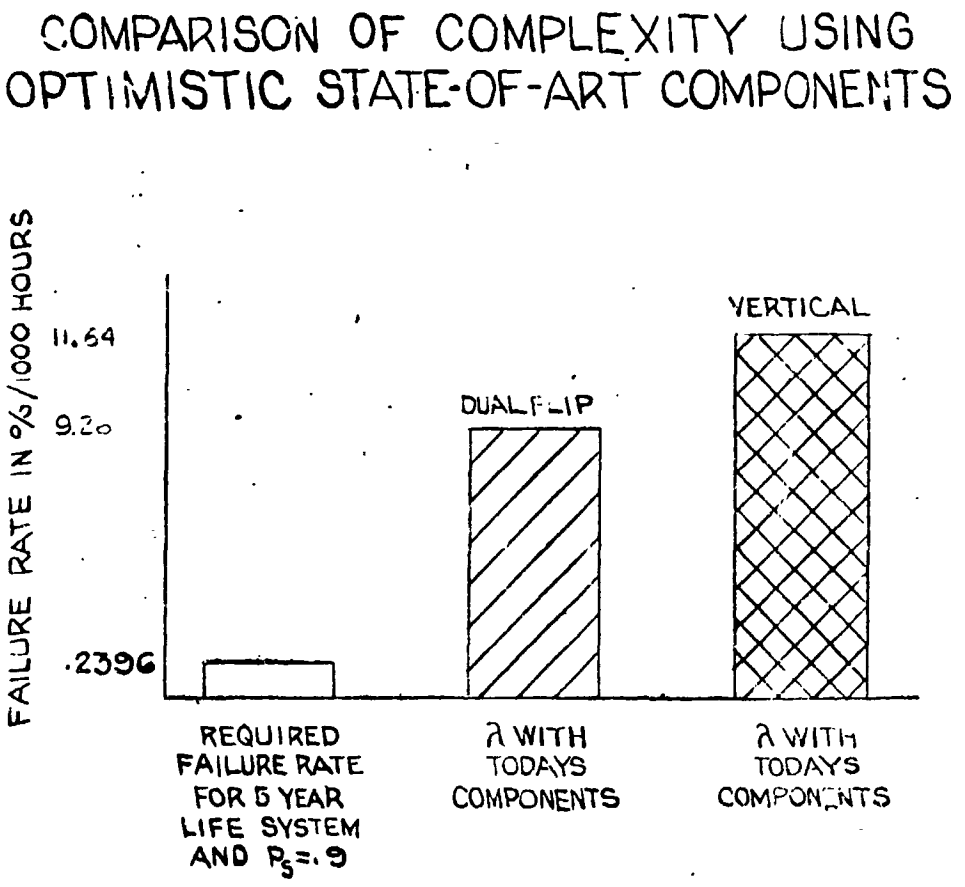

Figure 4.7-1 Failure Rate Comparison

of the 49, or more than one half of them, had failed in less than 4 months. Failure is defined as being no longer capable of transmitting any useful data from any experiment on board. Initial or partial failure occurred much sooner than this.

4.7.3 Reliability Growth Potentials

The inherent characteristics of the Orbit Position Control system will permit and foster the reliability growth potential of the system. The system is predominately digital in nature with no items experiencing high electrical stresses and hence of greater reliability. Mil-Std-756 emphasizes the expectation of improved item failure rates when used in digital applications. Capitalization of the basic reliability features of the design has been obtained by minimizing the electro-mechanical part applications in the system to two non-critical relays and by elim-

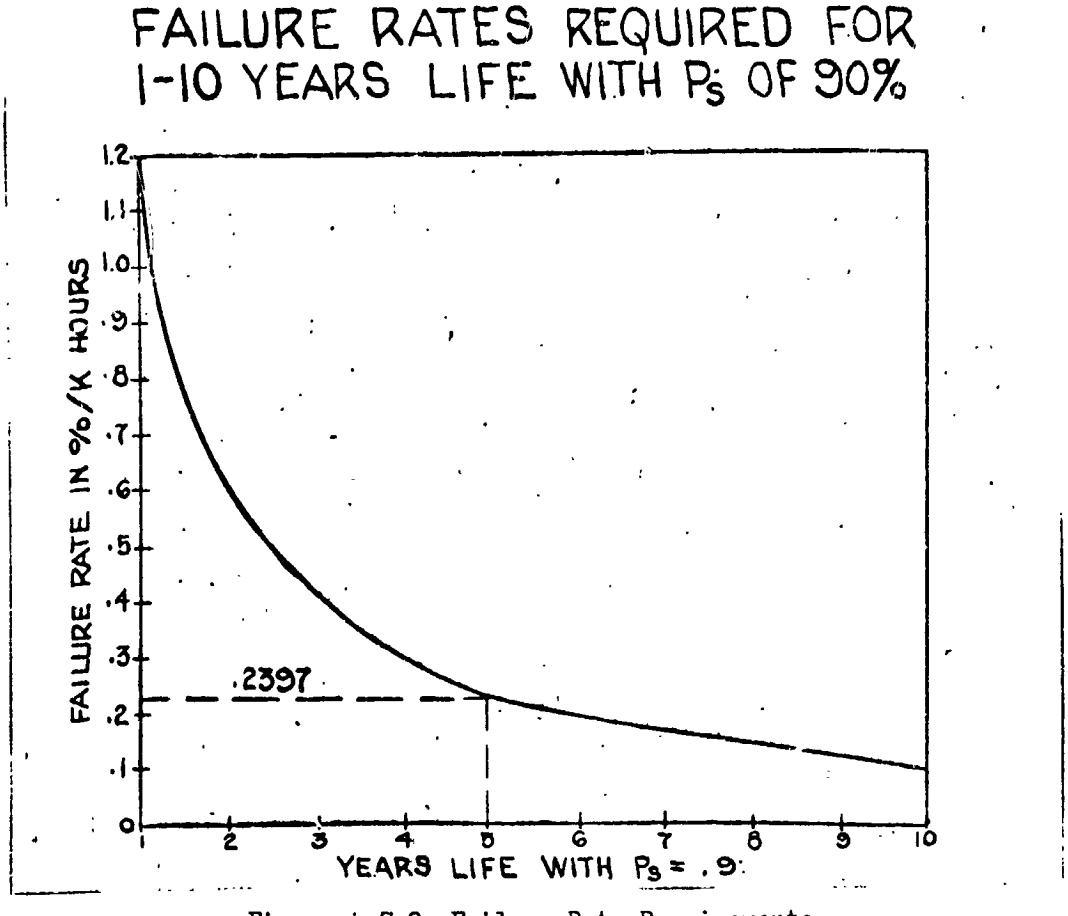

Figure 4.7-2 Failure Rate Requirements

inating failure prone decision switching functions. The life of the system, especially important for an Orbit Position Control system, has been enhanced by reducing those parts in the design where an early life wearout mechanism exists. Full attention can now be devoted to those parts where a known wearout mechanism exists, such as in the power supplies and sun sensors, to eliminate this reliability problem. Perhaps the greatest reliability growth potential feature of the system is the extensive use of integrated circuits. Use of integrated circuits permits redundancy of critical circuits with negligible penalties in space and weight requirements. Thus the inherent characteristics of the system will foster reliability growth.

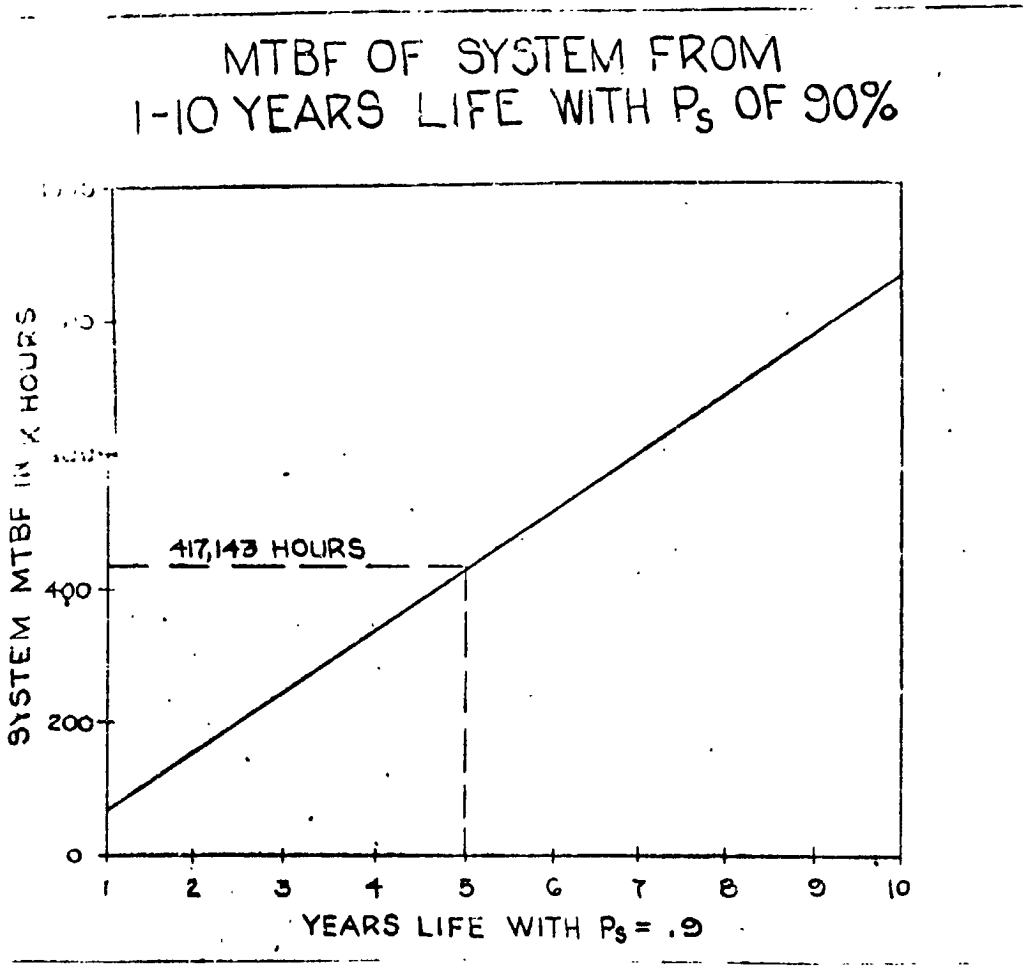

Figure 4.7-3 MTBF Requirements

4.7.4 Redundancy

Possibly the area wherein greatest reliability gains can be made is through the use of redundancy. Preliminary studies made indicates that the desired mission of 5 years life with P_S = 90% can be achieved through considerable redundancy. This study is as follows:

Assumptions made include those stated in paragraph 4.7.1 plus the following: (1) The number of redundant units, x, is such that there is equal probability of system failure from each of the subsystems. (2) All redundant units are active although only one is required for system operation. (3) No allowances were made for interconnection or interaction of units. (4) One entire system is composed of 10 subunits. The number of redundant units is such that their combined

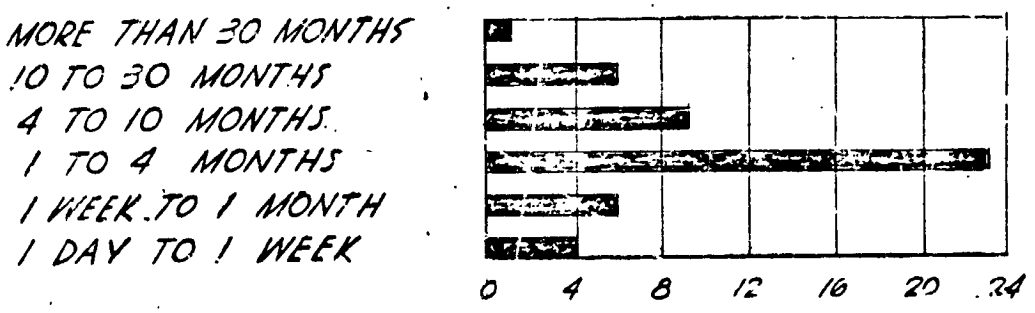

Figure 4.7-4, Satellite Failure History

reliability is just sufficient to exceed $(P_B)^{1/10} = .9^{1/10} = .9895$. With these assumptions and using the equation for parallel-series circuits

$$P_B = \left[1 - (1 - P)^x\right]^N$$

where $P_B = .9$, $N = 10$ $(1 - P)$ = failure rate of 1 unit. We obtain the following number of redundant units:

Unit	Dual Flip	Vertical
Receiver	3	3
Decoder	1	1
Data Storage	6	6
D-A Converter	3	3
Clock	2	2

Unit	Dual Flip	Vertical
Cross Multiplier	6	25
Sun Sensors	15	15
Damping Circuits	8	7
Torquing Circuits	4	4
Power Supply	7	7

4.7.5 Suggested Approach

Figure 4.7-5 depicts projected failure rates for integrated circuits. This improvement over today's circuits, plus the increased application of their use can only lead to improved system reliability. However, considerably more than overall reduction in generic failure rates is required for reliability improvements. The advances made in parts and their selection for the applicable system has been clearly demonstrated by the Bell Telephone Company in their Atlantic telephone cable. In brief, a three-phase program extending over a long period of time was their key to success. This program required:

(1) Proof of reliability potential of each part itself. Each part is severely tested for mechanical durability. These tests would be more severe than the part will endure during launch. They are then subjected to an equivalent proton and electron bombardment which they will experience in the satellite orbit. The parts then are evaluated to determine the reliability potential of the design.

(2) The second step is a screening and pre-aging phase to ferret out those parts not rejected earlier by quality control. All parts are subjected to mechanical shock and vibration tests. A portion of them is then selected for temperature test. The median temperature for failure is used for lot control and comparison. All parts receive a short term of high temperature aging.

(3) Parts which are acceptable through Phase 1 and 2 are then placed on an extended life test simulating in-use conditions. The quantity of parts in these tests is many times greater than will be required in the system. During life testing, the part's characteristics are frequently measured. Those parts exhibiting no change

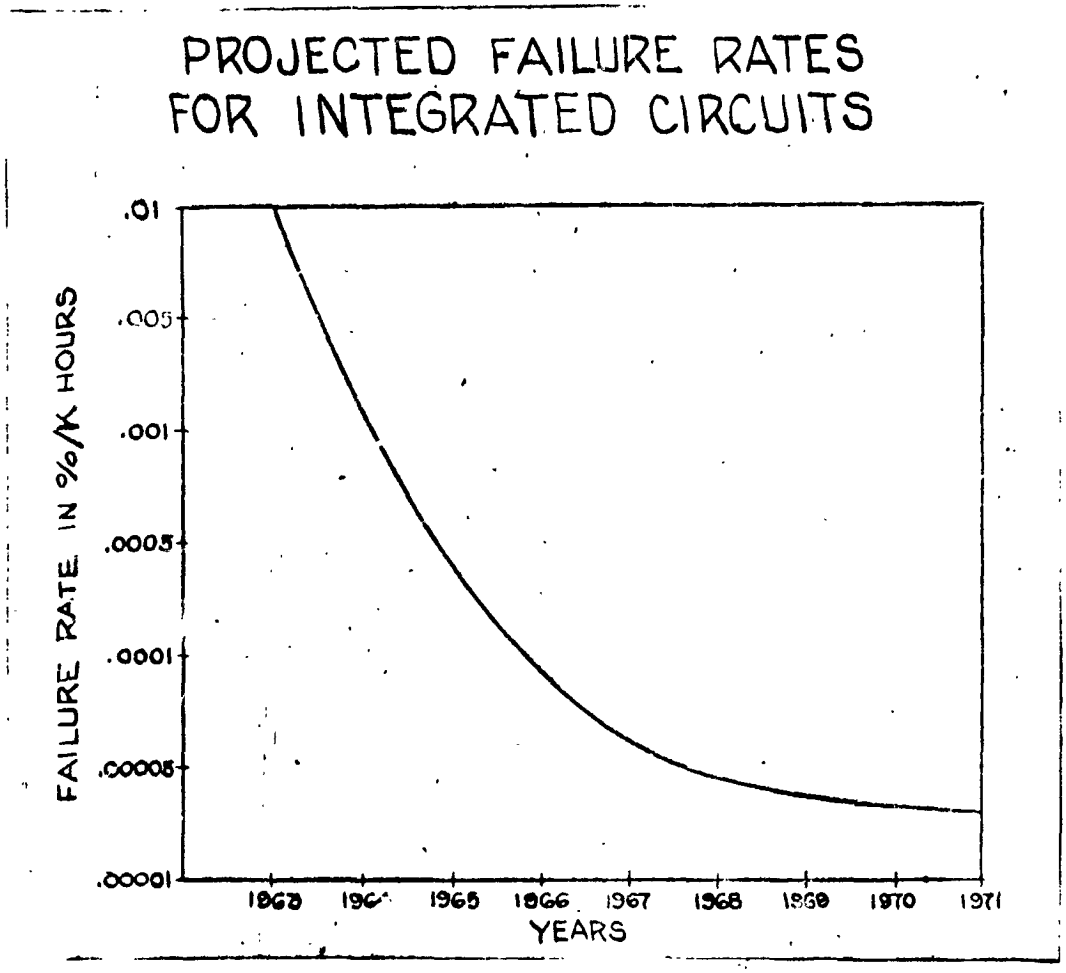

Figure 4.7-5 Projected Failure Rates

of characteristics during test are chosen for use in the system.

This conservative approach to the problem of parts selection has been proven successful, and coincident with an inherently reliable design offers the greatest promise of meeting the long life requirement of the Orbit Position Control System.

4.8 ORBITAL COMPUTATIONS

4.8.1 Orbit Determination Program

In order to study the effects of solar pressure on a spherical balloon type satellite, a digital computer program originally developed by the University of California Radiation Laboratory[1] was modified and used. This program, in its original form, performed a Cowell's method integration on the equations of motion and provided upon option the inclusion of the earth's bulge, atmospheric drag, and the gravitational effects of the sun, moon and other planets.

Since Cowell's method does not lend itself to the accurate computation of a large number of orbits, a more accurate method was needed. Encke's method was chosen because of the relative ease of program conversion and the greater accuracy that it offered. The program was also modified to include upon option the effects of solar pressure on a uniformly coated sphere and the effects of direct solar pressure, earth emitted pressure, earth reflected pressure and reradiation pressure on a patterned satellite.

A macro diagram of the program in its present form is shown in figures 4.8-1 and 2. This diagram by no means shows all the details contained in the program but is intended to show in general how the program is implemented and the order in which the computations are made. The program in this form was used to make the maximum eccentricity and mobility computation which are described later.

These computations pertaining to the force table option will be explained in detail in section 4.8.4. Associated with the program are a set of ephemerus tapes. These are magnetic tapes containing ephemerus information of the perturbing bodies (sun, moon, etc.) for the years 1800 A.D. through 2000 A.D.

The integration routine used by the program serves a dual purpose. Besides integrating the equations of motion, it also acts in a monitor like fashion

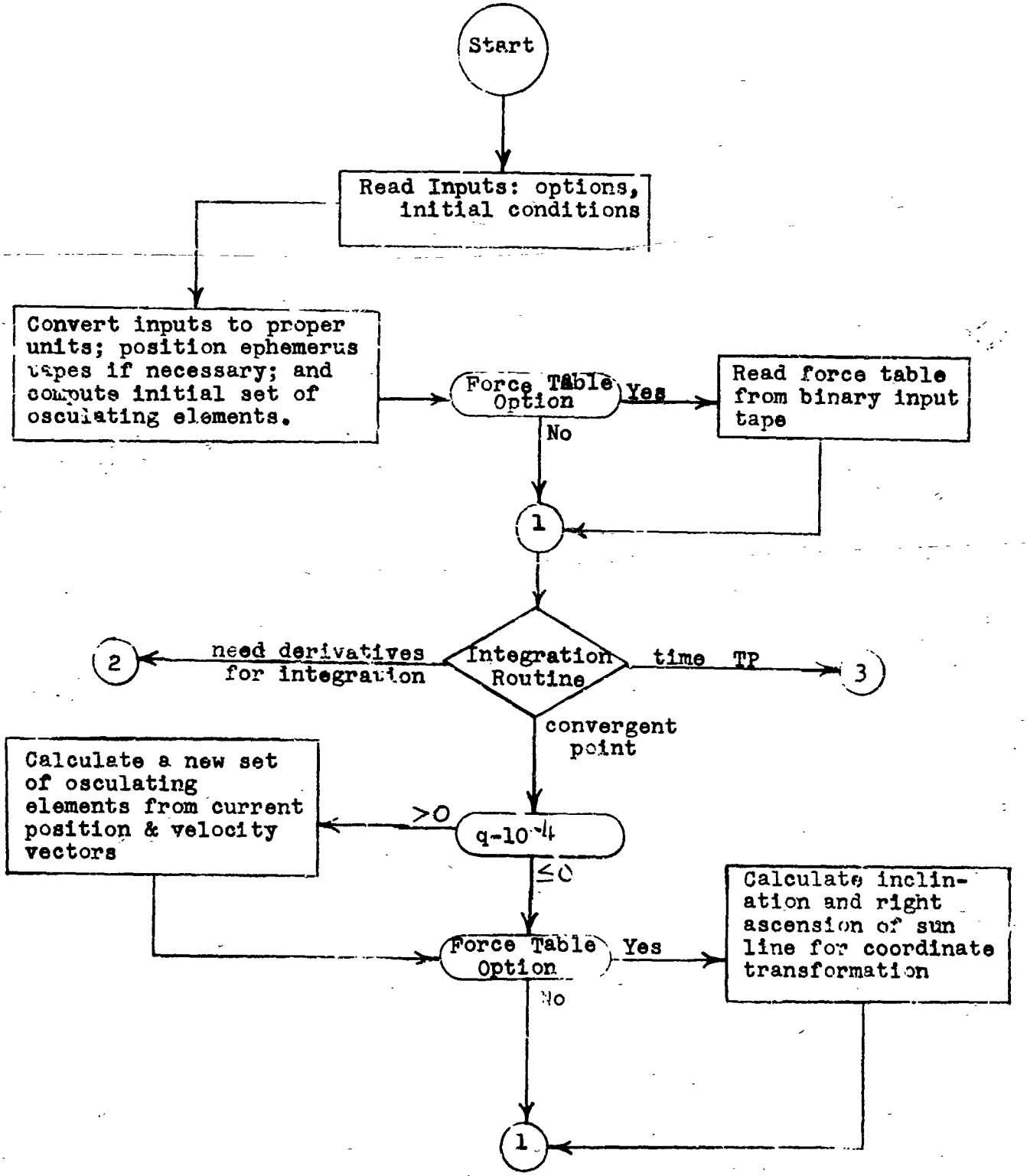
Start
Read Inputs: options, initial conditions
Convert inputs to proper units; position ephemerus tapes if necessary; and compute initial set of osculating elements.
Force Table Option
Yes
Read force table from binary input tape
No
1
Integration Routine
need derivatives for integration
2
time TP
3
convergent point
Calculate a new set of osculating elements from current position & velocity vectors
>0
q-10^-4
≤0
Force Table Option
Yes
Calculate inclination and right ascension of sun line for coordinate transformation
No
1

Figure 4.8-1

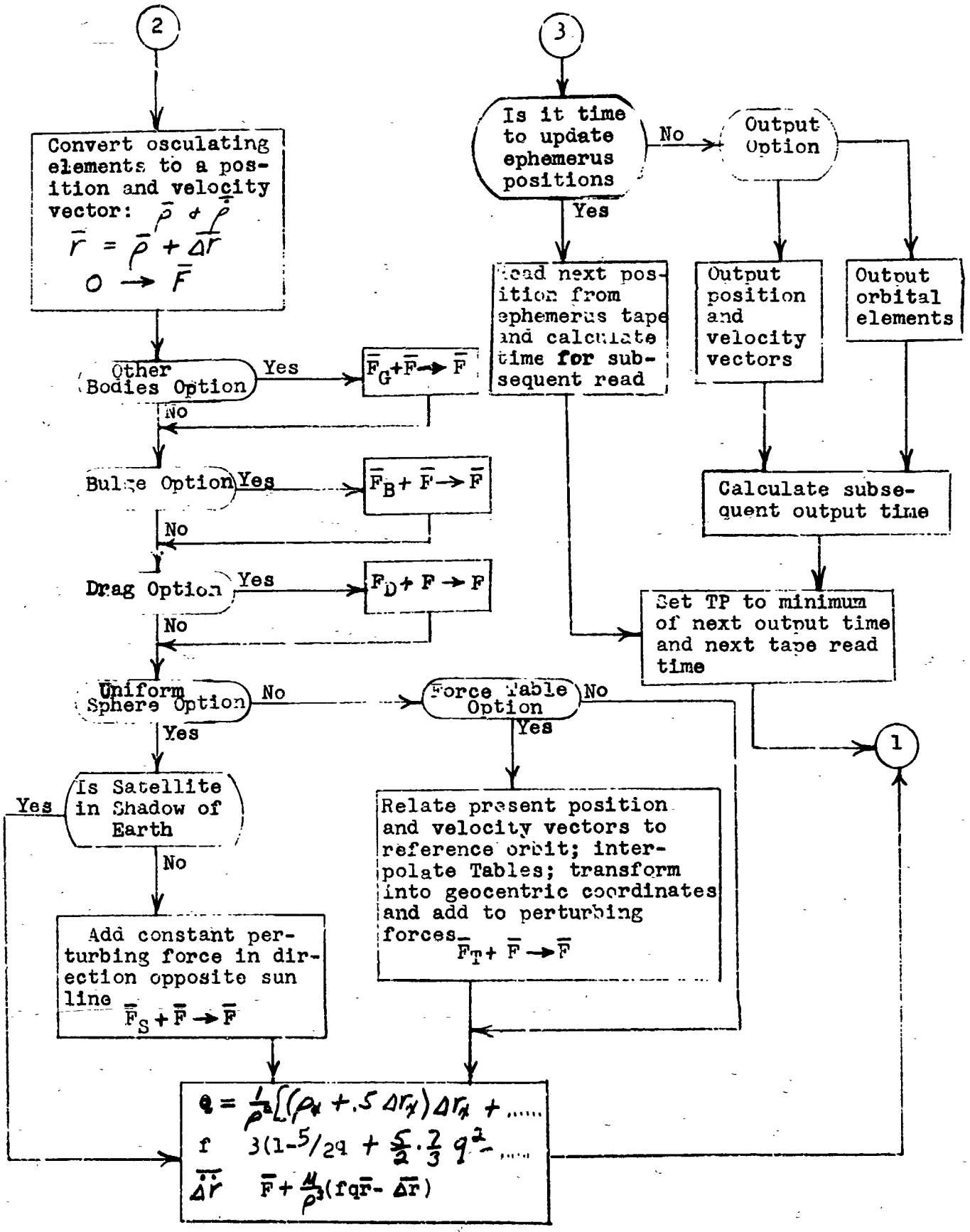
2
Convert osculating elements to a position and velocity vector: $\bar{\rho}$ & $\dot{\bar{\rho}}$
$\bar{r} = \bar{\rho} + \Delta\bar{r}$
$0 \rightarrow \bar{F}$
Other Bodies Option
Yes
$\bar{F}_G + \bar{F} \rightarrow \bar{F}$
No
Bulge Option
Yes
$\bar{F}_B + \bar{F} \rightarrow \bar{F}$
No
Drag Option
Yes
$F_D + F \rightarrow F$
No
Uniform Sphere Option
No
Yes
Is Satellite in Shadow of Earth
Yes
No
Add constant perturbing force in direction opposite sun line
$\bar{F}_S + \bar{F} \rightarrow \bar{F}$
Force Table Option
No
Yes
Relate present position and velocity vectors to reference orbit; interpolate Tables; transform into geocentric coordinates and add to perturbing forces
$\bar{F}_T + \bar{F} \rightarrow \bar{F}$
$q = \frac{1}{\rho^2}[(\rho_4 + .5\Delta r_4)\Delta r_4 + \ldots$
$f \quad 3(1 - 5/29 + \frac{5}{2}\cdot\frac{2}{3}q^2 - \ldots$
$\ddot{\Delta r} \quad \bar{F} + \frac{M}{\rho^3}(fq\bar{r} - \Delta\bar{r})$
3
Is it time to update ephemerus positions
No
Yes
Output Option
Read next position from ephemerus tape and calculate time for subsequent read
Output position and velocity vectors
Output orbital elements
Calculate subsequent output time
Set TP to minimum of next output time and next tape read time
1

Figure 4.8-2

controlling the flow through the program. Three separate exits from the integration routine are provided and program flow is controlled accordingly. One exit path is taken whenever derivatives are needed for the integration procedure, and, hence, this path must contain the evaluation of the perturbing forces. A second exit path is taken after each successful integration step. The third exit path is taken when the value of time becomes equal to an argument of the subroutine called TP. Operations which must be performed at some special time such as outputing and updating of the ephemerus information are included in this path.

The integration routine itself uses a fourth-order Runge-Kutta technique with an automatically controlled step size to perform the integration over one step within specified error limits.

In Encke's method, nominal position and velocity vectors are calculated at each time point from the set of osculating elements. Only the deviations from the nominal are integrated as a function of the perturbing forces. The quantity q is a measure of the deviations from nominal. If this quantity becomes greater than .5, it causes an infinite series expansion to diverge and the computations to blow up. In order to prevent this from happening, it becomes necessary to periodically reset the deviations to zero by calculating a new set of osculating elements. Based on experimentation with a set of runs, it was found that reseting the deviations whenever q became greater than 10^{-4} provided the best combination of accuracy and machine running time.

The other bodies option can be used to include the perturbing effects of the sun, moon or other planets. The perturbations are calculated in the following manner

$$\bar{F}_G = M_s \sum_i K^2 M_i \left(\frac{\bar{r}_i - \bar{r}}{\rho_i^3} - \frac{\bar{r}_i}{r_i^3} \right)$$

where $\bar{r}_i$ is the radius vector from the center of the earth to the ith perturbing body; $\bar{r}$ is the radius vector to the satellite and M_i is the mass of the ith perturbing body.

The bulge option of the program includes the effects of earth's bulge calculated from the second spherical harmonic in the following fashion.

$$\bar{F}_B = M_s \frac{\mu \bar{r}}{r^3} \left[J_2 \left(\frac{R}{r}\right)^2 \frac{3}{2} \left(\bar{C} - 5 \frac{\bar{z}^2}{r^2}\right) \right]$$

where J_2 is the coefficient of the second harmonic of the earth's potential function; $\bar{C}$ is a constant vector with components equal to 1, 1, and 3; and R is the equatorial radius of the earth.

The drag option of the program calculates the perturbing force due to atmospheric drag in the following manner.

$$\bar{F}_D = -\frac{1}{2} M_s C_D \sigma \left(\frac{A}{M}\right) V \bar{V}$$

where C_D is the coefficient of drag of the satellite, (A/M) is the area to mass ratio of the satellite and $\bar{V}$ is the velocity vector of the satellite.

4.6.2 Comparison with Echo I Observations

A comparison of program results using the uniform sphere option with Echo I observations offered an excellent means of checking the accuracy of the program. A force to mass ratio of 1.94×10^{-4} ft./sec^2 was calculated for the Echo I and put into the program along with a published set of orbital elements[2] as a starting point.

The results of this comparison are shown in figure 4.6-3 and 4. The solid black lines are the published Echo I orbital elements while the broken lines are the results of the computer runs. As can be seen all the elements appear to compare very closely out to 10 days with the possible exception of inclination angle which is on an exaggerated scale. Furthermore, the comparison remains fairly close out to 60 days where the period begins to decay more rapidly. In particular, the right ascension and argument of the perigee compare almost exactly for the entire length of the run.

A large number of phenomenon could have caused the deviations between the predicted and observed elements. Among them are the variations in the solar

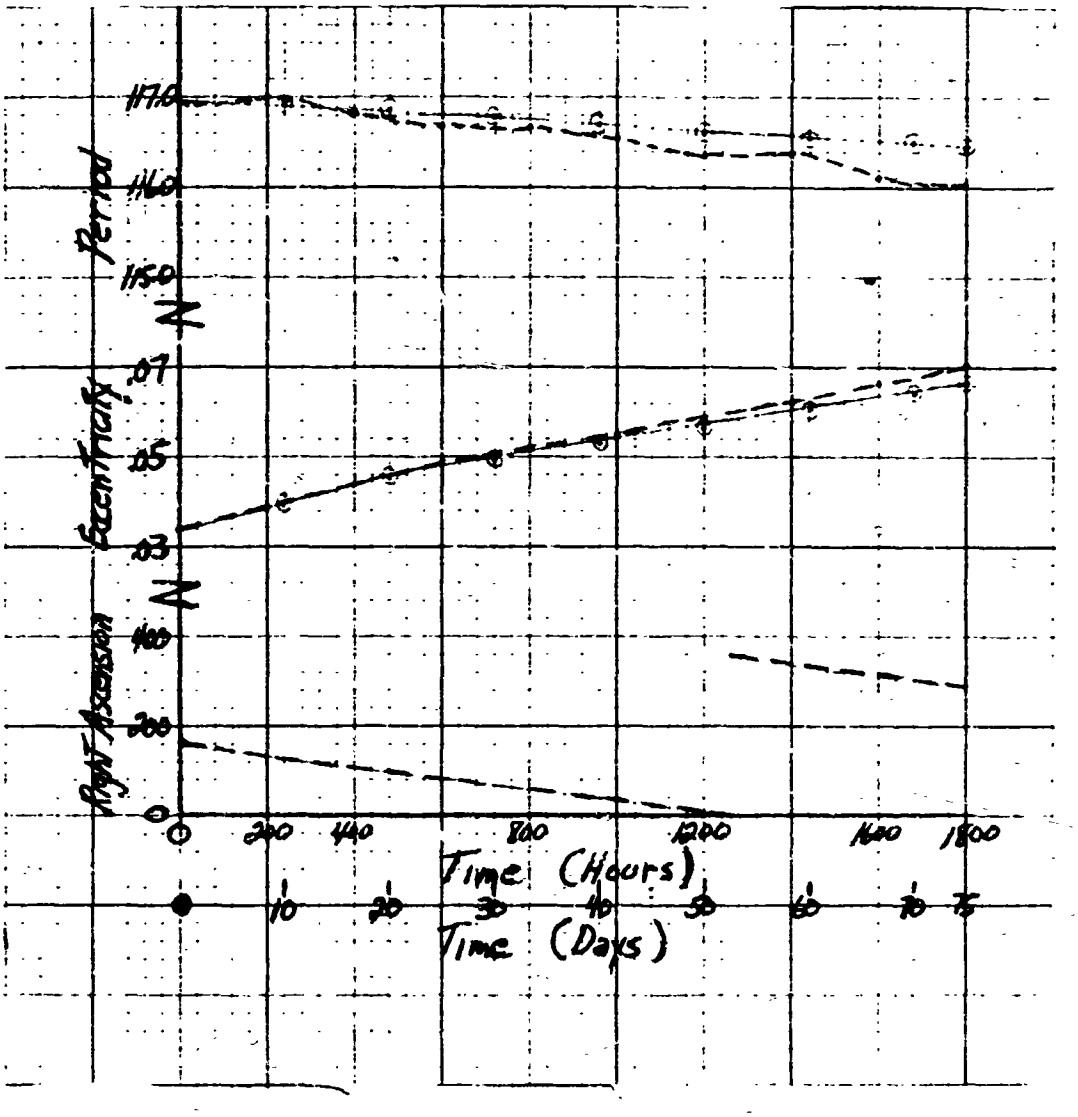
Period
Eccentricity
Right Ascension
1170
1160
1150
.07
.05
.03
200
0
200
440
800
1200
1600
1800
Time (Hours)
10
20
30
40
50
60
70
75
Time (Days)

Figure 4.8-3

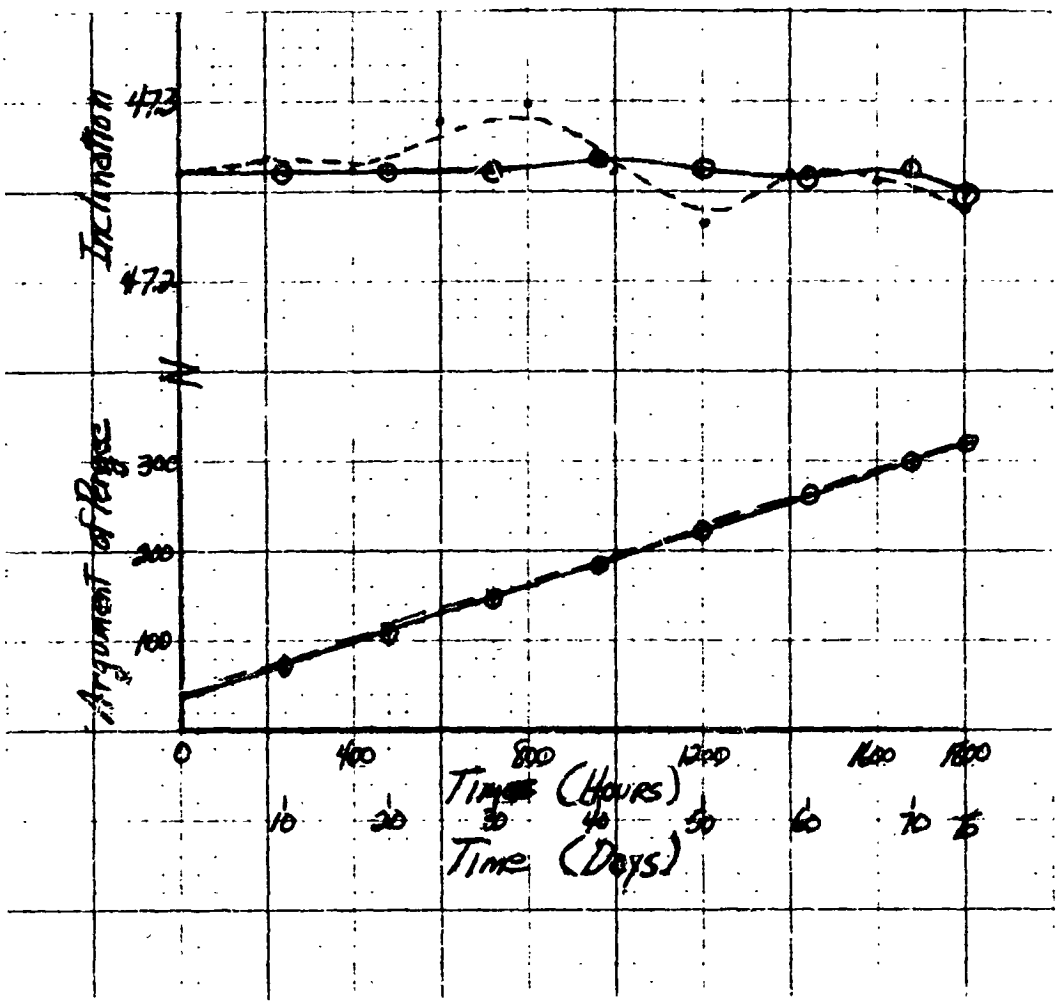
Inclination
473
472
Argument of Perigee
300
200
100
0
400
800
1200
1600
1800
Time (Hours)
10
20
30
40
50
60
70
75
Time (Days)

Figure 4.8-4

flux field, the neglecting of the secondary radiation pressures or the loss of accuracy in the integration procedure. It is very difficult to determine which one or which combination of these phenomena is causing the deviations. There are indications, however, that the integration does lose accuracy after some period of time. From these results, accuracy appears to be very good out to 40 days and reasonably good out to 60 days.

4.8.3 Maximum Eccentricity Computations

In order to attain efficient station keeping of a set of satellites staggered in approximately the same orbit, it becomes necessary to maintain the eccentricity of the orbit within some acceptable limits. As the eccentricity of an orbit becomes larger, the angular differences between two satellites will vary more and more. For instance, a satellite in an orbit of eccentricity equal to .05 may appear to move as much as 5.5 degrees with respect to a satellite in a circular orbit with the same semi-major axis. Furthermore, two satellites in orbits with the same semi-major axis and eccentricity of .05, but with the arguments of the perigee 180° out of phase may appear to move as much as 11 degrees with respect to each other.

These figures show the necessity for maintaining the satellites in as nearly circular orbits as possible. For this reason computations were made in order to estimate the maximum eccentricity which could be expected as a function of orbital inclination, satellite weight and satellite altitude.

Obviously, the best way to calculate the maximum eccentricity would be to use the orbital prediction program with the uniform sphere option. A circular orbit would be used as a starting point and the program would be run until a maximum eccentricity had been reached. However, this is not practical for two reasons. First, since the period of the eccentricity is so long (typical number is 200 days), the amount of computer time needed for a run of this type becomes prohibitive. Second, also because the period of the eccentricity is so long, a loss of accuracy in the integration procedure occurs after a period of time and the results become meaningless.

For these reasons it became necessary to approximate the maximum eccentricity in some manner. From the Echo I observations and from other computer runs, it became apparent that the eccentricity of the orbit varied between maximum and minimum values in a very nearly linear fashion. The maximum eccentricity can then be estimated by calculating the period of the eccentricity and extrapolating the slope of the eccentricity up to its maximum point.

The method for calculating the period of the eccentricity is illustrated in figure 4.8-5. If the circular orbit shown by the solid circle is used as a starting point, then initially solar pressure will add energy to the orbit in the vicinity of the point P. This will tend to create an apogee at a point 180 degrees away. Similarly, solar pressure will subtract energy from the orbit in the region of the orbit opposite the point P, thus tending to create a perigee near the point P. If both the orbit and the sun were to remain stationary in inertial space, it can be seen that the eccentricity of the orbit would keep increasing indefinitely and would soon become too large to be able to control the relative positions of a set of satellites.

However, the point of the perigee moves with relation to the sun line due to three separate considerations. First, the precession of the right ascension causes the perigee to move at a rate $\dot{\Omega}$ with respect to the sun line. The motion of the argument of the perigee also causes the perigee to move at a rate $\dot{\omega}$ with respect to the sun line and the apparent motion of the sun causes the sun line to move at a rate ω_s with respect to the perigee. When the combination of these three motions have caused the perigee to move 180 degrees with respect to the sun line, the solar pressure force will begin subtracting energy in the vicinity of the perigee and adding energy in the vicinity of the apogee thus causing the eccentricity of the orbit to decrease. Thus the period of the eccentricity is defined in the following manner.

$$(\dot{\Omega} + \dot{\omega} - \omega_s)\, P_e = 360$$

where P_e is the period of the eccentricity and all the angular rotations are defined as positive clockwise. This estimation procedure was tried on the Echo I data and

$$(\dot{\Omega} + \dot{\omega} - \omega_s) P_e = 360$$

Figure 4.8-5

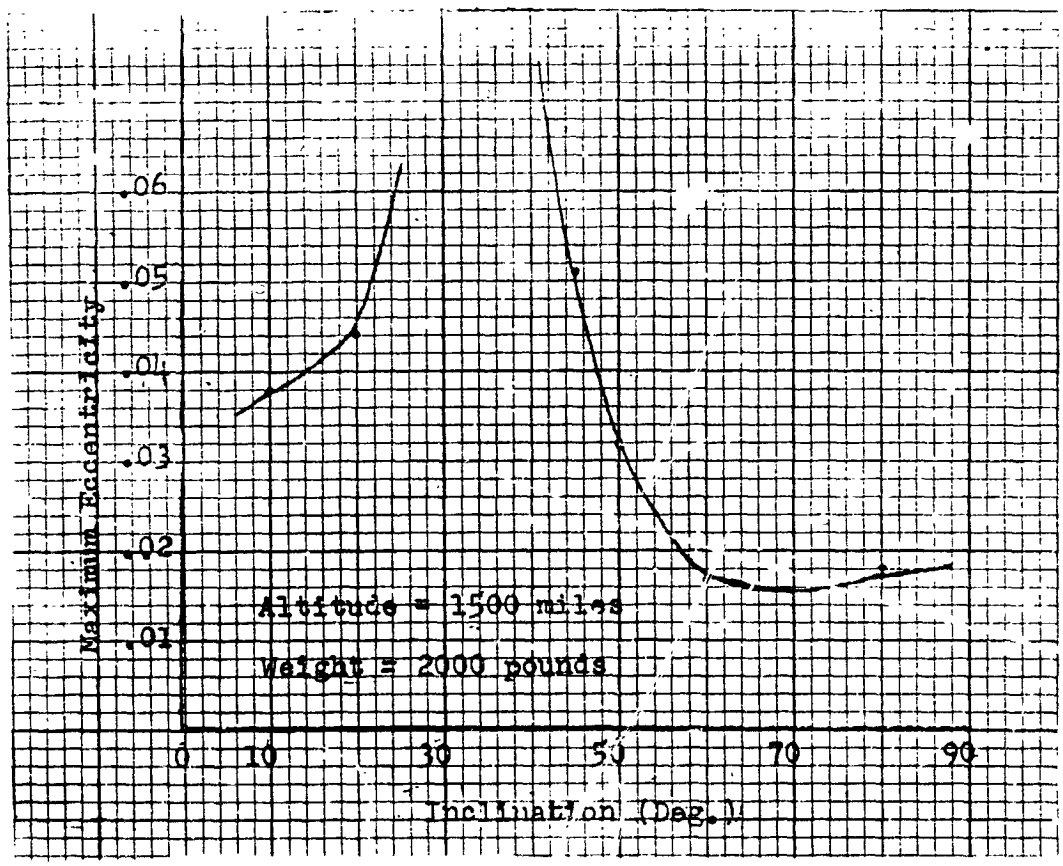
Maximum Eccentricity
.06
.05
.04
.03
.02
.01
Altitude = 1500 miles
Weight = 2000 pounds
0
10
30
50
70
90
Inclination (Deg.)

Figure 4.8-6

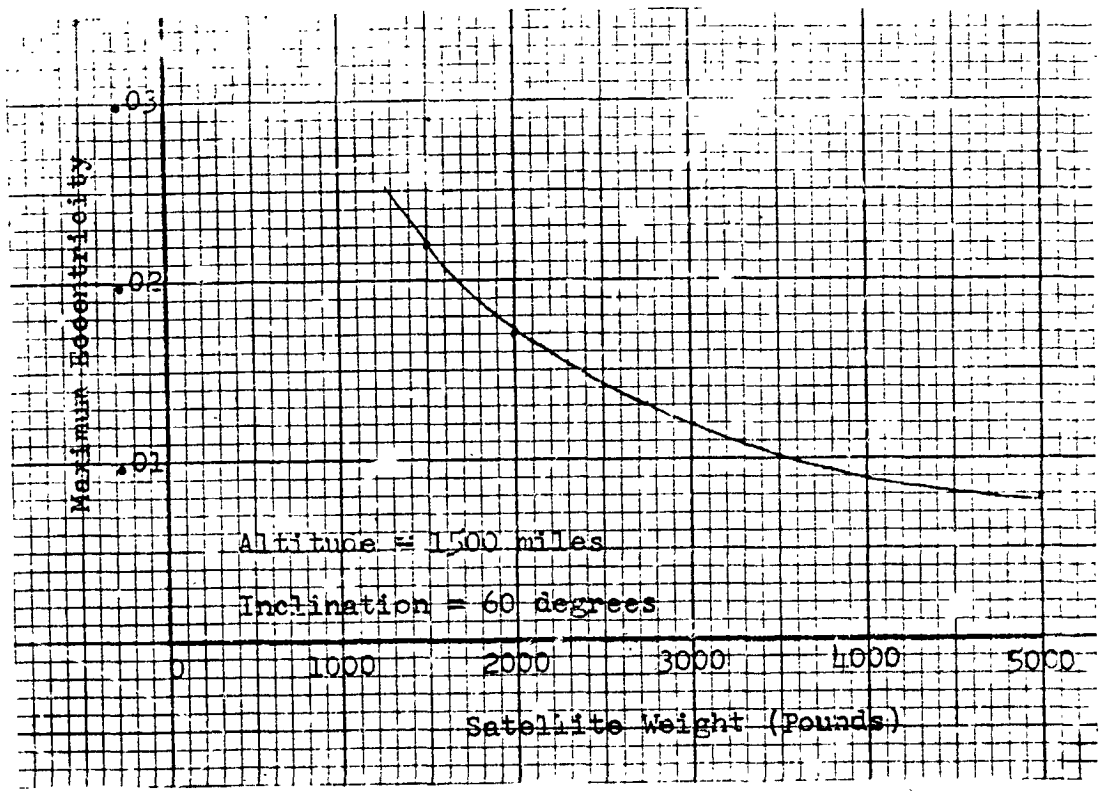
Maximum Eccentricity
.03
.02
.01
Altitude = 1,500 miles
Inclination = 60 degrees
0
1000
2000
3000
4000
5000
Satellite Weight (Pounds)

Figure 4.8-7

the results agreed very closely with the observations.

The orbital prediction program was used with the uniform sphere option to determine the slope of the eccentricity and the rates of motion of the right ascension and argument of the perigee. Figure 4.8-6 shows a curve of maximum eccentricity versus orbital inclination angle which was calculated by this procedure. These calculations were all made for a 200 foot diameter balloon with a weight ratio of about twice Echo I or 2000 pounds.

The region around 30 degrees where the maximum eccentricity becomes very large is caused by the resonance condition:

$$\dot{\Omega} + \dot{\omega} - \omega_s = 0$$

For this situation, the argument of the perigee effectively remains stationary in inertial space with respect to the sun line and the eccentricity keeps increasing indefinitely.

The curve shows that for this particular altitude of 1500 miles, the region around 60 degrees would be best for maintaining circularity of the orbit while the region around 30 degrees is not practical for station keeping purposes. Since the region of resonance is a function of altitude, the inclination angle of lowest maximum eccentricity will also vary as a function of altitude.

In figure 4.8-7 is shown a curve of maximum eccentricity versus satellite weight for a 200 foot diameter balloon at an altitude of 1500 miles and inclination angle of 60 degrees. As can be expected, the maximum eccentricity varies inversely with the satellite weight. Of course, the ability to control the satellite also varies inversely with satellite weight.

4.8.4 Mobility Study

In order to study the degree to which a particular satellite can be controlled by solar pressure forces it is necessary to calculate both the magnitude and direction of the direct solar foces, the earth emitted forces, the earth reflected forces and the reradiation forces on the patterned satellite as a function of the position and orientation of the satellite. Since the calculation

of all but the direct solar forces take a relatively large amount of computer time, it would be impossible to compute these forces directly in the orbit determination program. Thus it became necessary to develop a table of both direct solar forces and the secondary forces which would be general enough to be used for any position and orientation that might be encountered.

The method chosen was to calculate the forces on a satellite in some reference orbit which could then be related to any other orbit at the same altitude. In order to do this the reference orbit must be chosen to be in the plane of the sun line such that the points of equator crossings are at 90 degrees to the sun line. The forces on a satellite in this orbit can then be precomputed and stored in a table. In order to cover all possible positions and orientations the table must contain forces for orbit angles from 0 to 180 degrees with respect to the sun line. For each orbit angle the table must also include forces calculated for angles from 0 to 360 degrees between the axis of symmetry of the satellite and the velocity vector.

In actual computation an equational orbit with the sun directly over the equator is used as the reference orbit. The forces are precomputed in a satellite centered coordinate system which has the radius vector, velocity vector and normal as the x,y, and z axis respectively.

In figure 4.8-8 the method of relating any position and orientation to the corresponding one in the reference orbit is illustrated. The cross-hatched area of the figure represents the hemisphere of the earth that is in darkness. As can be seen the pattern of sunlight on the earth is symmetrical with respect to the sun line vector $\bar{r}_s$. The point S is some point on an orbit to be corresponded to the reference orbit which is shown as the equatorial orbit. Consider for the moment a sphere of uniform surface coating. Since the sunlight is symmetrical with respect to the sun line, the radius vector $\bar{r}$ of the satellite could be rotated anywhere around the sun line without changing the pattern of sunlight that the satellite would see. Hence a position in the reference orbit

PROPRIETARY

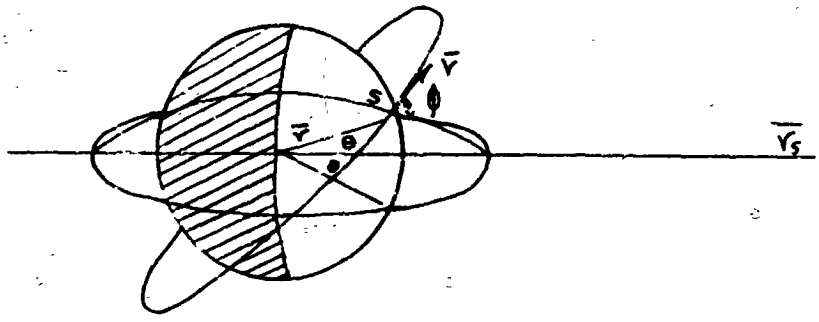

$$\theta = \cos^{-1}\left[\frac{\bar{r} \cdot \bar{r}_s}{r\, r_s}\right]$$

Figure 4.3-8

at an angle Θ with respect to the sun line where Θ is the angle between the sun line and the radius vector would see the same pattern of sunlight on the earth. The angle Θ is easily obtained in the following manner:

$$\Theta = \cos^{-1}\left[\frac{\bar{r}\cdot\bar{r}_s}{r\,r_s}\right]$$

However, with a nonuniform satellite the different surface coatings can have varying portions exposed to the sunlight pattern on the earth. In a vertically oriented control system for near circular orbits the rotation of the satellite pattern with respect to the sunlight pattern on the earth has only one degree of freedom. Hence, the angle σ between the axis of symmetry (velocity vector) and a great circle through the sun line will describe the orientation of the satellite in the reference orbit.

In figure 4.8-9 is shown a cutaway view of figure 4.8-8 in the plane of the sun line and the radius vector and a side view of that in the plane of the velocity vector. The vector $\bar{a}$ represents the direction of the great circle at the point of intersection with the radius vector and can be calculated as follows:

$$\bar{a} = \frac{r}{r_s \cos\Theta}\,\bar{r}_s - \bar{r}$$

The angle σ is then the angle between the vector $\bar{a}$ and the velocity vector:

$$\sigma = \cos^{-1}\left[\frac{\bar{a}\cdot\bar{v}}{av}\right]$$

Since four quadrant resolution is needed on the angle σ a second vector $\bar{b}$ can be made perpendicular to both the radius vector and $\bar{a}$ by taking the cross product:

$$\bar{b} = \bar{r} \times \bar{a}$$

Then if the angle between $\bar{b}$ and the velocity vector is less than 90 degrees the angle σ will be in the third or fourth quadrants.

If $\bar{b}\cdot\bar{v} <$ then $\sigma < 0$

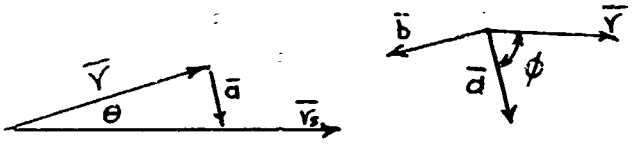

$$\bar{a} = \frac{r}{r_s \cos\theta}\,\bar{r}_s - \bar{r}$$

$$\bar{b} = \bar{r} \times \bar{a}$$

$$\phi = \cos^{-1}\left[\frac{\bar{a}\cdot\bar{r}}{a\,r}\right]$$

IF $\bar{b}\cdot\bar{r} < 0$ THEN $\phi < 0$

Figure 4.8 - 9

This procedure then gives the forces on the satellite in the coordinate system of the reference orbit. In order to be used in the orbital prediction program the forces must be transformed into a geocentric coordinate system. In figure 4.8-10 are shown the three rotations which must be made in the transformation.

The first rotation made is a clockwise rotation about the z' axis through an angle 90-G degrees. This defines a double prime coordinate system which has its x axis in the plane of the equator. If next a clockwise rotation about the x" axis through an angle i, which represents the inclination of the reference orbit with respect to the equator, is made a triple prime coordinate system is defined which has both its x and y axes in the plane of the equator. Furthermore, the y" axis will be parallel to the projection of the sun line in the plane of the equator. Thus a final rotation about the z" axis through an angle Ω, which is defined as the angle between the sun line and the positive y axis of the geocentric coordinate system. The angles i and Ω are expressed as follows:

$$i = \sin^{-1}\left(\frac{r_{s_z}}{r_s}\right)$$

$$\Omega = \tan^{-1}\left(\frac{-r_{s_x}}{r_{s_y}}\right)$$

and the forces can be transformed to the geocentric by:

$$\bar{F} = T_\Omega T_i T_{(90-\theta)} \bar{F}'$$

where $\bar{F}'$ are the forces in the reference orbit system, $\bar{F}$ are the forces in the geocentric system and $T_\Omega T_i T_{(90-\theta)}$ is:

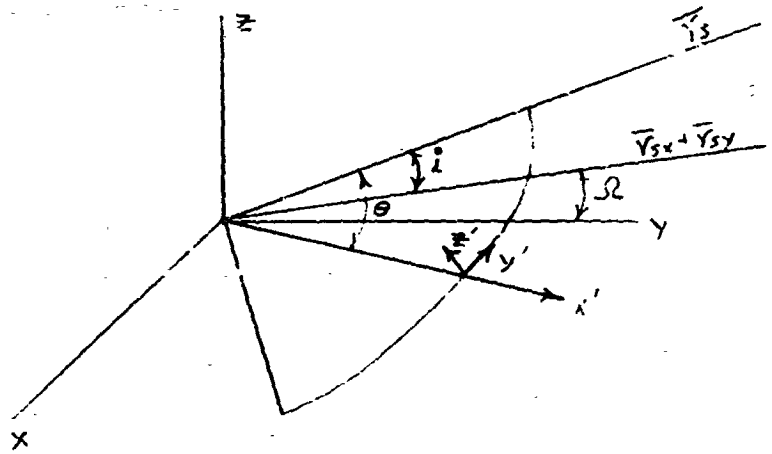

$$i = \sin^{-1}\left(\frac{r_{sz}}{r_s}\right)$$

$$\Omega = \tan^{-1}\left(\frac{-r_{sx}}{r_{sy}}\right)$$

Figure 4.8 -10

$$T_{\Omega} T_i T_{(90-\theta)} = \begin{bmatrix} \cos\Omega \sin\theta & -\cos\Omega \cos\theta & \sin\Omega \sin i \\ -\sin\Omega \cos i \cos\theta & -\sin\Omega \cos i \sin\theta & \\ \sin\Omega \sin\theta & -\sin\Omega \cos\theta & -\cos\Omega \sin i \\ +\cos\Omega \cos i \cos\theta & +\cos\Omega \cos i \sin\theta & \\ \sin i \cos\theta & \sin i \sin\theta & \cos i \end{bmatrix}$$

The model described above has been used to make computer runs showing the magnitude of mobility which can be expected. In the runs shown here only the direct solar force was included in the force table. This, however, is enough to show the degree of mobility which can be expected since the total mobility can be made either greater than or less than that calculated with only the direct solar forces by adjusting the coating parameters.

In figures 4.8-11 and 4.8-12 are shown the results of two mobility runs. These runs were made on a hemispherically coated satellite with emissivities of .90 and .50 for the two surfaces. The satellite was started in a circular orbit with an altitude of 1500 miles and an inclination angle of 45 degrees and allowed to run under the vertical control system.

Two separate runs were made with the axis of symmetry of the satellite at 0 and 180 degrees with respect to the velocity vector. When the hemisphere with the higher emissivity is directed along the velocity vector the solar pressure forces tend to decrease the energy in the orbit, thus increasing the period of the satellite and causing it to appear to slow down with respect to another satellite. This configuration will be referred to as the slow mode. Similarly, when the hemisphere with the lower emissivity is directed along the velocity vector the solar pressure forces tend to increase the energy in the orbit, thus causing it to appear to speed up with respect to another satellite. This configuration will be referred to as the fast mode.

In figure 4.8-11 is shown a plot of the orbital period for both the slow mode and the fast mode runs. The solid black line denotes the slow mode run

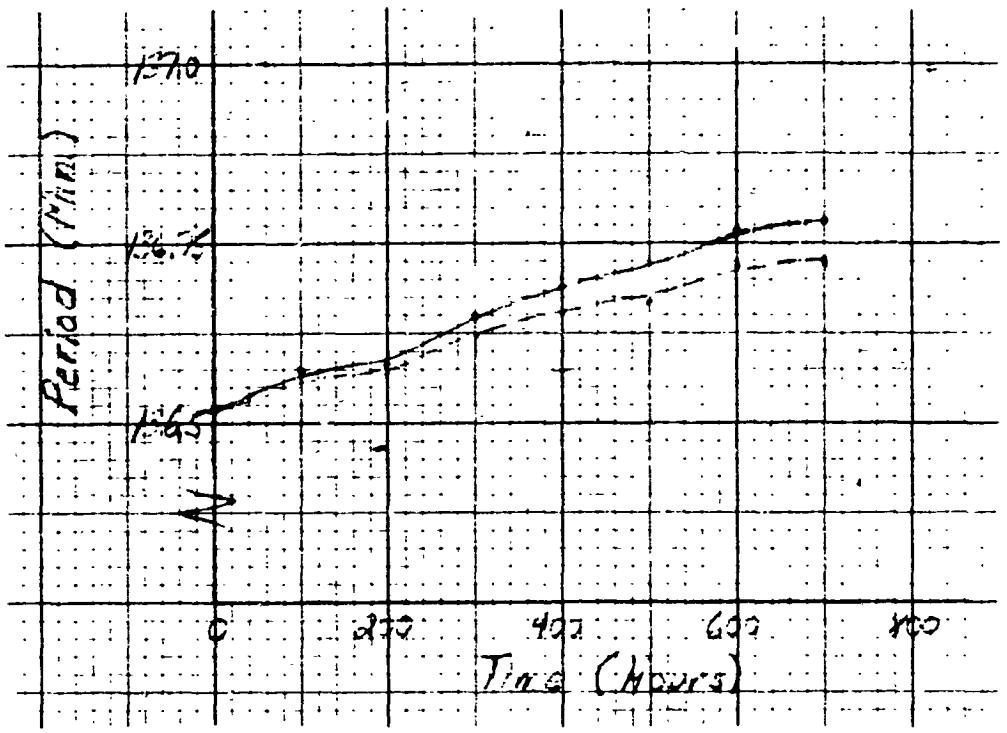

Figure 4.8-11

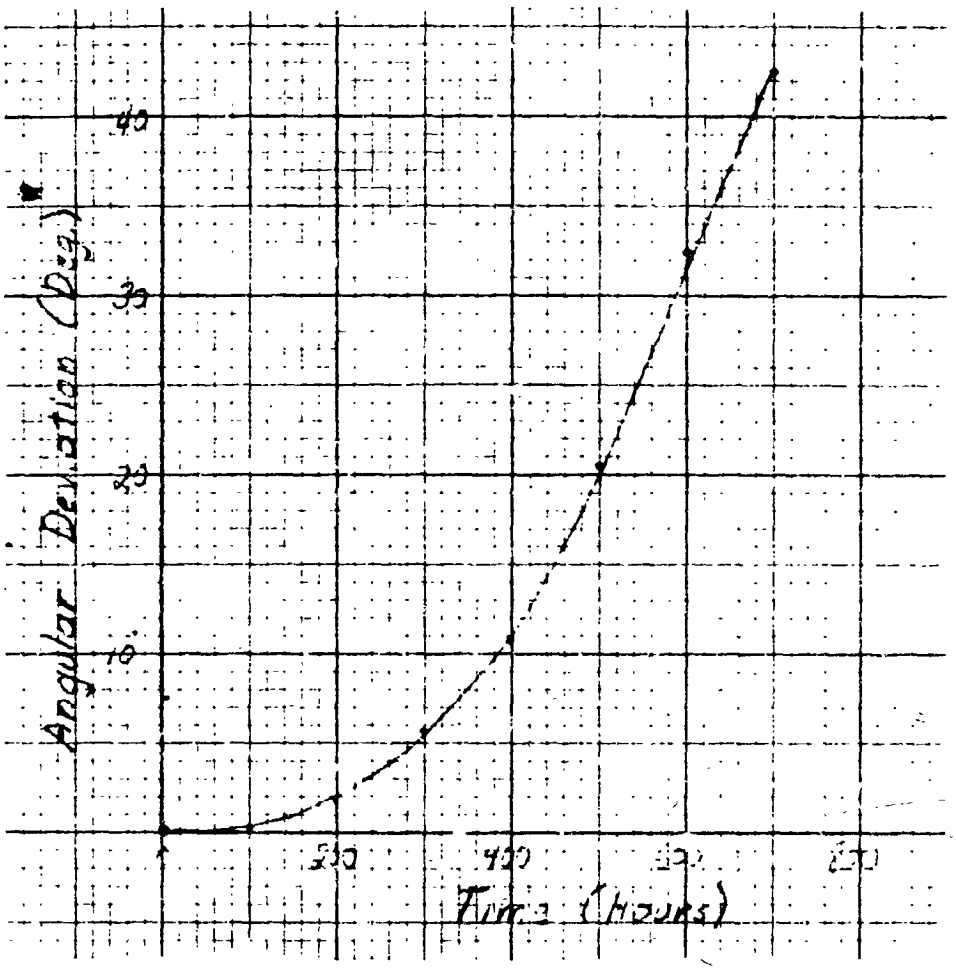

Figure 4.8-12

while the broken line denotes the fast mode run. As can be expected, the slow mode configuration causes the period of the satellite to become larger than does the fast mode.

Figure 4.8-12 shows the amount of angular difference which can be attained as a function of time for two satellites which originally have the same orbital period. During the first few days of the run the periods of the two satellites are still nearly equal and the amount of angular difference is very small. However, as the two periods become more divergent the larger angular difference over each orbit causes the total angular difference to build up somewhat exponentially. As can be seen from the curve, even though a difference of only three degrees can be achieved over the first ten days a difference of about 45 degrees can be achieved over a period of thirty days. This shows that station keeping corrections to the orbits of the satellites will probably have to be made over a period of approximately twenty days.

5.0 SUMMARY ASSESSMENT

A passive communications satellite vertically oriented with controllable mobility has been shown to be within the realm of possibility. This satellite could be constructed of materials similar to Echo II with approximately double the weight for a given diameter. The possible altitudes of operation fall in the range of 500 to 3500 statute miles. The evaluation of reduction in the number of satellites required over a system of random placement requires further computation of mobility. Optimization studies will probably improve some parameters.

One major area for further development is reliability to reduce the penalties for radiation damage and the need for redundant components. Another major area for further development is the satellite structure which will require the specification and performance of physical tests of materials, and effects encountered during inflation and deployment.